

UNCLASSIFIED

AD NUMBER
AD211874
NEW LIMITATION CHANGE
TO Approved for public release, distribution unlimited
FROM Distribution authorized to U.S. Gov't. agencies and their contractors; Foreign Gov't. Info.; Mar 1958. Other requests shall be referred to Central U.S. Registry, Rm. 1B889, The Pentagon, Washington, DC 20310-3072.
AUTHORITY
AGARD ltr, 24 Apr 1970

THIS PAGE IS UNCLASSIFIED

**UNCLASSIFIED**

**A 211874**

**Armed Services Technical Information Agency**

**ARLINGTON HALL STATION  
ARLINGTON 12 VIRGINIA**

**FOR  
MICRO-CARD  
CONTROL ONLY**

**1 OF 2**

**NOTICE: WHEN GOVERNMENT OR OTHER DRAWINGS, SPECIFICATIONS OR OTHER DATA ARE USED FOR ANY PURPOSE OTHER THAN IN CONNECTION WITH A DEFINITELY RELATED GOVERNMENT PROCUREMENT OPERATION, THE U. S. GOVERNMENT THEREBY INCURS NO RESPONSIBILITY, NOR ANY OBLIGATION WHATSOEVER; AND THE FACT THAT THE GOVERNMENT MAY HAVE FORMULATED, FURNISHED, OR IN ANY WAY SUPPLIED THE SAID DRAWINGS, SPECIFICATIONS, OR OTHER DATA IS NOT TO BE REGARDED BY IMPLICATION OR OTHERWISE AS IN ANY MANNER LICENSING THE HOLDER OR ANY OTHER PERSON OR CORPORATION, OR CONVEYING ANY RIGHTS OR PERMISSION TO MANUFACTURE, USE OR SELL ANY PATENTED INVENTION THAT MAY IN ANY WAY BE RELATED THERETO.**

**UNCLASSIFIED**

REPORT 172

ADVISORY GROUP FOR AERONAUTICAL  
RESEARCH AND DEVELOPMENT

**FC**

REPORT 172

**TECHNIQUES OF PRESSURE-FLUCTUATION  
MEASUREMENTS EMPLOYED IN THE  
RAE LOW-SPEED WIND-TUNNELS**

BY

T. B. OWEN

MARCH 1958



NORTH ATLANTIC TREATY ORGANIZATION  
PALAIS DE CHAILLOT, PARIS 16

FILE COPY

RETURN TO

ASTIA

ARLINGTON HALL STATION  
ARLINGTON 12, VIRGINIA

ATTN: TIS

ASTIA

RECORDED  
MAR 12 1959  
RECORDED  
TIPDR

AD No. 4  
211 874  
ASTIA FILE COPY

NORTH ATLANTIC TREATY ORGANIZATION  
ADVISORY GROUP FOR AERONAUTICAL RESEARCH AND DEVELOPMENT

TECHNIQUES OF PRESSURE-FLUCTUATION MEASUREMENTS  
EMPLOYED IN THE RAE LOW-SPEED WIND-TUNNELS

by

T.B. Owen

This Report was presented at the Pressure measurements Meetings, sponsored by the Agard  
Wind Tunnel and Model Testing Panel, held from 24th to 28th March, 1958, in London

## SUMMARY

A technique ~~has been~~ developed for examining, at model scale and in a low-speed wind-tunnel, the aerodynamic excitation responsible for aircraft vibration at flight speeds where Mach number does not have an important effect. The basic measurements are of the total intensity and spectrum function of the pressure fluctuations, and a description is given of the capacity-type transducers and the associated electronic equipment used. Problems of measurement, presentation and interpretation of the data are discussed; and, to illustrate the usefulness and limitations of the technique, examples are given of its application to the specific problems of aircraft vibration induced by flying with ~~either~~ open bomb-doors or extended air-brakes, or at an incidence where appreciable flow separation occurs over the wings. Consideration is given to the use of correlation measurements, and to the extension of the technique to testing at transonic speeds.

## SOMMAIRE

Une technique a été mise au point permettant d'examiner à l'échelle maquette en soufflerie à faible vitesse l'excitation aérodynamique pouvant donner lieu à des vibrations aux vitesses peu influencées par le nombre de Mach. Les mesures fondamentales effectuées ont porté sur l'intensité totale et la fonction spectrale des variations de pressions; on décrit les manomètres à capacité et l'électronique associé utilisés. Les questions intéressant la mesure, la présentation et l'interprétation des résultats obtenus sont ensuite discutées. Pour démontrer l'utilité ainsi que les limitations de cette technique, des exemples sont cités de l'application de la méthode aux problèmes particuliers des vibrations induites par le vol pendant lequel les trappes-bombes sont restées ouvertes ou les aéro-freins ont été sortis, ou bien par le vol à une incidence caractérisée par un décollement sensible sur les ailes. L'emploi de mesures corrélatives est considéré ainsi que l'extension de la technique à des essais aux vitesses transsoniques.

533.6.071.3

3b8b2

## CONTENTS

	Page
SUMMARY	ii
LIST OF FIGURES	v
NOTATION	ix
1. INTRODUCTION	1
2. METHODS OF MEASUREMENT AND PRESENTATION OF THE BASIC PRESSURE-FLUCTUATION DATA	3
2.1 Pressure-Transducers	3
2.2 Electronic Equipment	3
2.3 Calibrations	5
2.3.1 Transducer sensitivity	6
2.3.2 Amplifier frequency response	6
2.3.3 Analyser calibration	7
2.3.4 Tape recorder	7
2.4 Presentation of the Results	8
3. ACCURACY OF MEASUREMENT AND EXTENSIONS OF THE TECHNIQUE	9
3.1 Accuracy	9
3.2 Effect of Wind-Tunnel Airflow Unsteadiness	11
3.3 Additional Measurements	12
3.3.1 The use of pipes in pressure-fluctuation measurements	12
3.3.2 Correlation between pressure-fluctuations at two points	13
3.3.3 Estimation of normal-force fluctuations from pressure-fluctuation measurements	15
3.4 Further Developments	16
3.4.1 Extension of the present testing techniques to transonic and supersonic speeds	16
3.4.2 Automatic analyser	17
4. SOME PARTICULAR APPLICATIONS OF PRESSURE-FLUCTUATION MEASUREMENTS	17
4.1 Bomb-Bay Buffeting	17
4.2 Air-Brake Buffeting	18
4.3 Pressure Fluctuations of Thin Wings	18
4.3.1 Low-aspect-ratio unswept wing	19

	Page
4.3.2 Unswept wing panel	21
4.3.3 Wing panel with 30° leading-edge sweep	22
4.3.4 Low-aspect-ratio highly swept wings	23
5. CONCLUDING REMARKS	24
REFERENCES	25
FIGURES	26
DISTRIBUTION	

## LIST OF FIGURES

		Page
Fig. 1	Exploded sections of capacity-type pressure transducers	26
	(a) 0.7 in. pressure transducer	26
	(b) 1.5 in. pressure transducer	26
Fig. 2	General arrangement of apparatus for measurement and analysis of pressure fluctuations	27
Fig. 3	Typical bandwidth response curves for the Muirhead-Pametrada wave analyser type D-489	28
Fig. 4	Typical transducer calibration and sensitivity factor	29
	(a) Direct transducer calibration	29
	(b) Transducer sensitivity factor	29
Fig. 5	Frequency response of wide frequency-range amplifier	30
Fig. 6	Measured analyser characteristics	31
	(a) Measured bandwidth ratio	31
	(b) Overall analyser sensitivity factor (see Section 2.3.3)	31
Fig. 7	Frequency response using tape recorder	32
	(a) High frequency response of tape recorder and playback	32
	(b) Analyser sensitivity factor when used in conjunction with 6 in./sec recording and 60 in./sec playback	32
Fig. 8	Effect of record length on replay accuracy at low frequencies. Recording and replay at 60 in./sec tape speed	33
	(a) Analysis of two halves of a 75 ft recording	33
	(b) Analysis of four quarters of a 75 ft recording	33
Fig. 9	Effect of wind-speed on a spectrum of pressure fluctuations on the rear wall of a rectangular cavity in a cylindrical body. $L$ = cavity length	34
Fig. 10	Effect of bandwidth on a spectrum of pressure fluctuations on the upper surface of a highly swept wing	34

	Page	
Fig. 11	Measured spectrum showing separation of a peak, due to a discrete frequency oscillation, from the continuous spectrum	35
Fig. 12	Comparative measurements of a spectrum of pressure fluctuations behind a spoiler obtained by direct analysis, and by replay of recordings made at two tape speeds	36
	(a) Direct analysis. Analyses before and after recordings	36
	(b) Recording at 6 in./sec. Replay at 60 in./sec. Three 75 ft records	36
	(c) Recording at 60 in./sec. Replay at 60 in./sec. Three 75 ft records	36
Fig. 13	Model for comparative pressure-fluctuation measurements in two wind-tunnels	37
Fig. 14	Pressure fluctuations on a wing in two wind tunnels	38
Fig. 15	Attenuation due to use of a pipe between measuring point and transducer. Transducer as shown in Figure 1a, pipe 0.028 in. internal diameter	39
Fig. 16	Circuit variations for correlation measurements	40
	(a) Connections for measuring $\sqrt{A^2}$	40
	(b) Connections for measuring $\sqrt{B^2}$	40
	(c) Connections for measuring $\sqrt{(A + B)^2}$	40
Fig. 17	'Exploded' sections of a prototype transducer for the measurement of high-frequency pressure fluctuations	41
Fig. 18	Effect of rounding the rear bulkhead on bomb-bay pressure fluctuations	42
	(a) Bulkhead transducer	42
	(b) Body transducer	42
Fig. 19	Effect of rear bulkhead fairing on bomb-bay pressure fluctuations	43
Fig. 20	Installation of transducer for pressure-fluctuation measurements on body with air-brake	44

	Page	
Fig.21	Fluctuating and static pressure distributions on a body surface due to an air-brake	45
	(a) $\theta = 70^\circ$	45
	(b) $\theta = 90^\circ$	45
Fig.22	Pressure fluctuation spectra measured at points indicated in Figure 21	46
	(a) $\theta = 70^\circ$	46
	(b) $\theta = 90^\circ$	46
Fig.23	Effect of air-brake angle on the pressure excitation on a body	47
Fig.24	Variation of Strouhal number with air-brake angle	47
Fig.25	Wing for correlation coefficient measurements	48
Fig.26	Chordwise distribution of pressure fluctuations on wing shown in Figure 25, nacelle on	49
Fig.27	Chordwise variation of correlation coefficient on wing shown in Figure 25, nacelle on	50
Fig.28	Smoothed chordwise variation of correlation function on wing shown in Figure 25. Nacelle on	51
Fig.29	Variation of section normal-force fluctuation on wing shown in Figure 25. Nacelle on	51
Fig.30	Chordwise variation of correlation coefficient on wing shown in Figure 25. Nacelle on. Wing incidence $4^\circ$	52
Fig.31	Unswep wing with sharp leading edge	53
	(a) Details of model	53
	(b) Variation of bubble length with incidence	53
Fig.32	Unswep wing with sharp leading edge. Fluctuations in pressure difference between upper and lower surfaces	54
	(a) r.m.s. pressure fluctuation	54
	(b) Spectra of pressure fluctuations at 0.85c	54
	(c) 'Low frequency component' of pressure fluctuations	54

	Page	
Fig.33	Unswept wing with sharp leading edge. Comparison of pressure fluctuations on upper and lower surfaces. Transducer at 0.85c	55
	(a) r.m.s. pressure fluctuation	55
	(b) Spectra of pressure fluctuations, $\alpha = 14^\circ$	55
Fig.34	Sharp-edged wing with $30^\circ$ leading edge sweep	56
	(a) Model details	56
	(b) Position of attachment point at spanwise positions of pressure transducers	56
Fig.35	Pressure fluctuation measurements on a sharp-edged wing with $30^\circ$ leading edge sweep as shown in Figure 34	57
	(a) r.m.s. pressure fluctuation at the three transducer positions	57
	(b) Spectra of pressure fluctuations at middle transducer position	57
	(c) 'Low-frequency component' of pressure fluctuations at the three transducer positions	57
Fig.36	Upper-surface contours of $\sqrt{vnF(n)}$ at $n = 0.2$ on a low-aspect-ratio sharp-edged wing at $8^\circ$ incidence: $n = f\bar{c}/V$	58
Fig.37	Variation of r.m.s. upper-surface value of $\sqrt{vnF(n)}$ at $n = 0.2$ with incidence for the sharp-edged wing shown in Figure 36, assuming a correlation coefficient of 1.0 throughout	58
Fig.38	$81^\circ$ swept wing-RAE 101 section: fluctuations in pressure difference between upper and lower surface	59
	(a) Details of model	59
	(b) r.m.s. pressure fluctuation	59
	(c) Spectra of pressure fluctuations	59
	(d) 'Low frequency component' of pressure fluctuations	59

Best Available Copy

NOTATION

A, B	instantaneous values of two fluctuating quantities
$\bar{A}, \bar{B}$	mean values of A and B
$\overline{AB}$	mean value of product AB
$\sqrt{A^2}$	root-mean-square value of A
$\sqrt{B^2}$	root-mean-square value of B
c	local wing chord
$\bar{c}$	standard mean chord
$\bar{c}$	aerodynamic mean chord
$C_L$	lift coefficient
$C_D$	drag coefficient
$C_N$	instantaneous load
f	input frequency; buffeting frequency
$\Delta f$	acceptance frequency bandwidth
$f_w$	wing fundamental frequency
F(n)	spectrum function
l	a representative length (Air brake chord in Figures 20-24)
L	length of bomb bay
n	a non-dimensional frequency parameter ( $= fl/V$ )
p	root-mean-square of pressure fluctuation
$p_x, p_{x'}$	root-mean-square values of pressure fluctuations at x and x'
$P_x, P_{x'}$	instantaneous pressures at two points x and x' along wing chord
q	dynamic head ( $= \frac{1}{2}\rho V^2$ )
r	$ x' - x $
$R_{ab}, R_{xx'}, R_{xr}$	correlation coefficients
t	number of points on chord line at which pressure is measured

$V$  free-stream velocity  
 $V_A$  approach speed  
 $x, x'$  distances measured along a chord line from the leading edge  
 $\alpha$  wing incidence  
 $\Sigma$  bandwidth ratio (=  $\Delta f/f$ )  
 $\eta$  distance of pressure transducer from centre line (see Figure 22)  
 $\theta$  angular deflection of air brake  
 $\rho$  air density

Best Available Copy

TECHNIQUES OF PRESSURE-FLUCTUATION MEASUREMENTS  
EMPLOYED IN THE RAE LOW-SPEED WIND-TUNNELS

T.B. Owen\*

1. INTRODUCTION

There are many instances where aircraft vibration can be excited aerodynamically: for example, in flight with open bomb-doors, with extended airbrakes, or at speeds or attitudes at which extensive flow separations occur. The measurement, at model scale, of the pressure fluctuations which excite the vibration, and the subsequent extrapolation to full-scale conditions are therefore of considerable importance; and some of the techniques and methods of approach which may be used are considered in detail in this paper. The problems discussed are all ones in which Mach number does not have an appreciable effect, and the techniques described have been developed specifically for use in low-speed wind-tunnels; some mention is made, however, of the further problems expected in extending the model techniques to transonic speeds.

The first application of the technique was to a problem of aircraft vibration which occurred when the bomb-doors were open; a brief historical summary of this investigation, given below, brings out a number of points which have been found relevant to all subsequent investigations. A flight investigation had disclosed three characteristic properties of the vibration: its intensity was, at all points measured, approximately proportional to the dynamic head ( $\frac{1}{2}\rho V^2$ ) and independent of Mach number, within the speed range of the aircraft in question; the greater part of the vibration corresponded to excitation of the vertical and lateral flexural modes of the fuselage, within the frequency range 6 to 10 cycles/sec. and the vibration at points on the rear fuselage was very irregular, with no preferred frequency, suggesting its cause to be a random aerodynamic disturbance. Since these characteristics were consistent with forced vibrations of the aircraft structure, it seemed worthwhile to examine the nature of the aerodynamic forcing field in the absence of response effects and at model scale. The measurement and analysis of the fluctuating-pressure field on an effectively rigid model of the aircraft in a low-speed wind-tunnel was therefore undertaken to throw light upon the basic causes of the aircraft vibration, and to indicate the effectiveness of modifications designed to reduce them.

Preliminary tests were made in late 1952 using some existing transducers of the variable-capacitance type together with their associated pre-amplifier, and in conjunction with a wave-analyser which operated on the scanning principle. The results obtained showed that significant pressure fluctuations were confined to the neighbourhood of the rear bulkhead of the bomb-bay, but that they were of too random a nature for a spectrum analysis to be possible with the equipment used. The original analyser was accordingly discarded and replaced by the final stage of an existing amplifier (originally designed for use with hot-wire anemometers) together with a tunable wave-analyser, and further experiments immediately established the important result that both the root-mean-square intensity and the spectrum function of the pressure-fluctuations were proportional to the dynamic head, and could consequently be usefully expressed non-dimensionally in the same way as steady pressures.

---

\* United Kingdom

These results agreed qualitatively with those obtained in flight in that they indicated random aerodynamic excitation with no detectable scale effect. They therefore suggested that the non-dimensional results were applicable to the full-scale aircraft, and in particular it became possible to define, and to concentrate attention upon, a frequency range for the model scale which corresponded to the band containing the dominant full-scale vibrations. In view of the narrowness of the frequency band in question, the intensity in this band seemed to offer a better indication of the relevant excitation than did the total intensity, especially when considering the probable effectiveness of modifications, which are apt to change both total intensity and the spectrum shape.

These early wind-tunnel experiments established the usefulness of the technique and, with improvements in both the transducers and the associated electronic equipment, further applications followed, notably to the examination of the fluctuating-pressure fields:

- (a) Associated with bomb-bay buffeting, using a generalised model consisting of a cylindrical body in which the cavity shape could be systematically varied with various bomb-door configurations fitted
- (b) On a body in the vicinity of an air-brake
- (c) On thin wings under various mean-flow conditions.

All the experiments were confined to low speeds (below  $M = 0.3$ ), and the absence of scale effect, within the available wind-tunnel speed range, was again confirmed in all cases. The further experience with the technique served also to emphasize the earlier conclusion that it was essential to determine spectra as well as the total intensity of the pressure fluctuations, and these together were considered to provide the minimum amount of data from which useful inferences could be drawn.

In addition to the application of the pressure-transducer considered here, both the hot-wire and the strain-gauge are available for the measurement of velocity fluctuations and load or moment fluctuations respectively. Each of these techniques may be used in low-speed wind-tunnel investigations into the causes of buffeting; but a complete examination of their relative usefulness is beyond the scope of this paper, the purpose of which is to demonstrate the experimental methods, and the particular advantages and limitations, associated with the use of the pressure-transducer. The equipment required is considered in Section 2 of the paper, where the present designs of transducer and the associated electronic equipment are described in detail. This section also includes a discussion of the methods of reduction and presentation of the basic measurements, the total intensity, and spectra of the pressure-fluctuations. This is followed, in Section 3, by a discussion of the accuracy of the basic measurements, and of the methods available for widening the scope of the technique, additional measurements which can be made are considered in the same section. The use and limitations of the data which can be obtained are indicated finally, in Section 4, where a number of particular applications of the technique are discussed. Consideration is given in this section to the difficulties both of measurements and of interpretation, and to situations where other techniques might be more appropriate.

## 2. METHODS OF MEASUREMENT AND PRESENTATION OF THE BASIC PRESSURE-FLUCTUATION DATA

### 2.1 Pressure-Transducers

The transducers are of the variable-capacitance type and the two designs most used are those shown in Figures 1a and 1b. The diaphragms are of beryllium copper and the transducer bodies of brass, which has a similar coefficient of expansion. The fixed plate of the condenser is insulated from the body of the transducer by a Tufnol cup, the three parts being cemented together with Araldite. After cementing, the common face is machined flat and a small step introduced at the rim, as shown in Figure 1. This step, of 0.0030 in. for the larger transducer and 0.0035 in. for the smaller, in conjunction with a shim 0.0040 in. thick, gives a nominal gap between the diaphragm and fixed plate of 0.0010 in. for the larger transducer and 0.0005 in. for the smaller one.

For investigations in separated air-flows at wind-tunnel speeds of 100 to 150 ft/sec the two requirements for the transducers are:

- (a) A sensitivity of about 0.5 Pf/in. of water
- (b) An ability to withstand a positive pressure difference of at least 4 in. of water without the diaphragm coming into contact with the fixed plate.

These two conditions are satisfied with a diaphragm thickness of 0.007 in. for the larger transducer and 0.004 in. for the smaller. The inevitable slight lack of flatness the diaphragms makes it necessary to tune each individual transducer by trial assembly, using each of a number of diaphragms with various reduced shims, of from 0.0038 to 0.0040 in. in thickness, to find a suitable combination.

The sensitivity of about 0.5 Pf/in. of water appears to represent the highest value conveniently attainable with the smaller transducers as they are at present constructed. The larger transducers, however, can easily be made more sensitive by reduction of the diaphragm thickness and/or the gap between the diaphragm and the fixed plate, and sensitivities as high as 8 Pf/in. of water have been used for special purposes, though with a reduced maximum permissible pressure-difference.

### 2.2 Electronic Equipment

Figure 2 shows the general arrangement of the associated electronic equipment for the measurement and analysis of the pressure fluctuations. The transducers are used with a Southern Instruments oscillator and pre-amplifier. This is a frequency-modulated system using a 2-megacycle/sec carrier with an 'N-shaped' response curve, giving a nearly constant sensitivity of 0.4 volts/Pf over a range of 50 Pf. The output of the pre-amplifier can be taken to a high-resistance voltmeter (1 megohm/volt) for direct calibration of the transducer from pressure to voltage, or alternatively to an amplifier with a wide frequency-range for measurement of pressure fluctuations. This amplifier is basically the final stages of one designed<sup>1</sup> at the R.A.E. for use with hot-wire anemometers; its output stage has been modified for the present purpose, and it has a nominal usable frequency range from 1.4 to 50,000 cycles/sec. A thermojunction is incorporated in one of the final stages of the amplifier and is connected

to a suitable D.C. galvanometer. The reading of this galvanometer is then proportional to the mean-square amplitude of any alternating input voltage irrespective of frequency, within the frequency range of the amplifier. An uncalibrated input attenuator on the amplifier can be adjusted to give a standard reading on the thermo-junction-galvanometer irrespective of input, in the range 3.5mV to 350mV; the input to the amplifier can then be taken from the microvolter, the output of which can be adjusted to give the same reading on the thermo-junction-galvanometer as that produced by the signal from the pre-amplifier; the reading of the microvolter, which when excited from a suitable oscillator acts as a calibrated attenuator covering a root-mean-square range of 1 $\mu$ V to 1V, is then equal to the root-mean-square output of the pre-amplifier. This value may finally be converted into the root-mean-square total intensity of the pressure fluctuation by means of the calibration between steady pressures and voltages previously obtained.

If it is required to measure the spectrum density of the pressure-fluctuations, the amplifier output can be fed direct into the analyser section or recorded on magnetic tape for subsequent play-back into the analyser. The analyser used is the Muirhead-Pametrada D-489 which covers the frequency range 20 cycles/sec to 20,000 cycles/sec and has four possible bandwidth ratios: 1.5%, 3.0%, 4.8% and 15.5% of the tuned frequency. The method of obtaining these four bandwidths is of interest. The analyser consists of two tuned amplifiers in series; to obtain the 1.5% bandwidth ratio both amplifiers are in series giving a combined Q-factor of 80, and for the 3.0% bandwidth ratio one amplifier is switched out giving a Q-factor of 50. For the 4.8% bandwidth ratio the two amplifiers are again in series, but the tuned frequencies of the amplifiers are respectively +1.5% and -1.5% from the frequency set on the analyser; similarly the 15.5% bandwidth ratio is obtained with both amplifiers in series, with their frequencies +5% and -5% from the selected frequency. Typical response curves are shown in Figure 3 and it can be seen that the 4.8%, and more particularly the 15.5%, bandwidth ratio obtained in this way is a better approximation to the ideal 'square' response curve than the single tuned circuit curves of the 1.5% and 3.0% bandwidth ratios. The low-frequency range of the analyser is extended to include 2 to 20 cycles/sec by introducing a low-frequency modulator, which basically adds 50 cycles/sec to the frequency of any incoming signal, so that this range becomes 52 to 70 cycles/sec, which is then within the range of the analyser. This method of obtaining the low-frequency range leads to some complications with regard to bandwidth variation which will be discussed in Section 2.3.3.

Two modifications have been made to the analyser as supplied by the makers. Firstly a thermo-junction feeding a suitable D.C. galvanometer has been introduced into the output circuit, and the rectifier-type instrument on the analyser switched out. The operator takes a mean of the galvanometer reading by eye, and this modification enables the required mean of a squared output to be taken rather than a simple mean, as would have been obtained from the instrument fed through a rectifier; also, some necessary damping of the analysed signal, which may be varying rapidly by as much as two or three to one, is introduced. Secondly, the three-to-one steps of the analyser input-attenuator were then too large for an output-instrument reading proportional to the square of the signal, and a logarithmic potentiometer was constructed to replace the analyser attenuator, which was then locked on its 3mV setting. The logarithmic potentiometer covers a 1000 to 1 range in 100 steps (i.e. with a gain of 1.072 per step), and the output-galvanometer is scaled over the range 0.90 to 1.10.

In use the amplifier, adjusted as described earlier, supplies the fluctuating signal for analysis at a root-mean-square level of 3.5V to the analyser section. The frequency range is covered using a standardised set of frequencies in which the ratio of each higher frequency to the preceding one is approximately in the ratio of  $\sqrt{2}:1$ , the most usual range (3 to 2000 cycles/sec) requiring 22 measurements; measurements at these frequencies alone are normally sufficient, but the steps are small enough for the readings to reveal any sharp peaks in the spectrum, the presence of which would require additional points to be interpolated. Calibrations are performed at intervals by taking the amplifier input from the microvolter, with zero setting on the logarithmic potentiometer and at a medium frequency of 280 cycles/sec, and determining the exact input voltage required to produce a reading of unity on the analyser output-galvanometer; allowance can then be made for any drift in the gain of the amplifier or analyser.

The analysis of one signal requires steady wind-tunnel conditions to be maintained for about 20 minutes. This is usually feasible for small low-speed wind-tunnels, but for larger or higher-speed wind-tunnels the cost in power and tunnel-running time, together with difficulties in maintaining constant conditions in some cases, makes a reduction in this time desirable. Provision has accordingly been made for recording the amplifier output onto magnetic-tape, for subsequent re-play into the analyser, so cutting the tunnel-running time to about 5 minutes, though the time taken for the analysis is hardly affected.

The tape recorder used is a two-channel Ampex Type 306-2 with recording speeds of 6, 12, 30 and 60 in./sec; re-play is on an Ampex Type 3-3559 75 ft loop playback system with a speed of 60 in./sec only. The only modification required for recording is attenuation of the amplifier output from 3.5V r.m.s. to 0.5V r.m.s., the recommended signal voltage for the recorder; this is then compensated by the addition of a seven-to-one amplifier to the replay electronics, so that 3.5V r.m.s. is again supplied to the analyser section. The Ampex equipment works on the frequency-modulated principle using a carrier frequency of 54,000 cycles/sec at 60 in./sec, with proportionately reduced carrier frequencies at lower tape speeds.

In use, channel 1 of the recorder is supplied continuously with 0.4V r.m.s.\* at 280 cycles/sec. After measuring the equivalent r.m.s. voltage of the pre-amplifier output signal, as described earlier, the amplifier is left connected to the microvolter and a short tape (about 8 ft) recorded; 75 ft is then recorded, taking the amplifier input from the pre-amplifier, and this is followed by another short tape using the microvolter output. By reference to channel 1, and using the two short tapes, any drift in channel 2 gain during recording or playback can be allowed for.

### 2.3 Calibrations

In order to obtain an acceptable accuracy it has been found necessary to calibrate the whole system at intervals; this is required so that allowances can be made for small steady drifts in gain of all the electronic items and in the sensitivity of the transducers. The various calibrations are considered separately below.

---

\* 0.4V r.m.s. rather than 0.5V is supplied to channel 1 so that incorrect loading of calibrating tapes into the replay equipment can be detected.

### 2.3.1 Transducer sensitivity

The transducers, while having the merit of being simple to construct, and adaptable to a number of forms, suffer from two main drawbacks, non-linearity of calibration, and variation with temperature both of zero and sensitivity. Considering first non-linearity, a typical transducer calibration is shown in Figure 4a, where the D.C. voltage output of the pre-amplifier is plotted against steady pressure difference across the transducer diaphragm. The corresponding transducer sensitivity in volts/in. of water is shown in Figure 4b plotted against the output voltage. In a typical low-speed test on a wing the pressure difference across the transducer may vary from 0 to 5 in. of water, causing a variation in sensitivity of 10%. However, this can be allowed for by using the relation shown in Figure 4b, provided that the mean pressure difference, in terms of output-voltage from the pre-amplifier, is noted during the tests. The peak-to-peak amplitude of the pressure-fluctuation would not normally exceed 3 in. of water, so that non-linearity does not distort the fluctuating signal appreciably.

10°C rise in temperature may raise the transducer sensitivity by as much as 10%, and cause a zero-shift equivalent to 5 in. of water. For low-speed wind-tunnel tests it is normally sufficient to calibrate the transducers at the beginning, middle and end of the morning and either twice or three times again in the afternoon; the order of drift between successive calibrations is shown in Figure 4. The zero-drift and sensitivity-drift can then be allowed for on a time basis if one tunnel-speed is being used, or otherwise on a temperature basis. Appreciable zero-drift occurs in the pre-amplifier when it is first switched on, and it has been found necessary to use a time-switch, so that the pre-amplifier may have been switched on for two to three hours before it is used. An accuracy of  $\pm 2\%$  on the transducer sensitivity appears reasonable using these methods.

Preliminary tests on the possibility of using the present transducers in a model in a transonic wind-tunnel, with temperature rises of up to 45°C, suggested however that, even with preliminary calibration of the temperature effects, an accuracy of  $\pm 5\%$  on transducer sensitivity would be difficult to attain.

The author is not aware of any satisfactory and simple method of measuring the frequency response of pressure transducers at frequencies above about 100 cycles/sec, and no attempt has been made to examine the frequency response of the transducers used. The Southern Instruments equipment, which uses a 2-megacycle/sec carrier frequency, would be expected to have a flat response to considerably above the 20,000 cycles/sec limit of the rest of the equipment; the natural frequency of the transducer diaphragms is about 6000 cycles/sec, and it is assumed that the transducers have a flat response to about a third of this, say 2000 cycles/sec. The transducer sensitivity to steady pressures is therefore used throughout and an upper limit of 2000 cycles/sec is applied to the spectrum analysis. For low-speed tests this upper limit excludes very little of the total energy in the spectrum.

### 2.3.2 Amplifier frequency response

The amplifier response curve is shown in Figure 5. The r.m.s. amplitude of the signal passed by the amplifier is taken as representing the total intensity of the pressure fluctuation. The upper frequency limit is well above any signal passed by the transducer, but the low frequency cut-off sometimes results in too low a value for the total intensity being obtained.

### 2.3.3 Analyser calibration

The analyser is designed so that the whole frequency range from 2 cycles/sec to 20,000 cycles/sec is divided into 11 sub-ranges, and it has been found necessary to measure the bandwidth and the amplitude response at a number of points in each sub-range. A typical bandwidth calibration curve is shown in Figure 6a; the full lines show the bandwidth condition normally used. A compromise must be made in choosing the bandwidth; a narrow bandwidth gives a better definition of a function which varies rapidly with frequency; but, if it is too narrow, large fluctuations in amplitude of the signal passed by the band occur, and a mean reading is difficult to obtain. Above 20 cycles/sec the nominal 15.5% bandwidth ratio appears to give the right kind of compromise; it also has the additional advantage that it provides the best cut-off at the edges of the band (see Section 2.2). Below 20 cycles/sec the use of the low-frequency modulator, which adds 50 cycles/sec to the frequency of any input signal, means that the bandwidth ratio is increased by a factor of  $(50 + f)/f$ , where  $f$  is the input frequency. This necessitates the use of the 1.5% bandwidth from 3 cycles/sec to 11 cycles/sec, and the 3.0% bandwidth from 11 cycles/sec to 20 cycles/sec, with the results shown in Figure 6a. Using these measured bandwidth ratios a satisfactory smooth spectrum is obtained, provided a genuinely random signal is being analysed. However, the differences in discrimination between the three bandwidth settings lead to apparent discontinuities in the spectrum at 11 cycles/sec and 20 cycles/sec, if a large single frequency fluctuation is present below about 50 cycles/sec.

In order to calibrate the system for direct analysis, the microvolter is first replaced by an attenuator circuit containing a thermojunction so that a constant input (of about 100mV), irrespective of frequency, can be supplied to the amplifier. Using this, the bandwidth ratio of the analyser and the overall frequency response of the amplifier and analyser are measured at several frequencies in each of 11 sub-ranges of the analyser. An overall sensitivity factor is then computed, giving the actual output through the analyser band at each frequency, as a ratio to that which would be produced by an ideal analyser having a constant 15.5% bandwidth ratio, and with a flat frequency response for the analyser and amplifier; a typical calibration is shown in Figure 6b. This calibration takes about 10 days, but checks show that errors of only 1 to 2% occur over about a year, at the end of which time it is necessary to readjust the analyser settings, to correct distortion of the bandwidth response curves due to unequal deterioration of the valves.

Allowances are made for the effect of the input impedance of the amplifier on the pre-amplifier output; for the effect of the input impedance of the low frequency modulator on the logarithmic potentiometer calibration, and for the combined effect of these on the amplifier output.

### 2.3.4 Tape recorder

The introduction of the tape recorder into the system modifies the usable frequency ranges considerably. The measured frequency response of channel 2, recording at 6 and 60 in./sec and with 60 in./sec playback, is shown in Figure 7a. The overall frequency response of the whole system, from amplifier input to analyser output, is shown in Figure 7b for 6 in./sec recording speed; this shows a usable frequency range of 2 to 1000 cycles/sec.

Using 60 in./sec recording speed the upper frequency limit is raised to 10,000 cycles/sec, while the lower limit might appear to be 3 cycles/sec, as for direct analysis. However, in this case, the lower frequency limit is no longer simply defined, but has to be experimentally determined as the lowest frequency which is sufficiently accurately sampled in a 15-second recording (the maximum tape loop for playback is 75 ft). As a check on this, the results of analysing separately the two halves of a 75 ft recording are shown in Figure 8a, compared with a direct analysis, and the results for the four quarters are similarly shown in Figure 8b. Possible limits, on the assumption that the additional scatter is inversely proportional to the number of cycles recorded, are shown. Assuming a normal maximum scatter of  $\pm 10\%$ , twice the normal scatter seems reasonably acceptable at the limiting frequency; this requires a minimum of 150 cycles recorded. On this basis the usable frequency ranges of the equipment become

Recording speed (in./sec)	Usable frequency range (cycles/sec)
6	2* to 1,000
12	2 to 2,000
30	5 to 5,000
60	10 to 10,000

From this it would seem that the 12 in./sec recording speed matches the present transducers satisfactorily. Where 1000 cycles/sec is a sufficiently high upper limit, the 6 in./sec recording speed has the advantage of less tape being wasted while the recorder accelerates to its operating speed, and also the low-frequency modulator is not required for the subsequent analysis.

The overall frequency response of the system from amplifier input to analyser output is again determined at intervals using the calibrating circuit described in Section 2.3.3; short tapes, about 8 ft long, are recorded for a number of frequencies at each of the recording speeds. Measurements at about 12 frequencies at each tape-speed are sufficient to define a smooth curve of the ratio of the overall frequency response of the system using the tape recorder, to that measured with the amplifier connected directly to the analyser section; values of this ratio can then be read off the curve at intermediate frequencies and applied as an additional factor to the overall sensitivity factor for direct analysis determined as described in the previous section (2.3.3).

#### 2.4 Presentation of the Results

The root-mean-square intensity,  $p$ , of the pressure fluctuations is made non-dimensional by dividing it by the dynamic head  $q (= \frac{1}{2}\rho V^2)$ . A non-dimensional frequency parameter  $n = fl/V$  (where  $f$  is the frequency,  $l$  a representative length and  $V$  the free stream velocity) is then introduced, and a spectrum function  $F(n)$  is defined, such that  $F(n)\delta n$  is the contribution  $(p/q)^2$  in the frequency range  $n + \delta n$ . Thus

$$\delta \left( \frac{p}{q} \right)^2 = F(n)\delta n = nF(n) \delta(\log n)$$

The results of the spectrum analyses can therefore be plotted in the form  $F(n)$  against  $n$ , or  $nF(n)$  against  $\log n$ ; and, in either case, integration over any range of frequency

\* Limited by the amplifier response

gives the corresponding mean-square intensity of the fluctuation. In particular, the total area under either curve is equal to the total intensity, for

$$\left(\frac{p}{q}\right)^2 = \int_0^{\infty} F(n)dn = \int_{n=0}^{n=\infty} nF(n) d(\log n)$$

However, for the usual application of the analysis to the examination of buffeting excitation, a modified form of presentation is considered to be more appropriate. This is because aircraft buffeting normally takes the form of the excitation of a particular structural mode at nearly a discrete frequency; that is to say, a mode with a sharply tuned resonance curve, or a narrow acceptance band. If  $f$  is the buffeting frequency and  $\Delta f$  the acceptance bandwidth in such a case, the relevant root-mean-square intensity of the excitation  $\sqrt{\Delta p^2}$  is then given approximately,  $\Delta f/f$  being small, by

$$\frac{\sqrt{\Delta p^2}}{q} = \sqrt{nF(n)} \sqrt{\frac{\Delta f}{f}} \quad (1)$$

since  $\frac{\Delta f}{f} = \frac{\Delta n}{n}$

With the ratio  $(\Delta f/f)$  determined by the aircraft structural characteristics, and presumably independent of speed, the aerodynamic excitation expressed non-dimensionally,  $(\sqrt{\Delta p^2}/q)$ , is directly proportional to  $\sqrt{nF(n)}$ , which therefore provides a useful presentation of the spectrum. The abscissa is taken as  $\log n$ , because a more open scale is obtained at low frequencies, and because the integrable power spectrum may be readily obtained by squaring the ordinates. Equation (1) is also used to calculate  $\sqrt{nF(n)}$  from the measurements; the root-mean-square voltage passed by the analyser is first expressed as  $\sqrt{\Delta p_A^2}/q$ , using the transducer sensitivity factor; then, if the analyser bandwidth ratio  $(\Delta f_A/f)$  is written as  $\epsilon_A$ ,

$$\sqrt{\Delta p_A^2}/q = \sqrt{nF(n)} \epsilon_A$$

This is strictly correct only if  $\epsilon_A$  is infinitely small; and the errors introduced by the use of a small but finite bandwidth are considered in Section 3.1.

### 3. ACCURACY OF MEASUREMENT AND EXTENSIONS OF THE TECHNIQUE

#### 3.1 Accuracy

A number of checks have been made, at intervals, on the repeatability of results and, as far as possible, on the validity of the conclusion that there is no apparent scale-effect when the spectrum is presented in a non-dimensional form. An example is shown in Figure 9 where the pressure-fluctuations on the rear wall of a rectangular cavity in a cylindrical body have been analysed at three windspeeds: 108, 150 and 218 ft/sec. These results show no apparent scale-effect for the range of windspeed covered, and, in all the series of tests made, a few checks have been made that the same

spectrum is obtained at two windspeeds differing by a factor of about two. So far no discrepancies worse than those shown in Figure 9 have been found; the Mach number in all cases has been less than 0.3. The scatter shown, amounting to a maximum of  $\pm 10\%$ , is about what can normally be achieved, although in a specific case this could be reduced to nearer  $\pm 5\%$  by spending longer over taking the visual mean of the analyser output-galvanometer reading at each frequency. The additional time required is not normally considered justified as sufficient points are measured for a smoothed curve to be drawn.

As a check on the effect of analyser bandwidth, the same signal, in this case of the pressure fluctuations on a highly swept wing, was analysed using both the nominal 4.8% and 15.5% bandwidths shown in Figure 6a; the results are shown in Figure 10. In this case the frequency range was extended to include the resonance of the transducer diaphragm. The discrepancies between the two curves are less than  $\pm 10\%$  except in the neighbourhood of the resonance peak. In addition, the intensity of pressure-fluctuations ( $p/q$ ), deduced from integrating  $nF(n)$  with respect to  $\log n$ , is 0.0085 for the analysis using the 4.8% bandwidth and 0.0084 using the 15.5% bandwidth, compared with 0.0087 by direct measurement. These measurements demonstrate that the 15.5% bandwidth is satisfactory for the continuous part of the spectrum up to about 1500 cycles/sec.

The presence of sharp peaks in the spectrum leads however to differences in the measured spectra, in the neighbourhood of the peak, which depend on the bandwidth used. In particular, if the true spectrum is a continuous smooth curve with the addition of an oscillation at a discrete frequency, the correct representation will be the continuous spectrum with a single line to infinity at the discrete frequency; while the measured spectrum, deduced in the usual way from the analyser readings, will be the continuous spectrum with the addition of the product of the amplitude of the discrete frequency oscillation and the analyser response curve. Figure 11 shows such a measured spectrum and demonstrates that it is possible to find, by trial and error, an amplitude for the discrete frequency oscillation which, multiplied by the analyser response curve, enables the smooth continuous spectrum to be inferred. This dividing of the spectrum into its two components can only be made directly if the data is plotted in the form of an integrable power-spectrum, e.g. as  $nF(n)$  against  $\log n$  as in Figure 11. The area under the continuous-spectrum curve can then be integrated to give the mean-square intensity of the random pressure fluctuation, while the area under the peak, but above the continuous-spectrum curve, should be equal to the mean-square amplitude of the discrete frequency oscillation.

In most cases, however, this division of the spectrum is not possible, as the peak is produced, not by a discrete frequency oscillation, but is correctly a smooth peak in the spectrum. The curves shown in Figure 10 are of this form, since it is apparent that the width of the peak is large compared with that of the analyser response curves (Fig. 3). Only at the centre of the peak do the two curves differ appreciably.

An important point to note is that regardless of how the peaks arise, and of what bandwidth is used, the area under a peak, when the results are presented in the form of an integrable power spectrum, is a fairly correct measure of the energy in the corresponding frequency range. The results are therefore normally given as measured, with no attempt to apply corrections to the exact shape of any peak present.

To check the effect of the tape-recorder on the accuracy with which a spectrum is determined, a particular signal produced by a transducer behind a spoiler was analysed directly, recorded at 6 in./sec on 225 ft of tape, recorded at 60 in./sec on another 225 ft of tape, and finally analysed directly again. Each of the 225-ft lengths of tape was cut into three and the portions analysed separately; the resulting spectra are compared in Figure 12 with the spectrum resulting from the direct analyses.

### 3.2 Effect of Wind-Tunnel Airflow Unsteadiness

Early tests were made in the RAE 4 ft x 3 ft and No.2 11½ ft wind-tunnels on cylindrical bodies having either a cavity to represent a bomb-bay or an external air-brake. Both tunnels have screens in the maximum sections and hot-wire measurements have shown low turbulence levels\*. Datum checks of the pressure fluctuations on the surfaces of the plain bodies gave values of  $p/q$  of about 0.005, which were small compared with the maxima of about 0.15 measured in the cavity or behind the air-brake. The spectra for these datum tests were consistent with the pressure-fluctuations being mainly due to the turbulent boundary-layers on the bodies.

However, preliminary measurements of pressure-fluctuations on a thin wing in the No.1 11½ ft wind-tunnel, which is of earlier design, and has no screens, with a contraction ratio of 4.75 to 1, showed spectra with a sharp rise in amplitude at low frequencies, even with the wing at zero incidence. This was attributed to the unsteadiness of the airflow in the tunnel working-section and, in order to investigate it, a special model was constructed (Fig.13), consisting of a rectangular wing of 1 ft span and 6 in. chord, with a single transducer at its centre measuring the pressure difference between the upper and lower surfaces at this point. The transducer was basically of the design shown in Figure 1a, but with a different front casing, and also with a thinner diaphragm to increase the sensitivity; this enabled values of  $p/q$  as low as 0.0003 at 150 ft/sec to be measured and analysed.

The results of these tests are shown in Figure 14. The No.1 11½ ft wind-tunnel in its original form gave results with a very large increase of amplitude towards the low-frequency end of the spectrum. Fitting an available honeycomb at the beginning of the working-section reduced the fluctuations considerably as shown; though, as compared with the results from the No.2 11½ ft wind-tunnel, they were still large. While reducing the fluctuations to a level which might have been acceptable for some types of test, the honeycomb was not a satisfactory solution, as its positioning at the beginning of the working-section lead to a threefold increase in the power required to drive the tunnel, with a consequent rapid rise in the temperature of the air at the normal operating speed of the tunnel.

The low-frequency nature of the fluctuations suggested an intermittent breakaway in the tunnel return circuit, and one possible source was located by inspection. Vortex-generators were installed ahead of this section, but, though this led to a considerable reduction in the level of the fluctuations, as shown in Figure 14, the

\* At the usual test speed of 150 ft/sec the longitudinal and lateral components of the turbulence in the 4 ft x 3 ft wind-tunnel are about 0.01% and 0.02% respectively, while the longitudinal component in the No.2 11½ ft wind-tunnel is about 0.04%.

level of  $\sqrt{nF(n)}$  at low frequencies is still high. This indicates that the tunnel is still unsuitable for pressure-fluctuation measurements on wings, or for any other tests where incidence fluctuations can affect the results.

Provided that the pressure-fluctuations are large compared with those produced by the boundary-layer alone, this type of test can be regarded as a method of obtaining incidence-fluctuation values at low frequencies, where the equivalent wave-length is large compared with the wing chord: 10 cycles/sec for instance corresponds to 30 wing chords. The pressure-fluctuations can be converted to incidence-fluctuations by dividing by  $ds/d\alpha^*$ , where  $s$  is the difference between the static pressure coefficients across the transducer, and  $\alpha$  is the wing incidence. As a check on the nature of the pressure fluctuations on the wing in the No.2 11½ ft wind-tunnel, a 26 s.w.g. transition wire was added at 10% of the wing chord. This led to an approximate doubling of  $nF(n)$  throughout the frequency range, suggesting that the measured pressure fluctuations on the plain wing were mainly due to the wing boundary-layer, and that only negligible fluctuations due to tunnel unsteadiness were present.

No tests were made in the 4 ft x 3 ft wind-tunnel, since measurements with hot-wire anemometers had shown an even smoother air flow there than in the No.2 11½ ft wind-tunnel. All subsequent pressure-fluctuation tests have been confined to these two tunnels.

### 3.3 Additional Measurements

In previous sections the methods used to produce the total intensity and spectrum density of the fluctuating pressures have been described. Two further types of measurement are now considered: (a) the use of pipes when only the amplitude of  $\sqrt{nF(n)}$  at low frequencies is required; and (b) the measurement of the correlation between pressure-fluctuations at two points.

#### 3.3.1. The use of pipes in pressure-fluctuation measurements

As will be discussed in Section 4.3, it has been found more appropriate, in some tests, to use the value of  $\sqrt{nF(n)}$  at a particular low frequency as a parameter, rather than  $p/q$ . For such tests the possibility arises of using a fairly long length of pipe between the measuring point and the transducer, so enabling the measuring point to be traversed over a large area of wing or body surface, without the necessity of moving and reinstalling the transducer. A suitable type of piping was found to be cupro-nickel hypodermic tube of 0.40 in. (nominal 1 mm) outside diameter and 0.028 in. inside diameter. This is sufficiently soft to be bent into various curves for traversing the measuring point a considerable number of times without fracture or reduction of the bore.

A wide-range spectrum similar to that shown in Figure 12 was recorded with no pipe and with a series of pipe lengths between the measuring point and the transducer. The results are shown in Figure 15 as the variation with frequency of the attenuation in amplitude produced by the introduction of the various lengths of pipe. These results only apply in detail to the design of transducer shown in Figure 1a, since the size of the chamber in the front casing influences the response of the system. The attenuation curve shown for the 60-in. pipe was obtained at both 80 and 140 ft/sec.

\*  $ds/d\alpha$  was 0.040 degree for the wing used.

the total r.m.s. intensity of the pressure fluctuation being about 0.05q. This independence of response with the amplitude of the pressure-fluctuation can, however, only be expected to apply at low windspeeds, where the amplitudes of the fluctuations are sufficiently small for the intermittent flow in the pipe not to be affected by the compressibility of the air.

It is suggested that a reasonable upper-frequency limit for the longer pipes is that at which the attenuation is 0.5, i.e. at 18, 50, 120 and 200 cycles/sec for the 60, 30, 15 and 7.5 in. pipes respectively. For shorter lengths of pipe the more rapid variation of attenuation with frequency, above the resonant frequency, would require very accurate frequency measurement and allowance for the variation of the speed of sound with temperature, if accuracy was to be maintained. In particular, for lengths of pipe shorter than about 2 in., a sharp resonance peak with further peaks at the higher harmonics would be expected, and the usual upper-frequency limit of half the resonant frequency would apply. For the system tested therefore, it would seem that about 8 in. is a reasonable minimum pipe-length, with no further useful gain in the upper-frequency limit unless the pipe can be reduced to less than about 1 in. in length.

### 3.3.2 Correlation between pressure-fluctuations at two points

Some measurements, described later in Section 4.3.1, have been made to determine the correlation coefficient  $R_{ab}$  defined in the usual way as

$$R_{ab} = \frac{\overline{AB}}{\sqrt{\overline{A^2} \overline{B^2}}}$$

where A and B are the instantaneous values of two fluctuating quantities, measured at points a and b,  $\overline{AB}$  is the mean of the instantaneous product AB, and  $\sqrt{\overline{A^2}}$  and  $\sqrt{\overline{B^2}}$  are the root-mean-square values of A and B. The usual method of obtaining  $\overline{AB}$  is to measure the mean square values,  $\overline{(A+B)^2}$  and  $\overline{(A-B)^2}$ , of the instantaneous quantities (A+B) and (A-B), obtained by electrically adding and subtracting voltages proportional to A and B, whence  $\overline{AB}$  can be calculated from

$$\overline{(A+B)^2} - \overline{(A-B)^2} = 4 \overline{AB}$$

There are considerable difficulties in using this method with the existing equipment. While the pre-amplifier (Fig.2) has two channels, and two transducers may readily be used to produce two fluctuating-voltage outputs, the circuits of both the pre-amplifier and the following amplifier have one side earthed, in order to reduce pick-up at the mains supply frequency and its higher harmonics. This earthing is basic to the construction of the apparatus and there appeared to be no simple methods of interconnection to obtain both (A+B) and (A-B). Eliminating the earthing from a second set of pre-amplifier equipment, while retaining rectified 50 cycles/sec voltage supplies, led to very large voltage pick-up at 50 cycles/sec and higher harmonics. Replacing this voltage supply by dry batteries reduced the pick-up to a tolerable level, but the very short life of readily available batteries used in this way made the technique very cumbersome. In addition, some complication was introduced by the need for complete insulation of the transducer and its connecting leads from the model, which in this case was of metal. The simpler method was therefore adopted of measuring  $\sqrt{\overline{A^2}}$ ,  $\sqrt{\overline{B^2}}$  and  $\sqrt{\overline{(A+B)^2}}$  and obtaining  $\overline{AB}$  from the relation

$$\overline{(A + B)^2} - \overline{A^2} - \overline{B^2} = 2 \overline{AB}$$

It should be noted that in the complete formula for  $R_{ab}$ ,

$$R_{ab} = \frac{\overline{(A + B)^2} - \overline{A^2} - \overline{B^2}}{2\sqrt{\overline{A^2} \overline{B^2}}} \quad (2)$$

the substitution of  $kA$  for  $A$  does not affect the result. It is not therefore necessary for the two voltages, or other quantities summed, to be in the same ratio to the original quantities  $A$  and  $B$ . In particular, if the two transducers are connected in parallel so as to sum the capacity fluctuations, the r.m.s. value of the resulting voltage output from the pre-amplifier can be used in Equation (2), together with the corresponding values obtained from the transducers connected singly, to give  $R_{ab}$ , irrespective of the transducer sensitivities. It is necessary, however, for the three measurements to be taken in sufficiently rapid succession for the transducer sensitivities to remain substantially unchanged.

To provide the interconnections of the transducers, three multi-way relays, contained in a screening box, are used. The circuit includes fixed and adjustable condensers, so that the total capacity of the system can be made the same, whether readings from either transducer or the combination are being made. This constancy of the total capacity is advisable as the pre-amplifier sensitivity (in volts/Pf) varies to some extent with the total capacity, and it is essential, either that this sensitivity should be the same for all three measurements, or that allowance should be made for the variation. The second alternative would require additional calibration, and introduce undesirable complication into the computation of the results. The circuits made by the relays are shown in Figure 16; when making measurements from a single transducer, the other is short-circuited.

To maintain accuracy, the three measurements required to obtain  $R_{ab}$  are always made consecutively, keeping conditions constant meanwhile; this applies to measurements at each particular frequency in a spectrum analysis, as well as to total intensity measurements. Since the estimation of  $R_{ab}$  is unaffected by any sensitivity factors of the system, it is best calculated as directly as possible; from the three microvoltage readings for total intensity measurements, and from the logarithmic potentiometer and output-galvanometer readings only in the case of spectrum measurements.  $R_{ab}$  is determined with acceptable accuracy by the above methods, provided that r.m.s. values of  $A$  and  $B$  do not differ appreciably in magnitude, but the accuracy falls off fairly rapidly as the ratio of  $\sqrt{\overline{A^2}}$  to  $\sqrt{\overline{B^2}}$  increases. As an illustration, the error in  $R_{ab}$  due to a 1% high reading of  $\sqrt{\overline{(A + B)^2}}$  and a 1% low reading of  $\sqrt{\overline{A^2}}$  is given below for a range of values of  $\sqrt{\overline{A^2}}/\sqrt{\overline{B^2}}$ :

Error in  $R_{ab}$

$\sqrt{\overline{A^2}}/\sqrt{\overline{B^2}}$	1	2	3	4	5
$R_{ab} = 1$	0.06	0.08	0.10	0.12	0.14
$R_{ab} = 0$	0.03	0.05	0.07	0.09	0.11
$R_{ab} = -1$	0.00	0.04	0.06	0.08	0.10

Best Available Copy

An accuracy of  $\pm 1\%$  in the r.m.s. amplitude of the total signals seems possible, and also in spectrum measurements at frequencies above 50 cycles/sec; at lower frequencies, however, the scatter increases and errors of up to  $\pm 5\%$  in amplitude may occur at 3 cycles/sec, with proportionately larger errors in  $R_{ab}$ . Since the estimate of  $R_{ab}$  is unaffected by any scaling ratios in the system, it is sometimes practicable to reduce the ratio of  $\sqrt{A^2}$  to  $\sqrt{B^2}$  by using the combination of a transducer of low sensitivity in a region of large pressure-fluctuations, with a transducer of high sensitivity in a region of small fluctuations.

### 3.3.3 Estimation of normal-force fluctuations from pressure-fluctuation measurements

If sufficient correlation measurements are made it is possible to calculate the normal-force fluctuation on a section or over an area. Such a series of measurements, discussed later in Section 4.3.1, has been made between a number of pairs of points along a wing chord-line, and the method of estimating the normal-force fluctuation for this case is discussed in this Section. Taking the origin at the wing leading-edge, and letting  $c$  be the wing chord, consider two points  $x$  and  $x'$  at which the instantaneous pressures are  $P_x$  and  $P_{x'}$ . The square of the instantaneous load is then

$$\Delta C_N^2 = \frac{1}{c^2} \int_0^c \int_0^c \frac{P_x P_{x'}}{q} dx dx'$$

with a mean square

$$\overline{\Delta C_N^2} = \frac{1}{c^2} \int_0^c \int_0^c \frac{\overline{P_x P_{x'}}}{q^2} dx dx' \quad (3)$$

It is necessary, therefore, to know the covariance between all pairs of points on the chord-line before  $\overline{\Delta C_N^2}$  can be estimated; suppose the number of measuring points to be  $t$ , then  $(t/2)(t-1)$  sets of measurements would be required. However, expressing the data in terms of correlation coefficients can sometimes lead to a reduction in the number of measurements required. The correlation coefficient, defined as before, is

$$R_{xx'} = \frac{\overline{P_x P_{x'}}}{\sqrt{\overline{P_x^2} \overline{P_{x'}^2}}} = \frac{\overline{P_x P_{x'}}}{p_x p_{x'}}$$

where  $p_x$  and  $p_{x'}$  are defined in the usual way as the r.m.s. intensities of the pressure-fluctuations at  $x$  and  $x'$ . Equation (3) can then be rewritten as

$$\overline{\Delta C_N^2} = \frac{1}{c^2} \int_0^c \int_0^c R_{xx'} \frac{p_x p_{x'}}{q} dx dx' \quad (4)$$

If now the curves of  $R_{xx'}$ , with  $x$  constant, show sufficient similarity, it is possible, in principle, to deduce the complete function of  $R_{xx'}$  from measurements for

only a few values of  $x$ . If for example it could be shown that  $R_{xr}$  (where  $r = |x' - x|$ ) was dependent only on  $r$  and independent of  $x$ ,  $(t - 1)$  measurements at one value of  $x$  would be sufficient, in principle, though in practice comparative measurements at two, or preferably three, values of  $x$  would be required to establish the validity or otherwise of such a relationship. If  $R_r$  is the correlation coefficient, dependent only on  $r$ , Equation (4) can be written as

$$\overline{\Delta C_N^2} = \frac{1}{c^2} \int_0^C \frac{p_x}{q} dx \int_{-x}^{C-x} \frac{p_x + r}{q} R_r dr \quad (5)$$

It should be noted that, even if the function  $R_{xr}$  does show some dependence upon  $x$ , the use of an approximate mean variation  $R_r$  in Equation (5), rather than the full set of data in Equation (4), would not be expected to introduce large errors into the estimate of  $\overline{\Delta C_N^2}$ , and this approach would seem to provide a useful method of reducing the number of measurements to be made.

### 3.4 Further Developments

#### 3.4.1 Extension of the present testing techniques to transonic and supersonic speeds

With the introduction of the tape-recorder into the system, the reduction of tunnel-running time at each test condition from 30 minutes for a direct spectrum analysis to 5 minutes using the recorder, makes testing in high-speed and high-power wind tunnels practicable. It is proposed, in the first place, to examine the suitability of two such wind tunnels, the 3 ft x 3 ft transonic and supersonic wind tunnel and the 8 ft x 6 ft transonic wind tunnel, for pressure-fluctuation tests by making measurements on a simple model at zero incidence, as was done for the low-speed tunnels (see Section 3.2). The model in this case is to be a delta-wing having a  $70^\circ$  leading-edge sweep, 9 in. long, with a single transducer of the type shown in Figure 1b, installed on the centre-line at 33% of the root-chord from the nose. With such a wing there should be no shocks across the model ahead of or near the transducer, within the Mach number range of the two wind tunnels, a maximum of 1.2 for the 8 ft x 6 ft tunnel and 2.0 for the 3 ft x 3 ft tunnel. The measurements should therefore give a good indication of the pressure-fluctuation datum in the two wind tunnels and its variation with Mach number.

If the wind tunnels should be suitable, further research will be required into temperature effects on transducer sensitivity, and into the constancy of the transducer calibration with continued use. For some tests also, the upper limit of 2000 cycles/sec imposed by the present transducers will be too low, and modified designs will be required; one possible design, to replace the low-speed type shown in Figure 1a, is shown in Figure 17. The diaphragm is tensioned and flattened by screwing down the front casing over the outer casing, giving a 0.40 in. diameter flush surface. The inner casing can be screwed in and out on a fine thread (100 threads per inch) to adjust the condenser gap and hence the transducer sensitivity. The natural frequency of the diaphragm, deduced from measurements of its deflections due to steady pressures, is about 100,000 cycles/sec. Effects of temperature and constancy of calibration have yet to be investigated.

### 3.4.2 Automatic analyser

When analysing recordings at present, the operator reads a mean value off the analyser output-galvanometer (Fig.2), as for direct analysis. To estimate a reasonably accurate mean reading, it is found necessary to observe the galvanometer for about 4 transits of the tape-loop at low frequencies, and 2 at high frequencies, each transit taking 15 seconds. The strain of the constant averaging prevents any one operator from performing this job for long periods. An automatic analyser, as well as reducing the strain on the operator, offers the possibility of reducing the analysis time to about a third, since only one transit of the tape-loop should be required for each reading.

Detailed plans for an automatic analyser have not yet been worked out, but it is envisaged as consisting of the following modifications to the existing system (Fig.2). The output could consist of some form of integrator with automatic read-out, operating off a squaring and rectifying circuit, preferably not a thermo-junction, as the thermal lag would introduce difficulties in this application. The analyser could, for most tests, be replaced by a set of 25 fixed filters, though some form of continuous tuning would sometimes be required. With an output proportional to the square of the signal, some form of calibrated gain control would still be required, though with less steps than the present logarithmic potentiometer; in principle this gain control could be set by the operator. Switching from one filter to the next, and the read-out, could be triggered by a photo-cell working off the tape-splice. This change-over should not take more than about 1 sec out of the 15 sec of the tape-transit time, so that only about 5 ft of tape, which should include the splice, would be lost.

## 4. SOME PARTICULAR APPLICATIONS OF PRESSURE-FLUCTUATION MEASUREMENTS

### 4.1 Bomb-Bay Buffeting

An investigation was made into the airflow in bomb-bays of various shapes, the drag to which they give rise, and the effectiveness of various flow-control devices; the model used was, basically, a cylindrical body, with a systematic series of cavities cut into it. Pressure fluctuations were measured, in some cases, using an earlier design of the transducer shown in Figure 1a, and it was found that the highest intensities were mainly concentrated on the rear bulkhead of the bomb-bay and on the body immediately behind it, with a fairly rapid reduction forward along the bomb-bay roof and rearward along the body. Two transducers only therefore were used, one in the rear bulkhead and one in the body just behind the bomb-bay, as shown in Figure 18. In general the total intensity of the pressure fluctuations and the form of the spectra were different for the two transducer positions; rounding off the lower edge of the rear bulkhead, in particular, reduced the intensity of the pressure fluctuations on the body very considerably, while having little effect on those on the remaining bulkhead (see Figure 18).

While there were minor differences in the total intensities and spectra between bomb-bays of various height-to-length ratios, the only modification which appreciably reduced the pressure fluctuations was the elimination of the vertical rear bulkhead, as shown in Figure 19; complete retraction of the bomb-doors still further increased the effectiveness of the sloping rear bulkhead.

#### 4.2 Air-Brake Buffeting

A series of tests<sup>2</sup> was made to examine the static and fluctuating pressure distributions on a cylindrical body with a square flat plate air-brake. A transducer of the type shown in Figure 1a was used and the model and transducer installation are shown in Figure 20. The portion of the body containing the transducer could be rotated, and also interchanged with other portions of the body for longitudinal positioning; the brake could also be moved longitudinally on the body. By this means it was possible to position the transducer orifice anywhere on the body in the region from  $2l$  ahead of the brake hinge to  $6l$  behind the brake hinge ( $l = \text{brake-chord}$ ). The rear orifice of the transducer was connected, through a small-bore metal pipe, to a long length of small-bore tubing outside the wind-tunnel to provide a steady datum.

Both static pressure and the total intensity of the fluctuating pressure were measured with the transducer, and contours of both were drawn, as shown in Figure 21. Spectra were measured at a few positions only, as shown in Figure 22. To obtain some impression of the variation of the aerodynamic excitation on the body with brake-angle, the total intensity of the pressure fluctuations was integrated over the area of the body affected and the result expressed non-dimensionally using the air-brake area; the results are shown in Figure 23. This integral has no quantitative value as no allowance has been made for the effects of correlation or of body curvature; but the variation with brake-angle is considered significant, and it was deduced that restriction of the brake-angle to  $50^\circ$  and mounting the brakes at the rear of the fuselage, to reduce the area of fuselage affected, should be effective in reducing the aerodynamic excitation associated with the brake.

This aerodynamic excitation appeared to be due to the unsteady nature of the flow behind the brake at high incidences. With the configuration tested (Fig. 20), the measured shedding frequency was nearly the same as for an isolated plate (Fig. 24); it was therefore considered that further attempts to reduce the unsteadiness of the wake, by means of modifications to the brake, could be compared more easily and quickly with the aid of hot-wire measurements<sup>3-5</sup> of velocity fluctuations in the wakes of isolated plates. The conclusions reached have not yet been confirmed by measurements of pressure fluctuations.

#### 4.3 Pressure Fluctuations of Thin Wings

The type of pressure transducer shown in Figure 1b was specially designed for use in metal wings. It is fitted into the wing with its flange-face flush with the upper surface, any excess of the body protruding through the lower surface being machined off; a minimum wing thickness of about 0.30 in. is required. A groove about 0.10 in. deep and 0.10 in. wide is machined into the lower surface of the wing, from the hole in the transducer body containing the rear plate connection to a suitable point on the wing, usually in a body or nacelle, at which the normal 0.25 in. diameter coaxial cable can be attached; a single insulated wire is fixed into the groove with Araldite cement and the surface smoothed off. There are three reasons for letting the transducer into the upper rather than the lower surface of the wing: firstly, the upper surface suction, whose magnitude is difficult to predict, then tends to increase the condenser gap, so that a short-circuit, which could otherwise only be avoided, with certainty, by using a large pre-set gap with a correspondingly low sensitivity, cannot occur; secondly, the variation with incidence of the differential static pressure

then leads to maximum sensitivity of the transducer at low incidence, where the pressure fluctuations to be measured are least; and thirdly, since the pipe through the transducer body is then connected to the lower surface of the wing, where the pressure fluctuations are normally small, any resonance due to its length will also be small.

A number of tests have been made on wings with approximately two-dimensional leading-edge flow separation. This is the simplest case, and investigations are now in progress to examine ways of measuring and presenting data for the more complicated types of flow separation associated with low-aspect-ratio highly-swept wings.

It is found that wing buffeting caused by shock-induced separations in high-speed flight consists almost entirely of the excitation of the fundamental flexural mode of the wing, and it is expected that this will also apply to low-speed buffeting at high incidences. Low-speed wind-tunnel tests are normally concerned with the possible occurrence of wing buffet during an airfield approach, and with the relative effectiveness of acceptable modifications to the wing configuration. It seems reasonable, in this case, to use as a criterion the aerodynamic excitation at a particular value of  $n$ , say  $n_A$ , defined by  $n_A = f_w(\bar{c}/V_A)$ , where  $f_w$  is the wing fundamental flexural frequency,  $\bar{c}$  is the wing mean chord and  $V_A$  is the approach speed. On projects so far examined  $n_A$  has been about 0.2; but with the relatively 'flat' spectra associated with flow separation on wings, the value of  $n$  chosen is not critical, and the conclusions reached would have been little affected if any other value of  $n$  between 0.1 and 0.4 had been used. A value of  $n$  of 0.2 corresponds to about 20 cycles/sec for a typical model wing and wind-tunnel speed; and for measurements at such a frequency it is possible to use a considerable length of pipe between the measuring point and the transducer, as described in Section 3.3.1, and to traverse the measuring point over the wing surface.

#### 4.3.1 Low-aspect-ratio unswept wing

The model shown in Figure 25 was constructed for measurements of the fluctuating-pressure field associated with flow separation from the leading edge of a low-aspect-ratio unswept wing; but since the addition of a nacelle, as shown in the figure, gave a region of approximately two-dimensional flow between the nacelle and the body, attention was confined, in the first instance, to this simpler flow regime. A pair of transducers, of the type illustrated in Figure 1b, can be set into any two of the twenty-two positions indicated in Figure 25, and soldered connections can be made to wires permanently installed in the lower surface of the wing; the remaining sockets may then be plugged with dummy transducers. Measuring the correlation between the pressure fluctuations at different points on the wing was the main purpose of the experimental programme.

The results discussed below all refer to the wing with the nacelle on, and with only the thirteen transducer positions between the nacelle and body in use. The total intensities of the pressure fluctuations measured in the chordwise traverse are shown for the range of incidence in Figure 26; and the corresponding correlation coefficients  $R_{xx}$  (see Section 3.3.3), for  $x = 0.1c$  and  $x = 0.8c$ , are shown in Figure 27. The measured values of  $R_{xx}$  show a fair amount of scatter, and a tendency to the constant value of 0.1, rather than zero, for large separations of the transducers. In order to reveal the dominant effects of incidence upon the correlation function, the measured coefficients were cross-plotted in the form  $R_{xx}$  against  $\alpha$  (where  $r = |x' - x|$ ); two sets of measured values, corresponding to the two values of  $x$ ,

were therefore plotted for each value of  $r$  and it was at once apparent that both sets could be represented by a single smooth curve, with an error not exceeding the experimental uncertainty; it follows that  $R_{xr}$  was effectively unaltered by changing  $x$  from 0.1c to 0.8c. The function of  $r$ ,  $R_r$  say, obtained in this way is plotted in Figure 28.

In view of these results it is natural to assume that  $R_r$  closely represents the correlation function for all values of  $x$ ; this implies that  $R_{xr}$  is not significantly dependent on  $x$ . In this case a fairly accurate estimate of the magnitude of the fluctuating normal force, on the section in question, may be made according to Equation (5), Section 3.3.3. Results so obtained are plotted in Figure 29; the same figure shows, for comparison, the total intensity of the normal-force fluctuation that results if the correlation coefficient is assumed to be unity everywhere, together with the total intensity of the pressure fluctuation measured at 0.8c. This assumption of unit correlation leads to the maximum force fluctuation compatible with the measured intensities of the fluctuating pressures; the computed fluctuating normal force on the section (expressed as a root-mean-square total intensity) ranges from 0.25 of the corresponding maximum at  $0^\circ$  incidence, to 0.50 at  $8^\circ$ , and 0.77 at  $16^\circ$ , thus indicating a marked effect of the increasing correlation with incidence. It is also interesting to notice that the total intensity of the pressure fluctuations at 0.8c shows some resemblance, in the form of its variation with incidence, to the normal-force fluctuations.

The spanwise correlations, with respect to the middle station of the five shown in Figure 25 at 0.8c, were also measured. In this case, however, insufficient data were obtained to justify a similar analysis to that applied to the chordwise traverse, but it is interesting to note that the results are adequately represented by the function  $R_p$ , determined from the chordwise traverse, at both high and low incidence; in the range  $4^\circ$  to  $8^\circ$  of incidence the spanwise correlations somewhat exceeded the corresponding chordwise values.

It is also possible, in principle, to derive the spectrum of the fluctuating normal force on a wing from the measured spectra of the two-point products of the pressure fluctuations at a sufficient number of points; the spectrum function for the force fluctuation is then obtained by successive application of either the complete form of computation described in Section 3.3.3, or, if the data are suitable, the forgoing shorter form, to a number of narrow bands of frequency. Some measurements have been made at one incidence ( $4^\circ$ ) of the variation with frequency of the chordwise correlation, and these results are shown in Figure 30 in the form of correlation coefficients; they exhibit a noticeable wave-form, and further measurements with respect to other reference points would be required to determine whether the correlation coefficient depends primarily on the separation of the two points in question at all frequencies, as is apparently true for the total intensity measurements.

In view of this wave-form, a single spectrum of the correlation between two points is of little value; it is clearly necessary to determine the manner in which the spectrum varies with the distance between the two points. The complete definition of the correlation function would also appear to require a closer spacing between successive stations than would be necessary if there were no wave-form. The results given in Figure 30, obtained in about 3 days of tunnel-running time, are not sufficient to give even an indication of the spectral density of the fluctuating normal force on the section, the definition of which must therefore be regarded as a lengthy process. As an illustration of the difficulties involved in deducing the spectra of

normal-force fluctuations from pressure-fluctuation measurements, consider, for example, the more general case of the wing shown in Figure 25, with the nacelle removed and with a full set of fourteen chordwise rows of nine transducer stations - 126 transducer positions in all. If no simplifying assumptions were permissible, the spectra of the correlations would be required between all pairs of these positions; using the present technique, the time taken, merely for the measurements - at the rate of three sets of spectra a day for fifty five-day weeks a year - would amount to about 10 years for each wing-incidence. Though there is little doubt that this figure would be considerably reduced in practice - permissible simplifications would be likely to become apparent as the results were collected, there is also little doubt that the total intensity and spectrum of a fluctuating load would be much better measured directly. On the other hand, a limited application of the procedure outlined here might help to throw light upon the causes of the load fluctuation; it is hoped, therefore, that the data already collected will be supplemented sufficiently to allow the computation of the spectrum of the fluctuation of the normal force on the wing section, for one or two angles of incidence, in order to investigate the significance of the periodic nature of the correlation function measured at different frequencies.

#### 4.3.2 Unswept wing panel

The effects of various leading-edge devices, and of plain and split flaps at the trailing-edge, have been examined, using the wing shown in Figure 31. Only two transducers were fitted, at 0.50c and 0.85c as shown, and the results for the plain wing are shown in Figure 32; these measurements are fairly similar for the two chordwise positions. The frequency at which buffeting might be expected to occur, at the approach speed of the full-scale aircraft, corresponds to a value of the frequency parameter,  $n$ , of about 0.2. At such a low value of  $n$  the correlation might be expected to be fairly high; this is supported by the solitary series of measurements plotted in Figure 30.

When the intensity of the pressure fluctuations shows a sharp rise with increasing incidence, as it does in this case (Fig.32), it is natural to suppose that the onset of buffeting - if it occurs - is likely to be associated in some way with this sharp rise. It is therefore suggested that the incidence, or more correctly the corresponding aircraft  $C_L$ , at which the value of  $\sqrt{nF(n)}$ , for  $n = 0.2$ , and  $x$  as large as practicable (in this case 0.85c), has risen appreciably - to 0.01 say - is likely to be a suitable criterion with which to establish the relative merits of the various leading-edge devices; according to this standard, a plain nose-flap of 10% chord was found to be the most effective of the devices tested.

Wherever possible, an attempt has been made to relate the fluctuating pressures to the mean flow field, which, for this particular wing panel, is dominated by a leading-edge separation which appears to give rise to an approximately two-dimensional flow of the 'bubble' type, with reattachment onto the upper surface of the wing up to about 11° of incidence (see Figure 31). It is interesting to note that while the low-frequency fluctuations reach their maximum intensity when the reattachment line lies along the trailing-edge of the wing, the sharp rise begins much sooner - at the incidence corresponding to about 0.3c, for the forward transducer, and 0.5c for the rearward one. Divergence of the trailing-edge static pressure, which is often used as a criterion for the onset of the type of wing-buffet associated with shock-induced separation of the flow over the rearward part of a wing, occurs when reattachment reaches 0.8c, so corresponding to nearly maximum intensity of the low-frequency

normal-force fluctuations from pressure-fluctuation measurements, consider, for example, the more general case of the wing shown in Figure 25, with the nacelle removed and with a full set of fourteen chordwise rows of nine transducer stations - 126 transducer positions in all. If no simplifying assumptions were permissible, the spectra of the correlations would be required between all pairs of these positions; using the present technique, the time taken, merely for the measurements - at the rate of three sets of spectra a day for fifty five-day weeks a year - would amount to about 10 years for each wing-incidence. Though there is little doubt that this figure would be considerably reduced in practice - permissible simplifications would be likely to become apparent as the results were collected, there is also little doubt that the total intensity and spectrum of a fluctuating load would be much better measured directly. On the other hand, a limited application of the procedure outlined here might help to throw light upon the causes of the load fluctuation; it is hoped, therefore, that the data already collected will be supplemented sufficiently to allow the computation of the spectrum of the fluctuation of the normal force on the wing section, for one or two angles of incidence, in order to investigate the significance of the periodic nature of the correlation function measured at different frequencies.

#### 4.3.2 Unswept wing panel

The effects of various leading-edge devices, and of plain and split flaps at the trailing-edge, have been examined, using the wing shown in Figure 31. Only two transducers were fitted, at 0.50c and 0.85c as shown, and the results for the plain wing are shown in Figure 32; these measurements are fairly similar for the two chordwise positions. The frequency at which buffeting might be expected to occur, at the approach speed of the full-scale aircraft, corresponds to a value of the frequency parameter,  $n$ , of about 0.2. At such a low value of  $n$  the correlation might be expected to be fairly high; this is supported by the solitary series of measurements plotted in Figure 30.

When the intensity of the pressure fluctuations shows a sharp rise with increasing incidence, as it does in this case (Fig.32), it is natural to suppose that the onset of buffeting - if it occurs - is likely to be associated in some way with this sharp rise. It is therefore suggested that the incidence, or more correctly the corresponding aircraft  $C_L$ , at which the value of  $\sqrt{nF(n)}$ , for  $n = 0.2$ , and  $x$  as large as practicable (in this case 0.85c), has risen appreciably - to 0.01 say - is likely to be a suitable criterion with which to establish the relative merits of the various leading-edge devices; according to this standard, a plain nose-flap of 10% chord was found to be the most effective of the devices tested.

Wherever possible, an attempt has been made to relate the fluctuating pressures to the mean flow field, which, for this particular wing panel, is dominated by a leading-edge separation which appears to give rise to an approximately two-dimensional flow of the 'bubble' type, with reattachment onto the upper surface of the wing up to about  $11^\circ$  of incidence (see Figure 31). It is interesting to note that while the low-frequency fluctuations reach their maximum intensity when the reattachment line lies along the trailing-edge of the wing, the sharp rise begins much sooner - at the incidence corresponding to about 0.3c, for the forward transducer, and 0.5c for the rearward one. Divergence of the trailing-edge static pressure, which is often used as a criterion for the onset of the type of wing-buffet associated with shock-induced separation of the flow over the rearward part of a wing, occurs when reattachment reaches 0.8c, so corresponding to nearly maximum intensity of the low-frequency

fluctuations, rather than their initial rise; it would seem, therefore, that this criterion is not directly applicable to buffeting associated with leading-edge flow separation at low speeds.

It seems likely that the marked increase in intensity of the low-frequency pressure fluctuations as the incidence increases from  $8^\circ$  to  $10^\circ$ , (see Figure 32b) is a result of the appearance of significant fluctuations in circulation, associated with intermittent changes in the flow structure; although the near position of reattachment line is still well forward of the trailing-edge of the wing at these incidences, its instantaneous position may approach, and perhaps reach, the trailing edge intermittently. Since tapped holes are provided in both sides of the type of the transducer shown in Figure 1b, either surface can be connected to a steady datum pressure by means of a metal pipe leading to a reservoir outside the wind-tunnel; the total intensities of the pressure fluctuations on the upper and lower surface, measured in this way at 0.85c, are compared in Figure 33a with the fluctuating differential pressures; it may be noticed that the rise in total intensity on the lower surface with increasing incidence is similar in form to that shown by the low-frequency fluctuations of the differential pressure in Figure 32c. The spectra of the lower-surface and the differential pressure fluctuations at 0.85c and  $14^\circ$  incidence are compared in Figure 33b; they show a marked similarity up to  $n = 0.5$ , the lower surface intensity being about one fifth of the corresponding differential values in this range. Above  $n = 0.5$  the lower surface intensity falls off rapidly until, above  $n = 2$ , it corresponds to a normal turbulent boundary-layer level.

These results all support the view that the large low-frequency content of the fluctuating pressure field, at incidences above about  $8^\circ$ , is associated with fluctuations in circulation, and that the chordwise correlation in this low-frequency range is likely to be high. It seems reasonable therefore to use, as a criterion for comparing the effectiveness of modifications, the first rise with incidence of the value of  $\sqrt{nF(n)}$  at a particular low frequency, and at a point sufficiently far back along the wing chord for most of the wing surface to be affected (see chordwise distribution of total intensity on a similar wing - Figure 26).

#### 4.3.3 Wing panel with $30^\circ$ leading-edge sweep

Pressure fluctuation measurements have been made on the wing panel shown in Figure 34. Surface flow patterns indicated leading-edge flow separation, with reattachment on to the upper surface of the wing, very similar to that observed on the unswept panel just described. Three transducers were installed as far back as possible (at 80% of the wing chord), as shown. The variation with incidence of the position of the reattachment line, at the three chordwise sections containing the transducers, is shown in Figure 34, and results of the pressure fluctuation measurements in Figure 35. It was expected that the critical full scale frequency range would again correspond to a value of  $n$  of about 0.2, and it is suggested that the incidence at which the value of  $\sqrt{nF(n)}$ , at  $n = 0.2$ , has risen appreciably for any of the three transducers is a reasonable criterion for comparing the effectiveness of modifications, as for the unswept wing panel. However, because of the more shallow initial rise in the low-frequency intensity, compared with that on the unswept wing panel, the incidence at which  $\sqrt{nF(n)}$ , at  $n = 0.2$ , first reaches 0.02 rather than 0.01 would probably yield a more reliable comparison in this case.

#### 4.3.4 Low-aspect-ratio highly swept wings

On wings of this class, surface flow patterns suggest that leading-edge flow separation gives rise to the vortex, rather than the bubble type of flow; the markedly three-dimensional nature of the mean flow then makes the choice of suitable transducer positions, and the interpretation of the results from them, much more difficult. However, some measurements have been made on the wing shown in Figure 36 using, in the first instance, four transducers at the positions indicated, but since the results obtained showed little relation to each other at any one incidence, a traverse of the upper surface of the wing was then made, using a single transducer fixed in the body together with a 16 in. length of pipe. The pipe ended in a piece of metal plate, 0.040 in. thick and 0.25 in. square, which was faired into the wing surface with plasticene, the pipe inlet being through a flush hole drilled in the centre of the plate; tests showed that variations in fairing shape were unimportant. The traverse results, for  $n = 0.2$ , showed excellent agreement with the corresponding results obtained with the four transducers let into the wing, although the former relate, strictly, only to the pressure fluctuations on the upper surface of the wing, while the latter relate to the fluctuations in differential pressure.

From the data presented in Figure 36, and corresponding data at other incidences, it appears that the dominant pressure fluctuations are confined to the part of the wing directly below the vortex. Very much more data would be required before an estimate of the fluctuating normal force could be made; though it is possible, of course, to estimate the maximum intensity of the normal force fluctuation, at  $n = 0.2$ , consistent with the local pressure fluctuation intensities, by assuming full correlation throughout. The mean-square intensity of the low-frequency pressure fluctuation, that is  $nF(n)$  at  $n = 0.2$ , has been integrated over the wing surface for the data shown in Figure 36, assuming unit correlation, and the result expressed as a mean over the whole wing area. The r.m.s. intensity of this quantity is 0.013 for the case illustrated, and its variation with incidence is shown in Figure 37, but unless it can be shown that the correlation is approximately constant, and independent of both incidence and any modifications which might be made, it is difficult to see how this, or any other, simple function of the data can be regarded as a reliable criterion for purposes of comparison. The possibility of direct measurements of the normal-force fluctuation is therefore under consideration, as an alternative approach.

Another interesting result was obtained on a wing of this class; this was a delta-wing with  $81^\circ$  leading-edge sweep, in which a single transducer was installed, for preliminary measurements, at 75% of the centre-line chord behind the nose and at 70% of the local semi-span. The results obtained are shown in Figure 38; it will be seen that the maximum intensity recorded is low, and even this is apparently confined to a narrow strip directly below each vortex, the peak value of  $\sqrt{nF(n)}$  for  $n = 0.2$  occurring when the vortex passes over the transducer position.

Further experiments have begun, with the object of determining contours of the low-frequency pressure fluctuations on a wing with  $60^\circ$  leading-edge sweep; these measurements are of particular interest, as there is a possibility of comparative full-scale data being obtained in flight. Preliminary results show levels of intensity under the vortices of the same order as those measured on unswept wings. This is not necessarily surprising since mean-flow measurements in wakes have suggested that the vortex structure caused by a leading-edge flow separation may change fairly abruptly with increasing angle of sweep; at moderate angles of sweep the vortex cores appear to be diffuse

and to exhibit either an instability or a large scale turbulent structure; at high angles of sweep - above  $70^{\circ}$ , it is thought - the vortex cores contract markedly, exhibiting high velocity components and no noticeable instability. Experiments are continuing for the purpose of examining the pressure fluctuations associated with these different types of vortex structure.

## 5. CONCLUDING REMARKS

The technique described in this paper has been proved, by use, to be satisfactory for the measurement and analysis of pressure fluctuations on wind-tunnel models at low speeds and, as indicated in Section 3.4.1, there is no reason to suppose that the additional difficulties arising from its use at transonic speeds - in so far as they affect the design and operation of the transducers and their associated electronic equipment - cannot be overcome. It remains to be proved, however, that the air flow in a transonic wind tunnel can be sufficiently steady for useful results to be obtained.

The applications of the technique to the low-speed investigations, described in some detail in Section 4, suggest certain broad conclusions in respect of its suitability for particular classes of problem and its general limitations. These may usefully be summarised here:

- (a) The technique is especially useful in fundamental research, since it provides local data in flow fields where other techniques (e.g. the hot-wire anemometer) cannot be used at all; some progress has already been made in relating the nature of the fluctuating pressure field on thin wings to the mean-flow structure, and further experiments (particularly if they include correlation measurements) may be expected to lead to a much greater understanding of the origins of the aerodynamic excitation which causes the full-scale vibration;
- (b) When applied to specific cases of aircraft-buffet, the techniques described can often be used, with fair certainty, to predict the effectiveness of modifications designed to reduce the buffeting;
- (c) The approach is not, in general, suitable for determining the resultant load fluctuation on a large area.

It should, perhaps, be emphasized that buffeting is regarded as the forced vibration of an aircraft structure, and that the present technique is intended solely for examination of the aerodynamic forcing excitation. However, the level of vibration to which the structure will be subjected depends also upon the aerodynamic and structural damping, so that knowledge only of the excitation cannot be expected, in general, to provide a sufficient indication of the onset of buffeting. This limitation must also be shared, to some extent, by all other techniques which aim at measuring aerodynamic excitation on rigid models, such as load or moment measurements, and it would appear that it is not completely overcome by techniques involving the measurement of vibration levels on dynamic models. These involve all the problems encountered in wind-tunnel flutter experiments, with the additional difficulties that there would be no precisely defined critical vibration, comparable to the self-excited flutter oscillation, and that, even if an accurate allowance could be made for differences

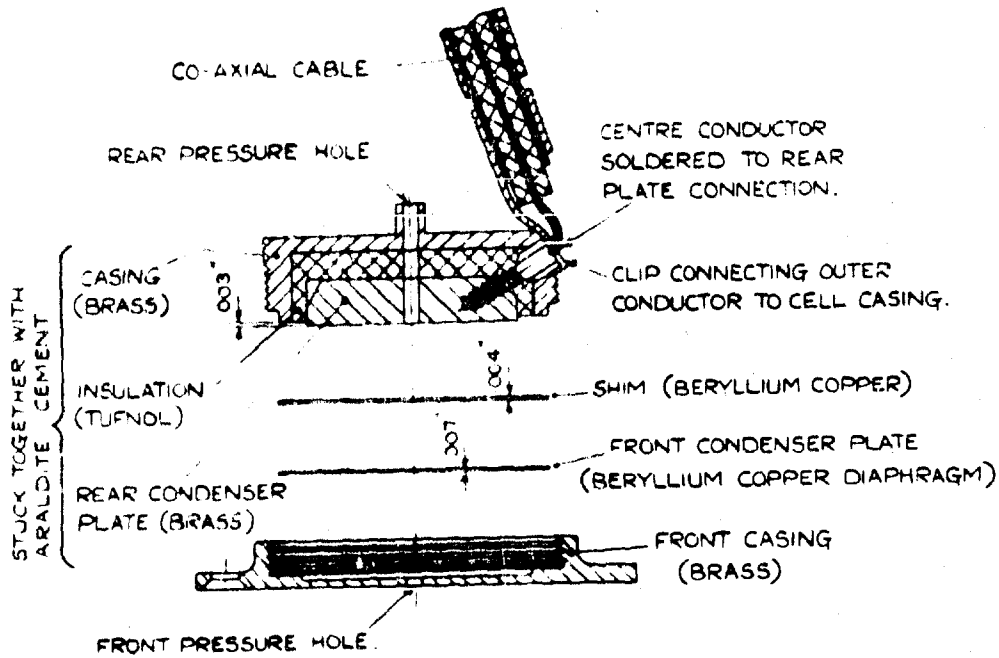
between the model and full-scale aerodynamic and structural damping, the tolerable level of vibration, full-scale, is not likely to be known.

On the other hand, it may often be assumed that the onset of buffet, should it occur, is likely to be sharply defined. A sharply defined change in the intensity and scale of the aerodynamic excitation might then be taken to indicate that the likelihood of buffeting exists and, to this extent, to provide a comparative criterion - that is to say, a criterion which may be used in comparing different curves of the same type. It is in this sense that the present technique has been used for the prediction of the effectiveness of modifications designed to reduce buffeting.

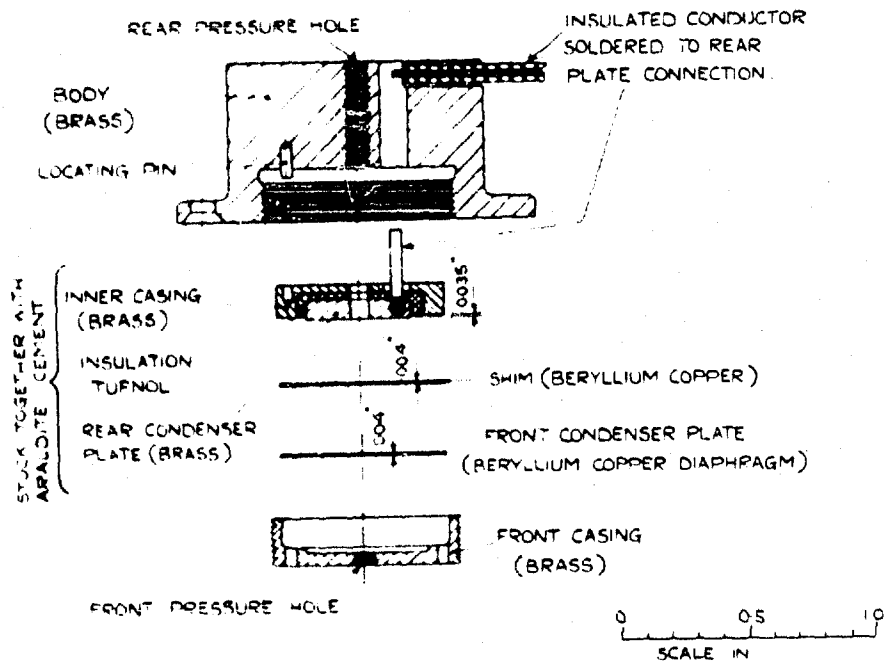
#### REFERENCES

1. Schuh, H.  
Walker, D. *Wide range amplifier for turbulence measurements with adjustable upper frequency limit.* (Unpublished M.O.S. report).
2. Owen, T.B. *Low speed static and fluctuating pressure distributions on a cylindrical body with a square flat plate airbrake.* C.P. No.288.
3. Fail, R. *Preliminary low-speed wind-tunnel tests on flat plates and air brakes: Flow, vibration and balance measurements.* C.P. No.251.
4. Fail, R.  
et alii *Low speed experiments on the wake characteristics of flat plates normal to an airstream.* (Unpublished M.O.S. report).
5. de Bray, B.G. *Low-speed wind-tunnel tests on perforated square flat plates normal to the airstream: Drag and velocity fluctuation measurements.* C.P. No.323.

Best Available Copy



(a) 0.7 in. pressure transducer



(b) 0.37 in. pressure transducer

Fig.1 Exploded sections of capacity-type pressure transducers

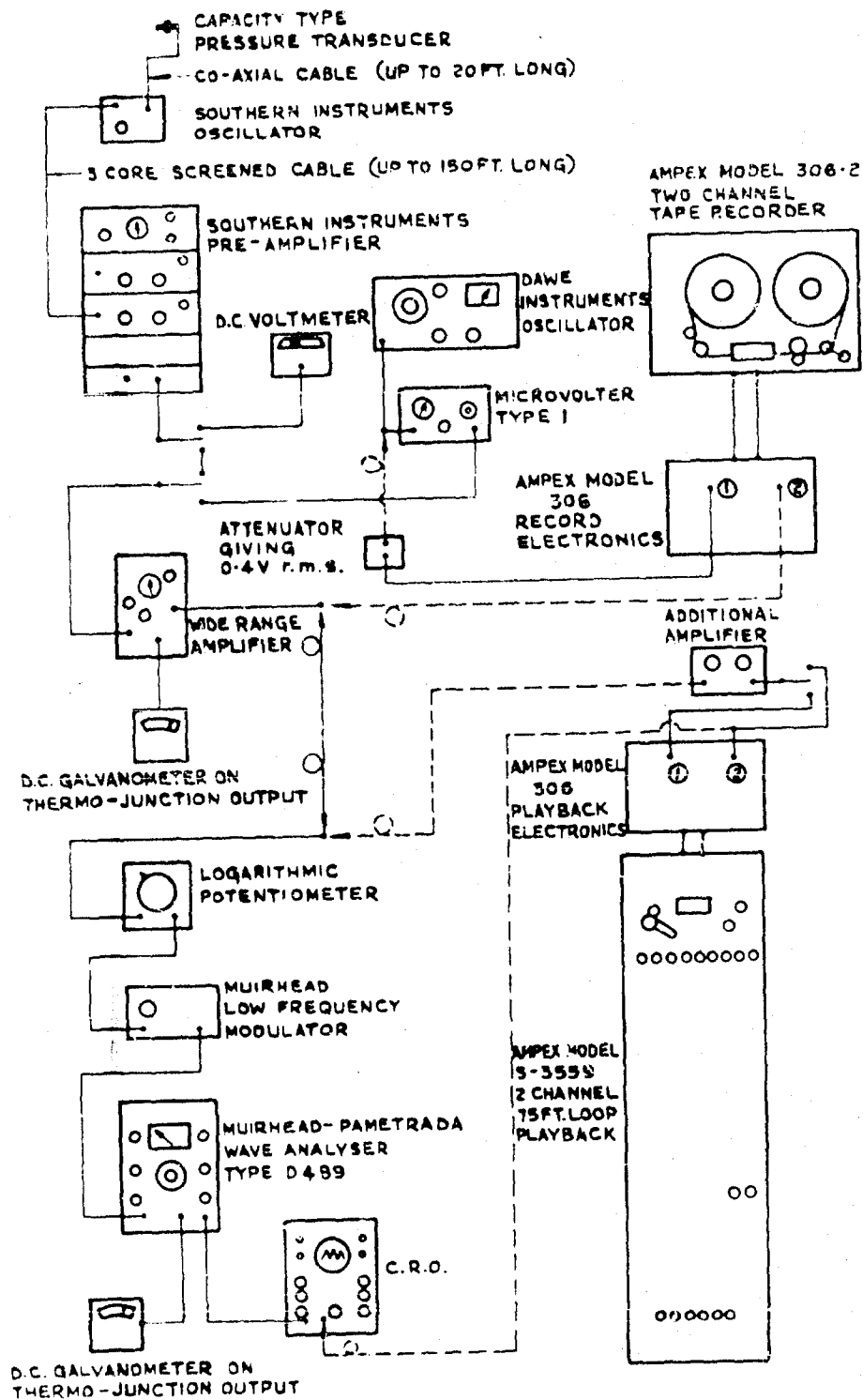


Fig.2 General arrangement of apparatus for measurement and analysis of pressure fluctuations

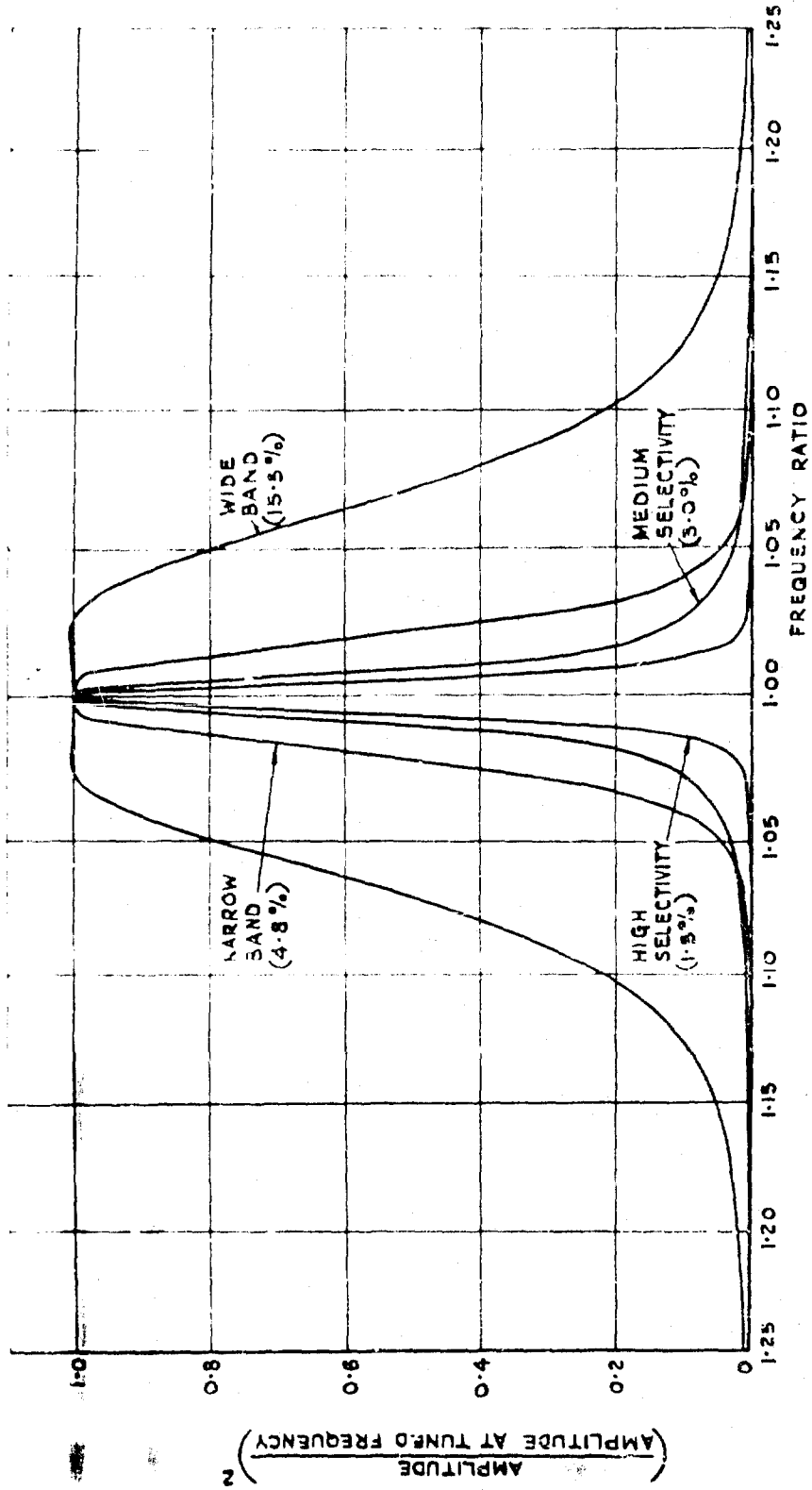
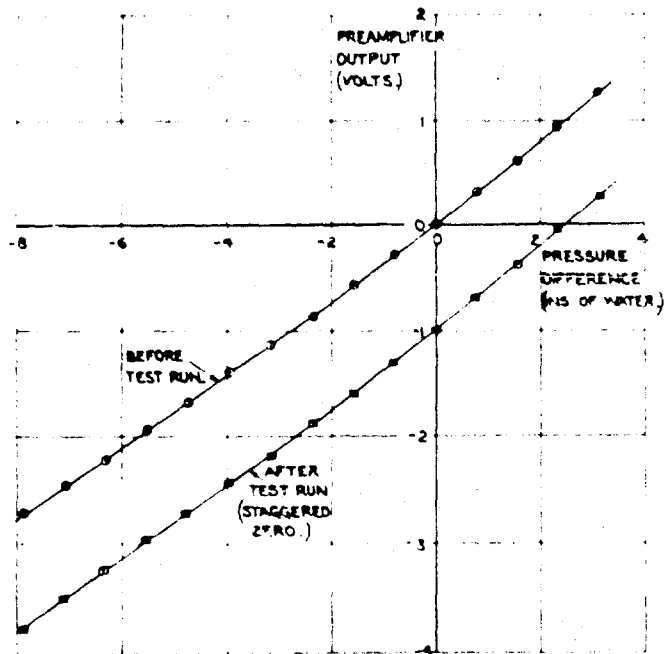
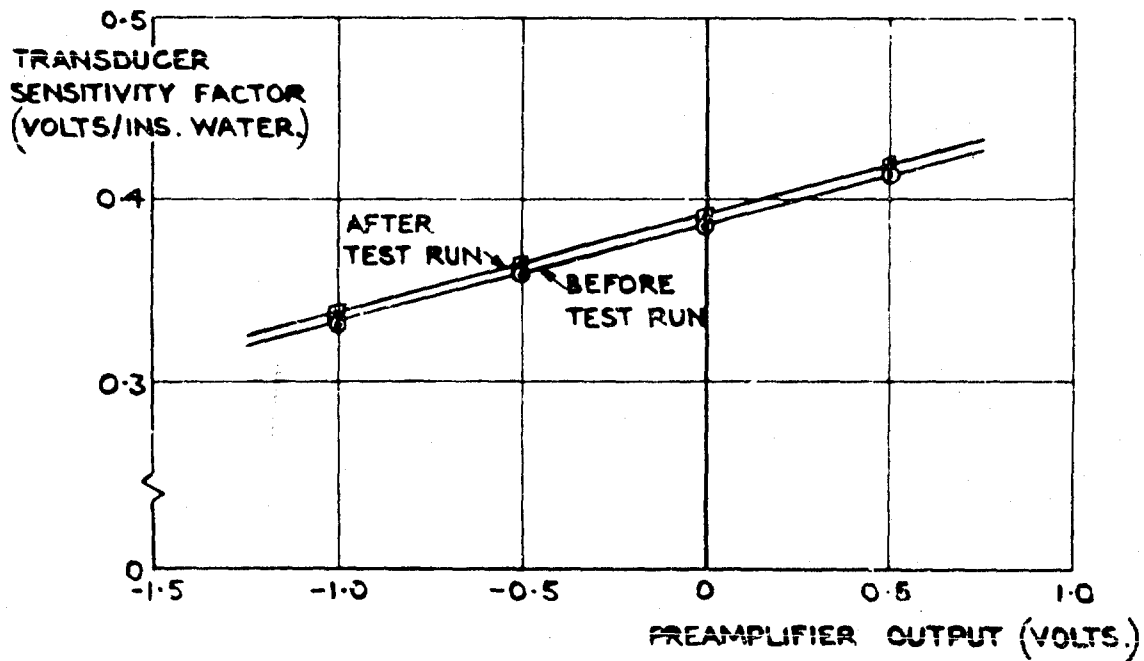


Fig. 3 Typical bandwidth response curves for the Muirhead-Pametrada wave analyser type D-489



(a) Direct transducer calibration



(b) Transducer sensitivity factor

FIG. 4 Typical transducer calibration and sensitivity factor

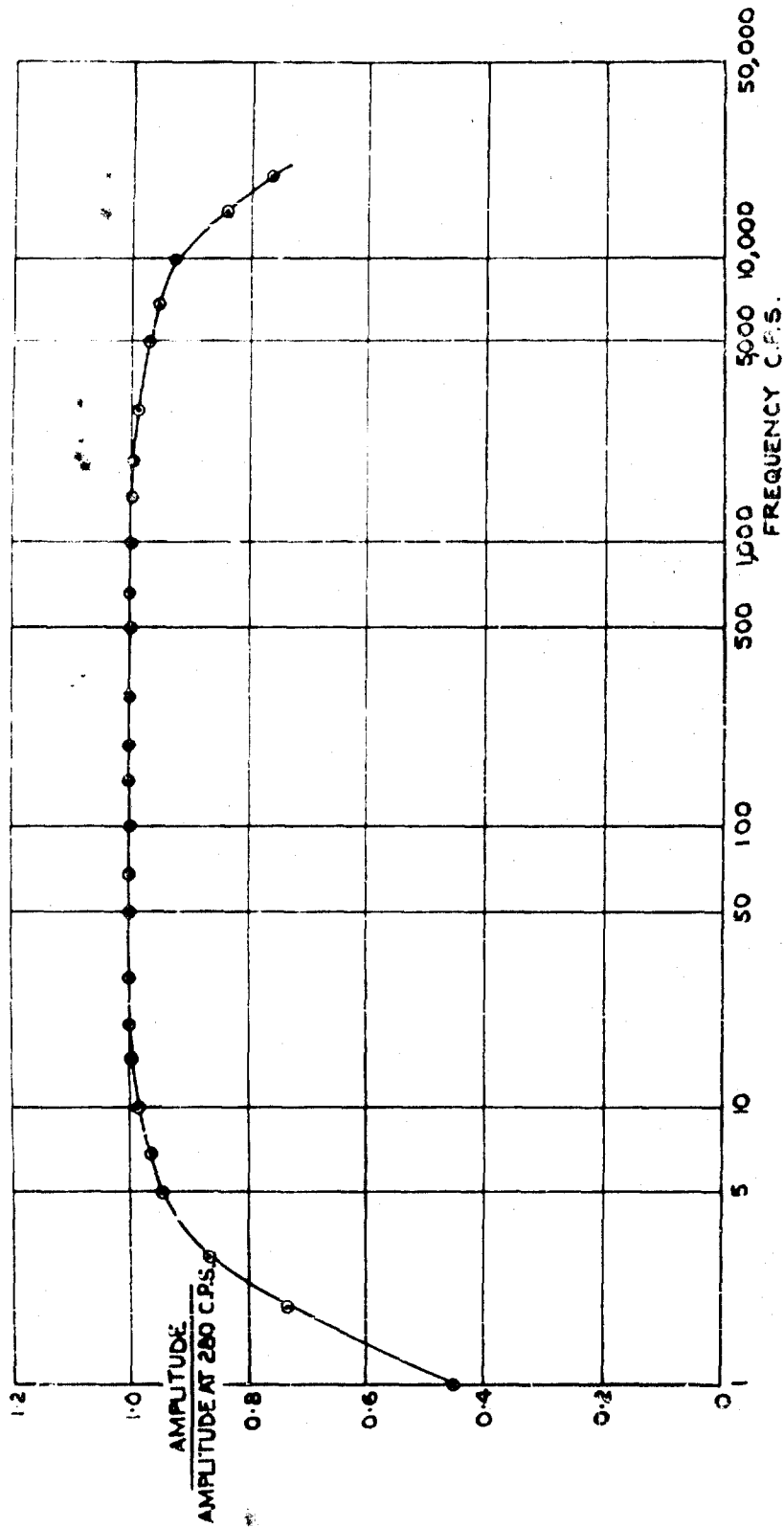
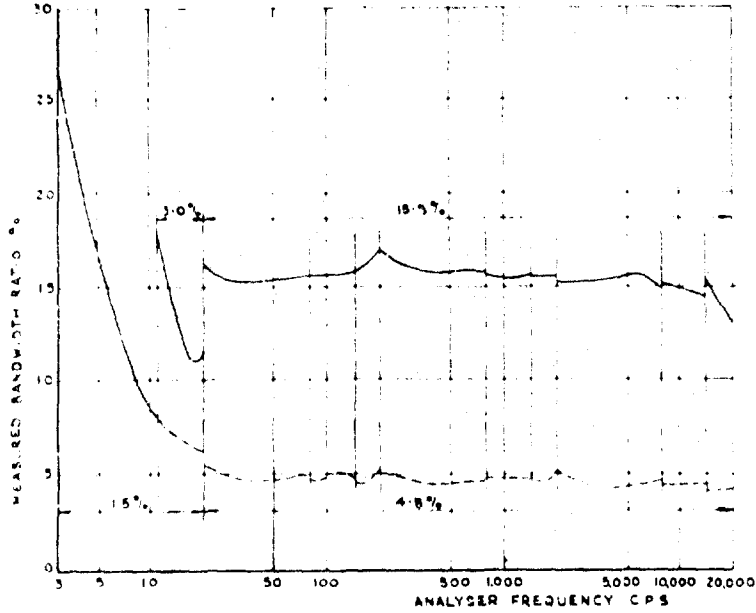
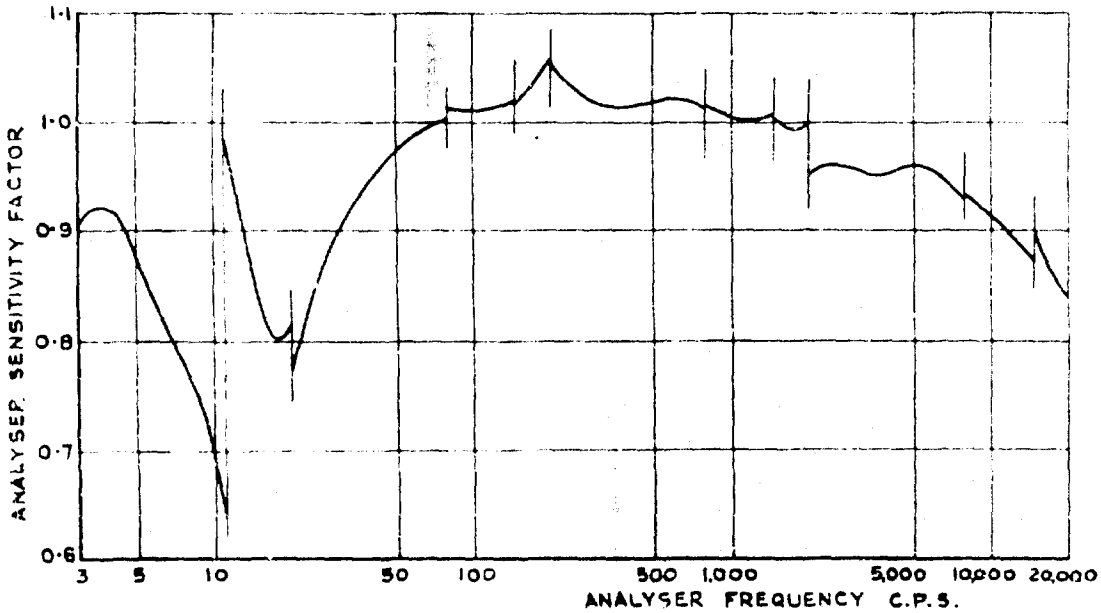


Fig.5 Frequency response of wide frequency-range amplifier



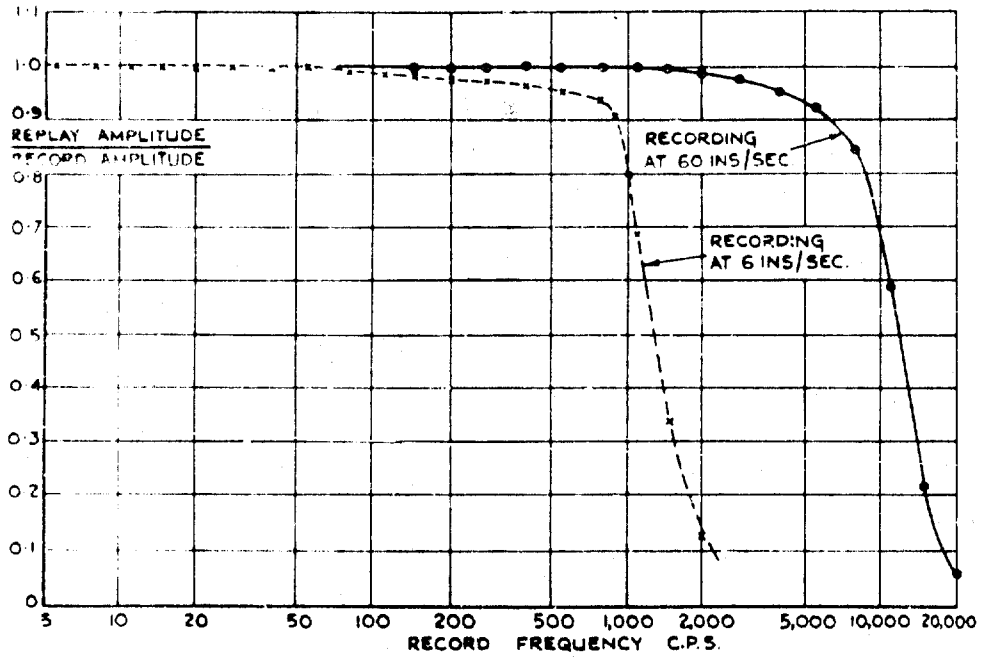
(a) Measured bandwidth ratio

(The figures are the nominal bandwidth settings, and the full curve refers to the settings normally used)

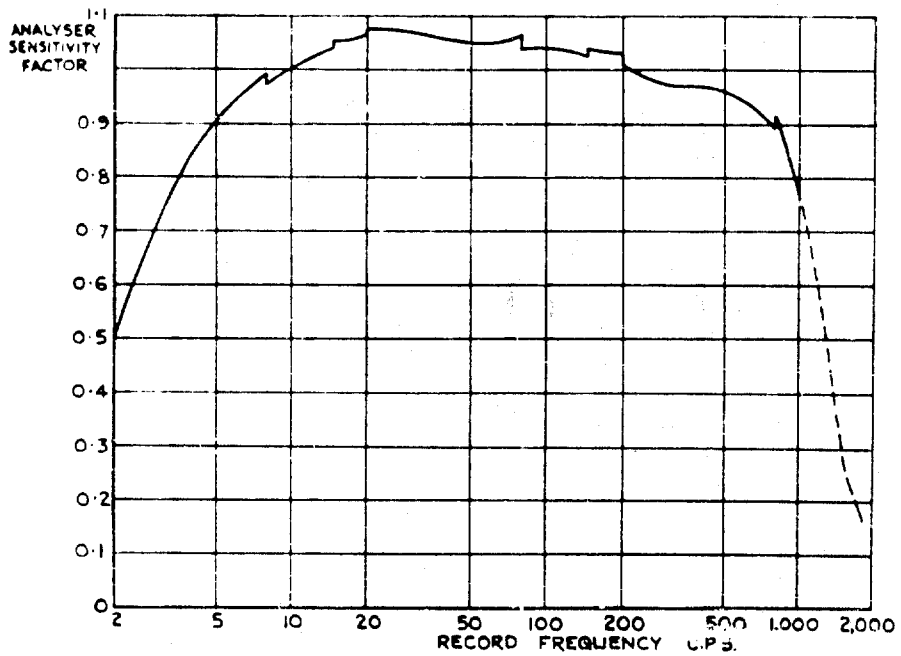


(b) Overall analyser sensitivity factor (see Section 2.3.3)

Fig. 6 Measured analyser characteristics

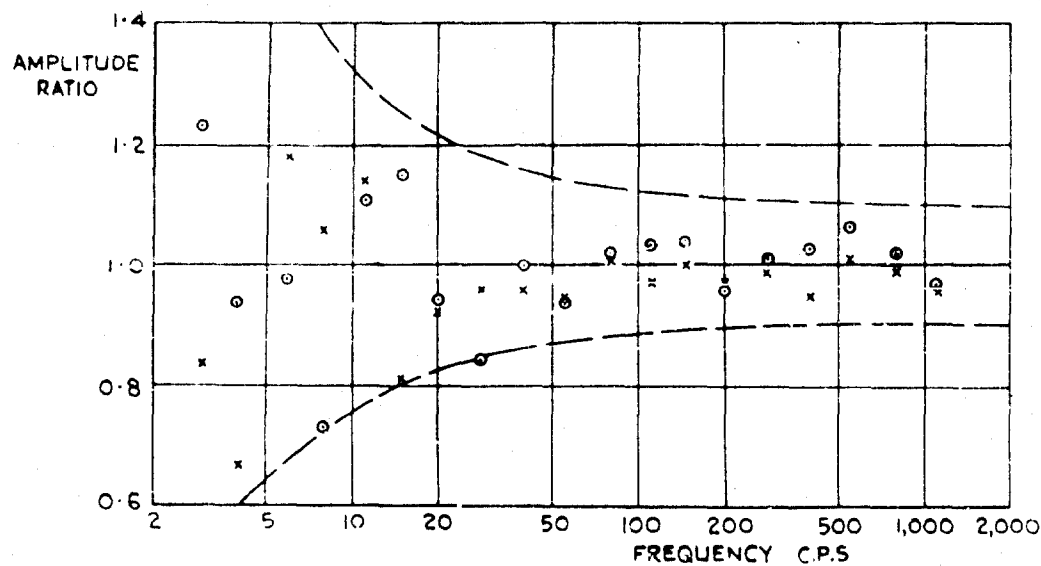


(a) High frequency response of tape recorder and playback

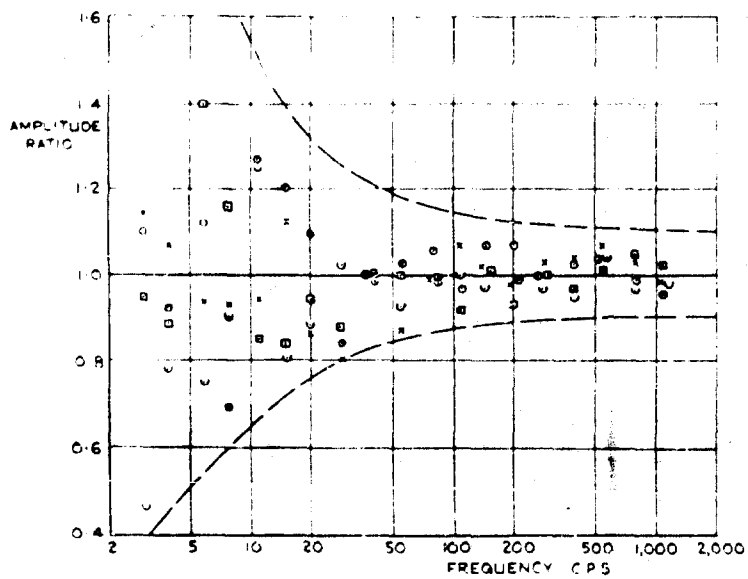


(b) Analyser sensitivity factor when used in conjunction with 6 in./sec recording and 60 in./sec playback

Fig. 7 Frequency response using tape recorder



(a) Analysis of two halves of a 75 ft recording



(b) Analysis of four quarters of a 75 ft recording

Fig. 8 Effect of record length on replay accuracy at low frequencies. Recording and replay at 60 in./sec tape speed

$$\text{Amplitude ratio} = \frac{\sqrt{nF(n)} \text{ from record replay}}{\sqrt{nF(n)} \text{ from direct analysis}}$$

Limit lines shown are  $1.1(1 + 15/N)$  and  $(1/1.1)(1 + 15/N)$   
 where N = number of cycles recorded

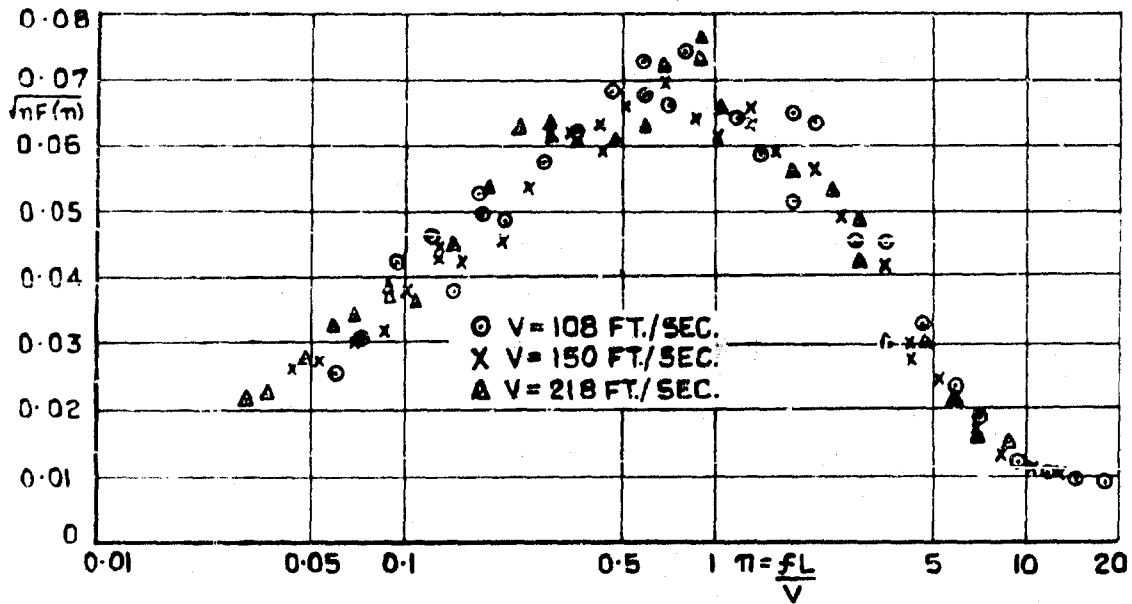


FIG. 9 Effect of wind-speed on a spectrum of pressure fluctuations on the rear wall of a rectangular cavity in a cylindrical body.  $L$  = cavity length

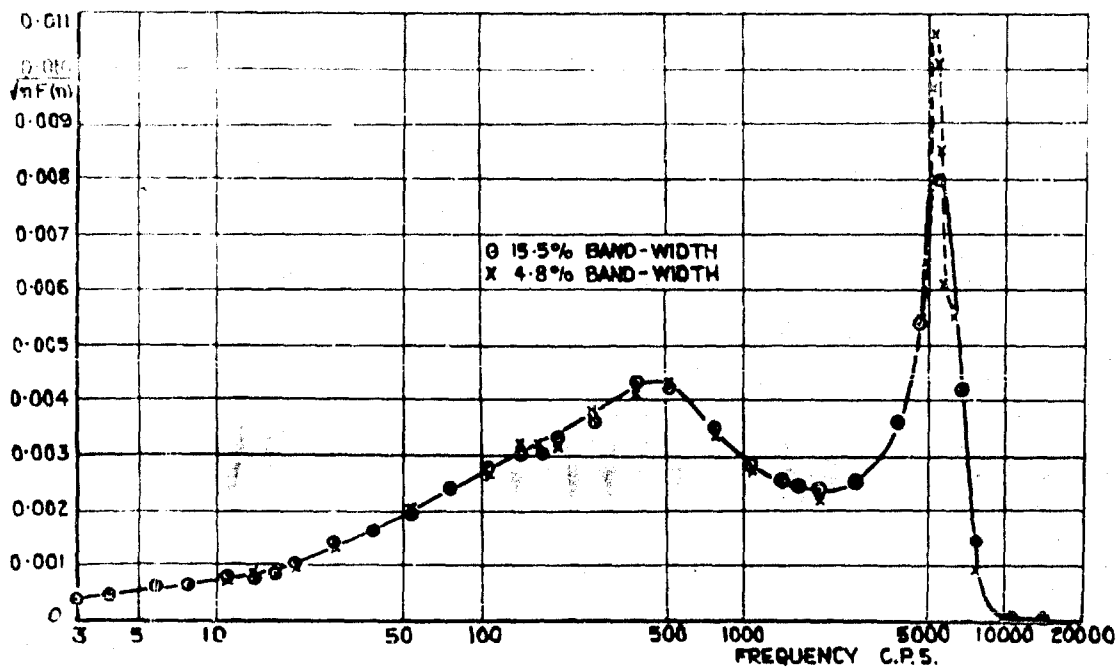


FIG. 10 Effect of a bandwidth on a spectrum of pressure fluctuations on the upper surface of a highly swept wing

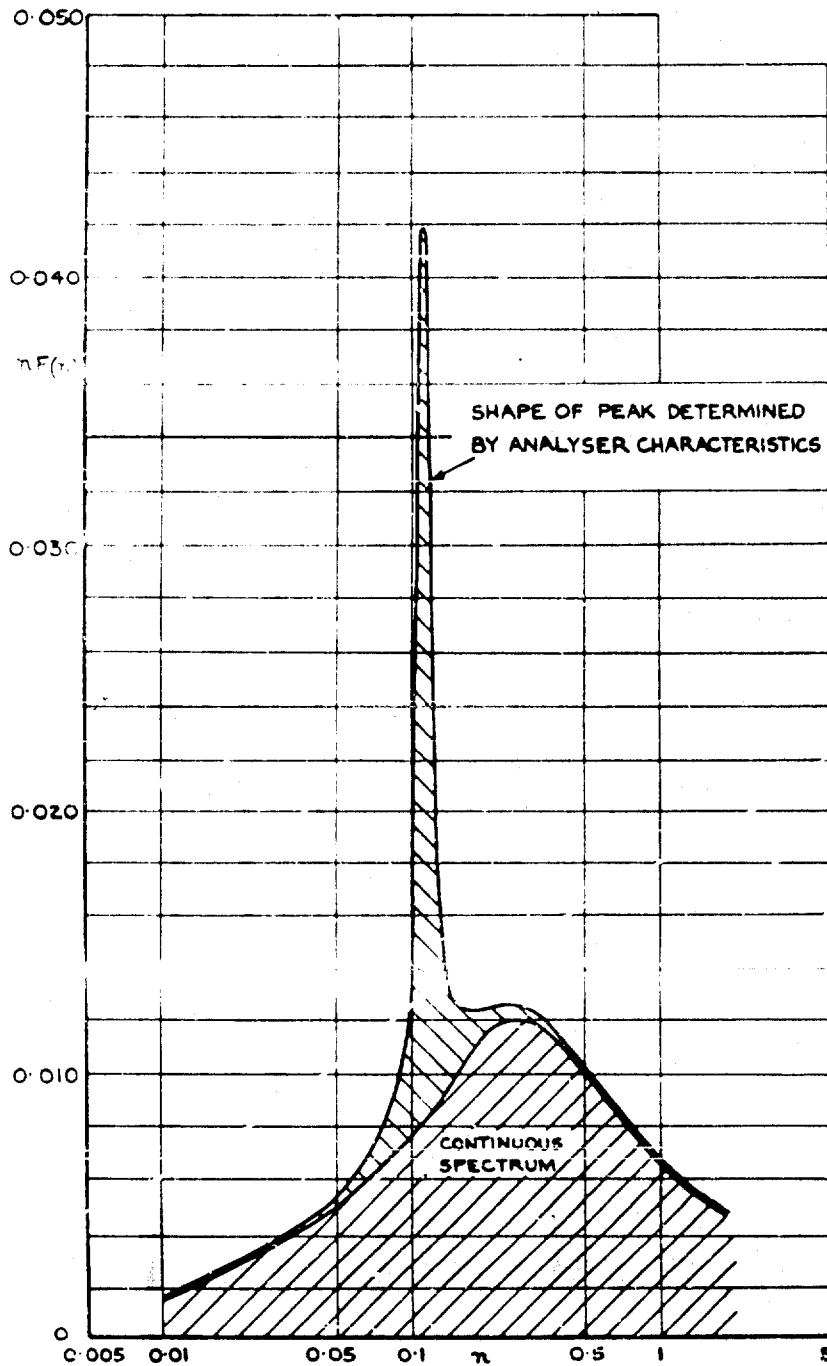
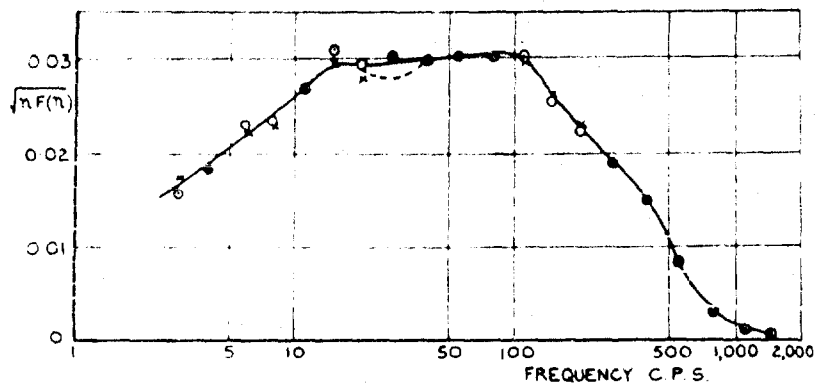
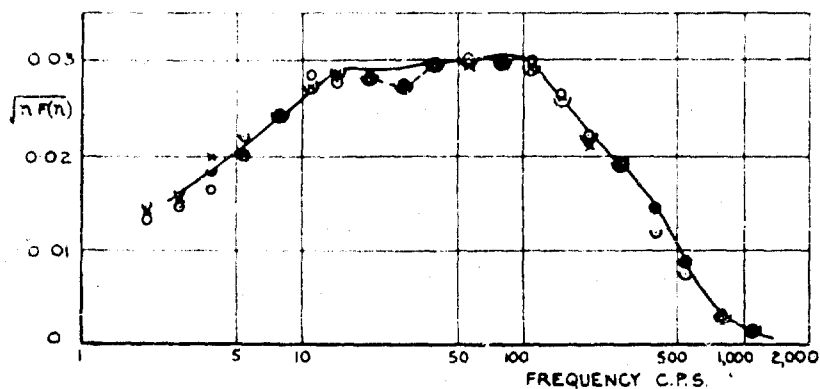


Fig.11 Measured spectrum showing separation of a peak, due to a discrete frequency oscillation, from the continuous spectrum

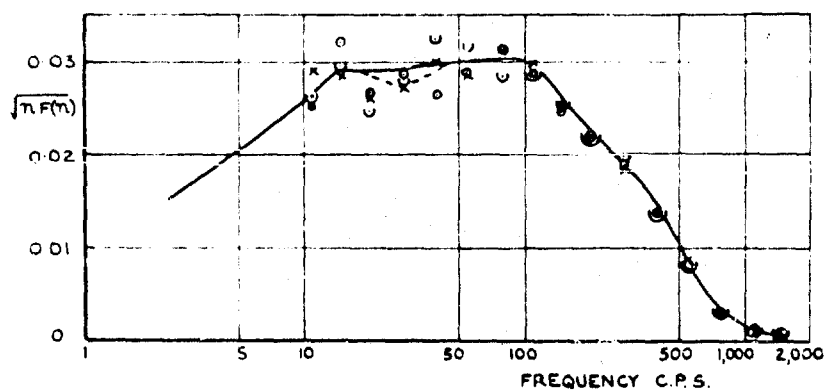
(The example is taken from velocity fluctuation measurements behind a square flat plate normal to the wind, using an earlier analyser with poorer discrimination than the Muirhead-Pametrada analyser)



(a) Direct analysis. Analyses before and after recordings



(b) Recording at 6 in./sec. Replay at 60 in./sec. Three 75 ft records



(c) Recording at 60 in./sec. Replay at 60 in./sec. Three 75 ft records

Fig.12 Comparative measurements of a spectrum of pressure fluctuations behind a spoiler obtained by direct analysis, and by replay of recordings made at two tape speeds

The full curve of Fig.12(a) is repeated in Fig.12(b) & 12(c)

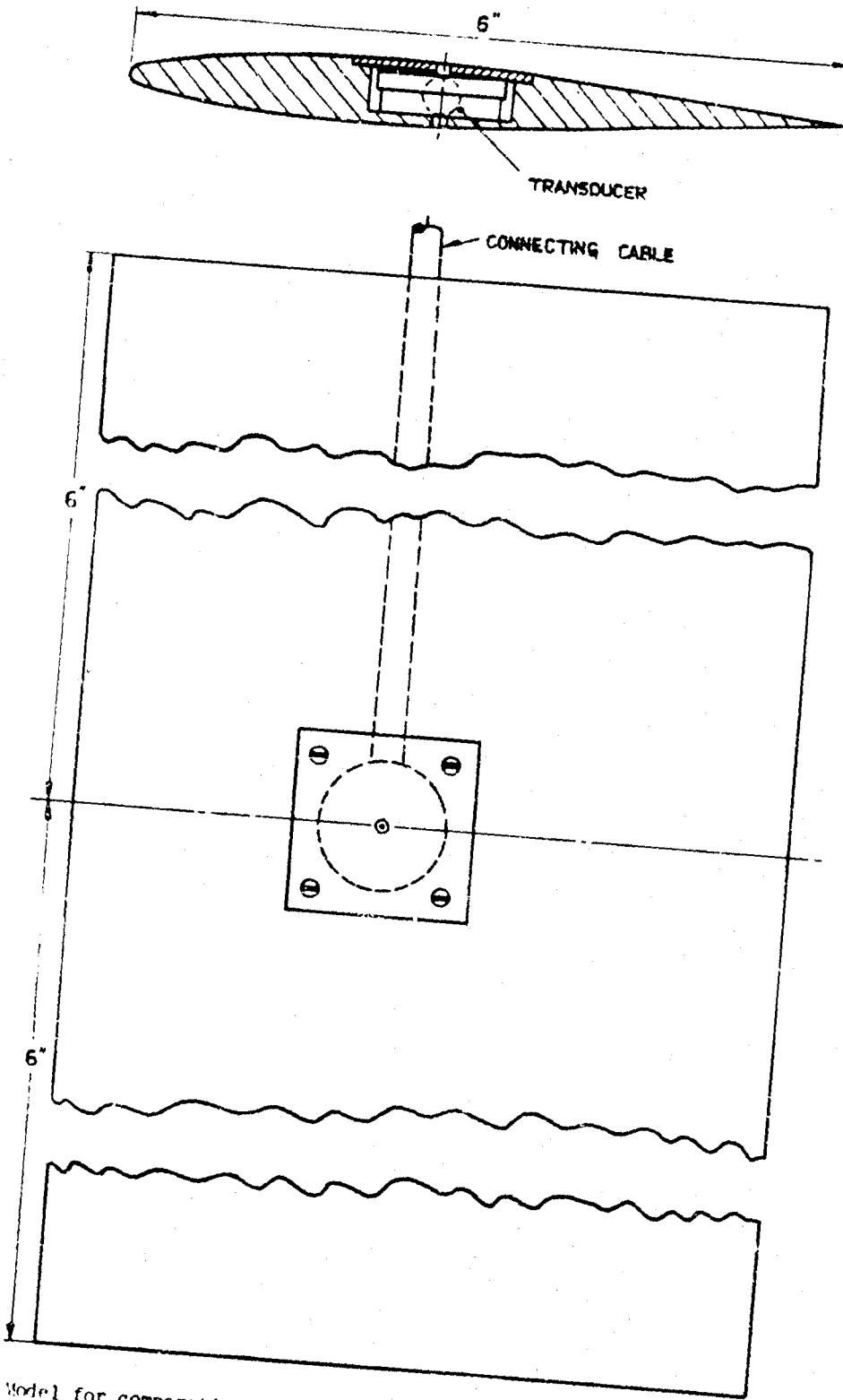


FIG. 13 Model for comparative pressure-fluctuation measurements in two wind-tunnels

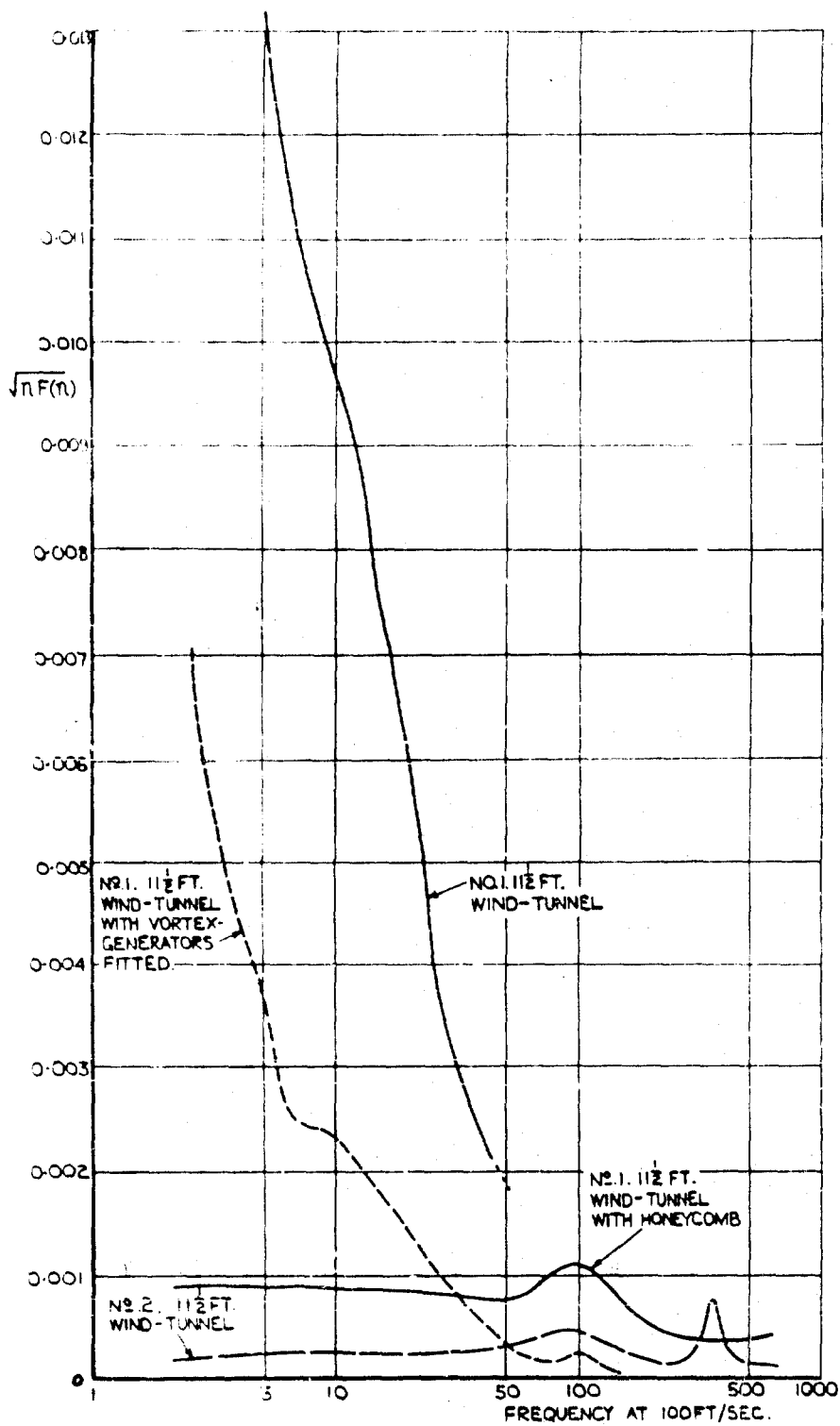


Fig. 14 Pressure fluctuations on a wing in two wind tunnels (see Section 3.2)

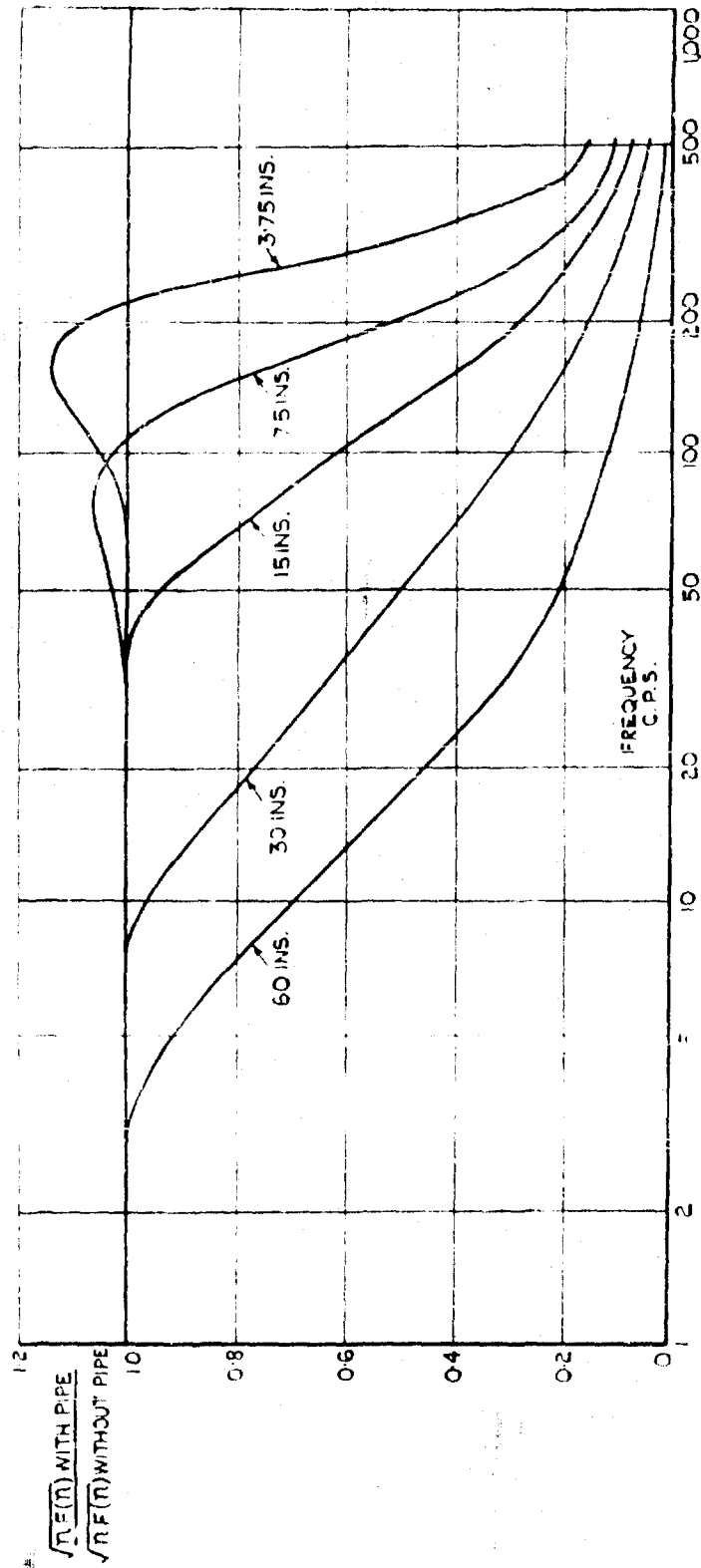


Fig. 15 Attenuation due to use of a pipe between measuring point and transducer. Transducer as shown in Figure 1a, pipe 0.028 in. internal diameter

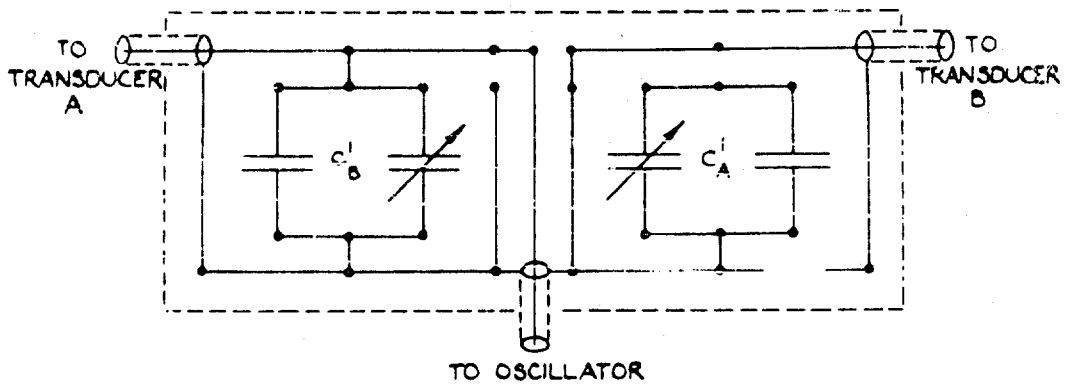
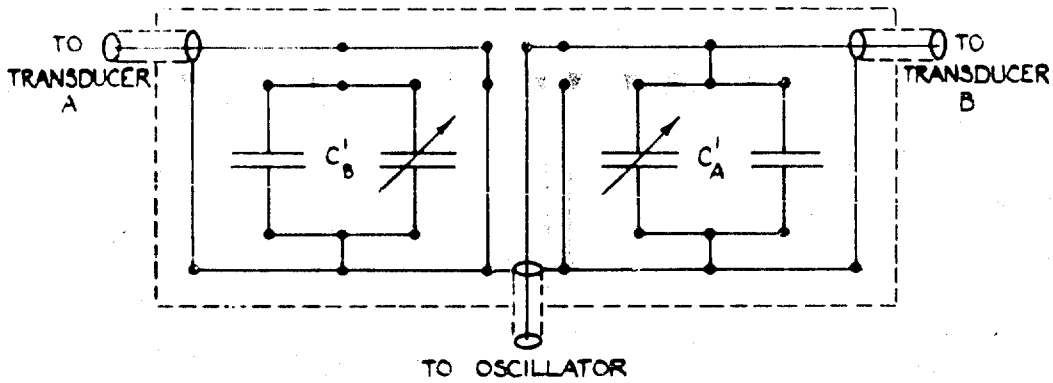
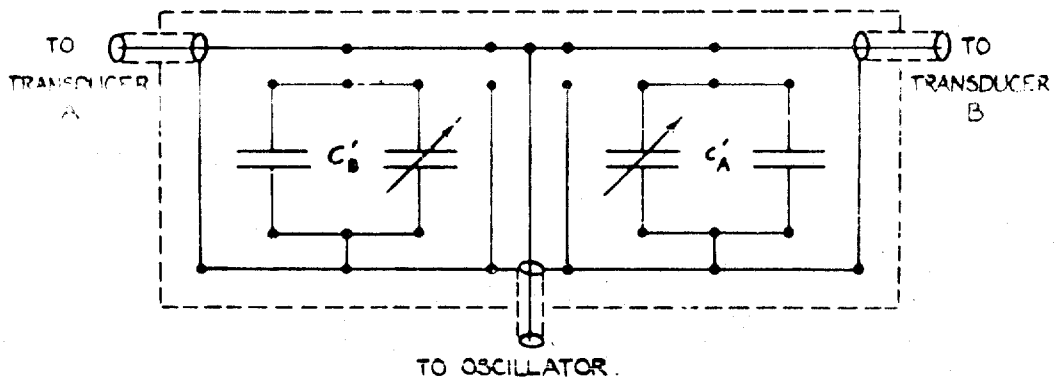
(a) Connections for measuring  $\sqrt{A^2}$ (b) Connections for measuring  $\sqrt{B^2}$ (c) Connections for measuring  $\sqrt{(A + B)^2}$ 

FIG. 16 Circuit variations for correlation measurements

$C'_A$  adjusted to be equal to  $C_A$  (the capacity of transducer A and its connecting cable)  
 $C'_B$  adjusted to be equal to  $C_B$  (the capacity of transducer B and its connecting cable)

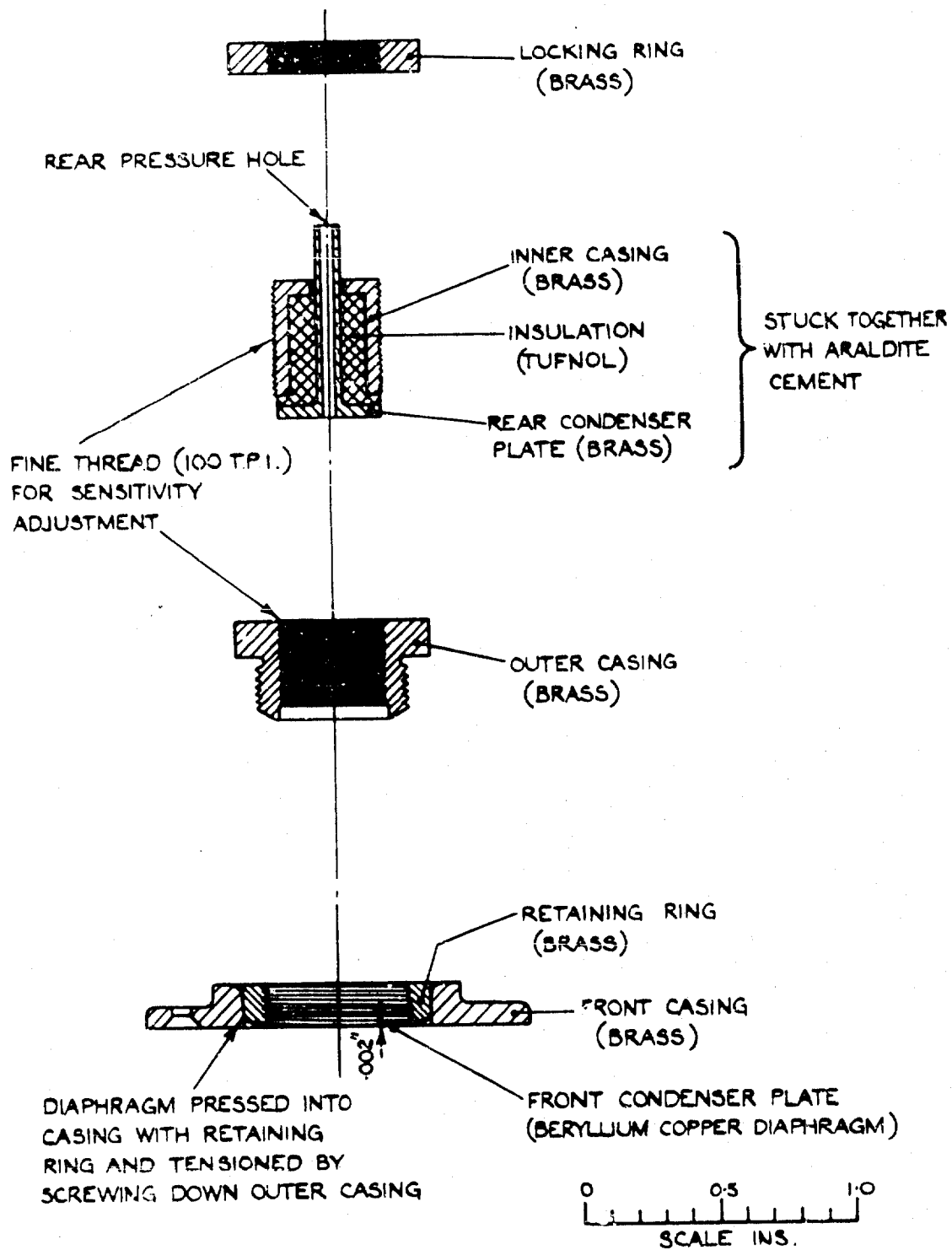
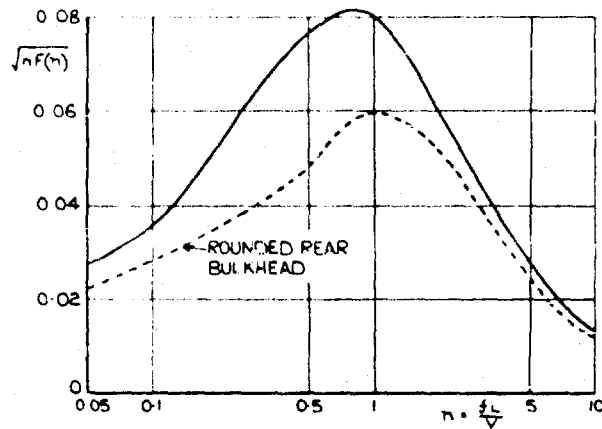
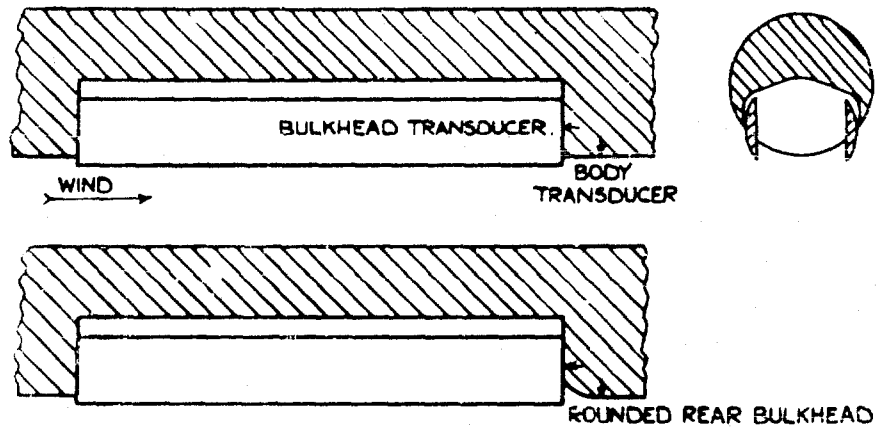
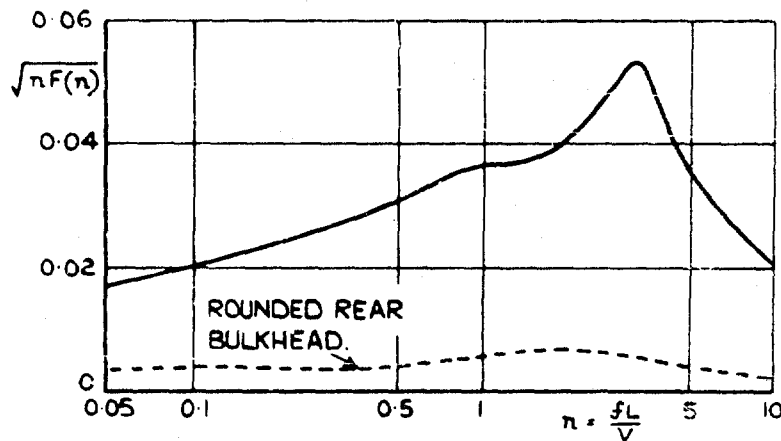


Fig. 17 'Exploded' sections of a prototype transducer for the measurement of high-frequency pressure fluctuations



(a) Bulkhead transducer



(b) Body transducer

Fig.18 Effect of rounding the rear bulkhead on bomb-bay pressure fluctuations

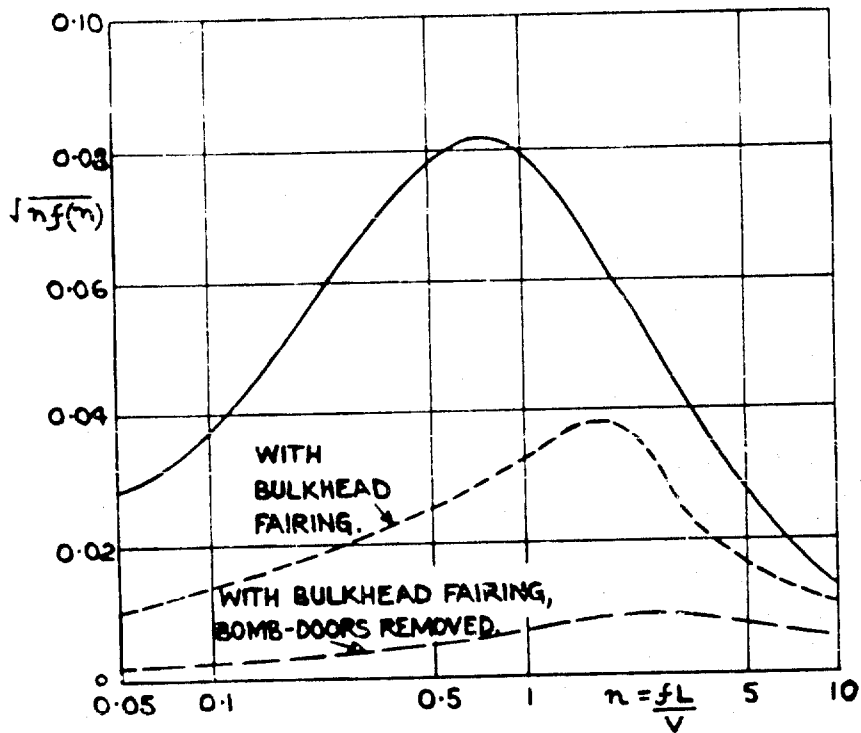
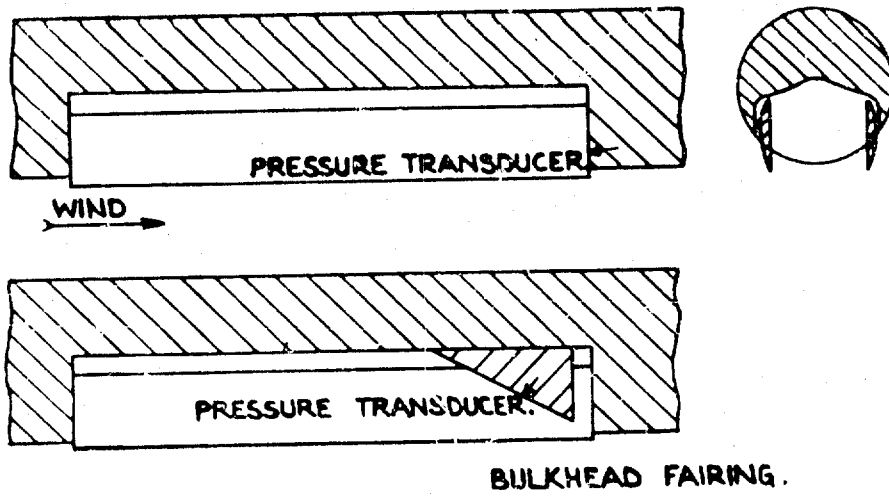


Fig. 19 Effect of rear bulkhead fairing on bomb-bay pressure fluctuations  
 $L$  = bomb-bay length

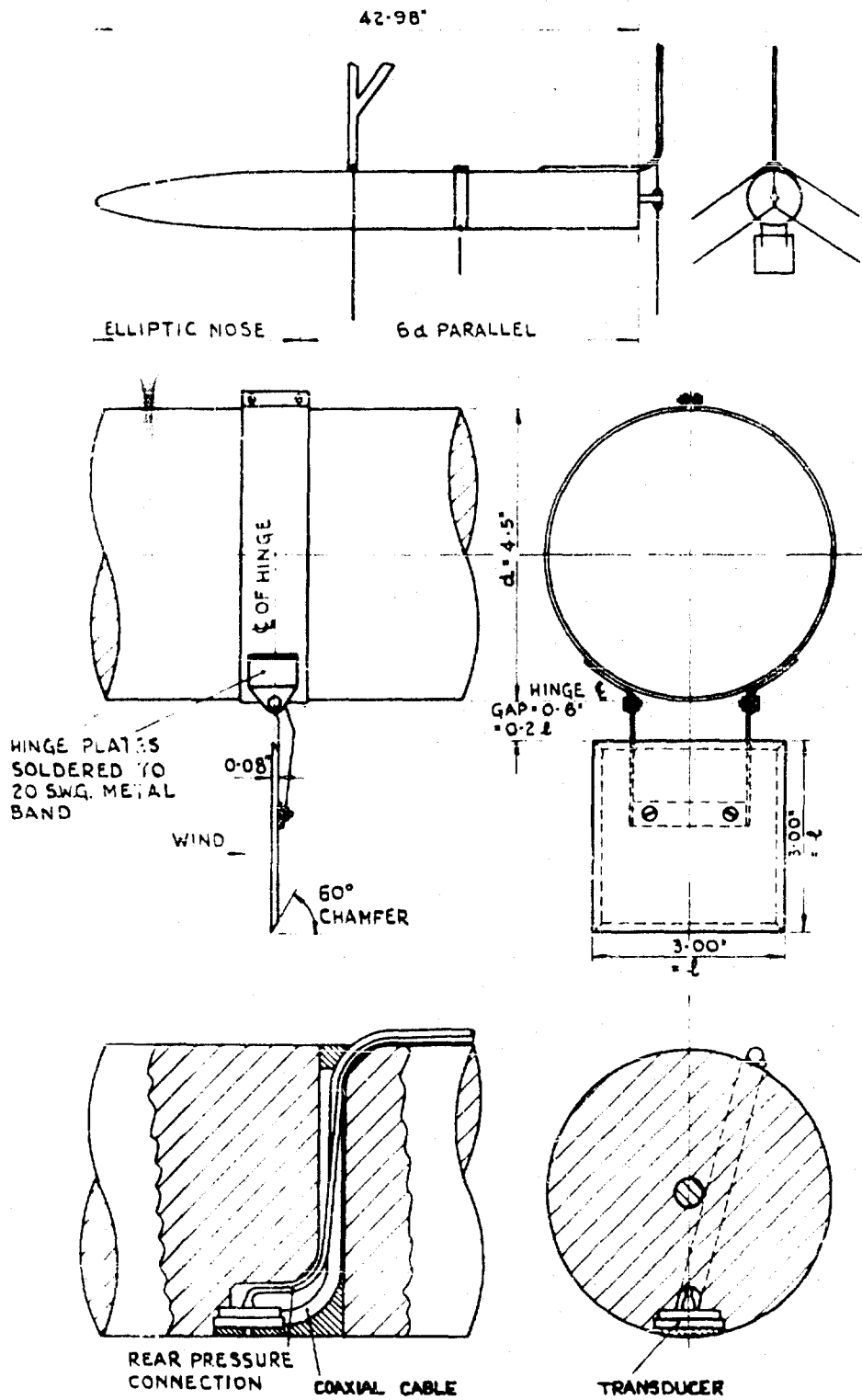
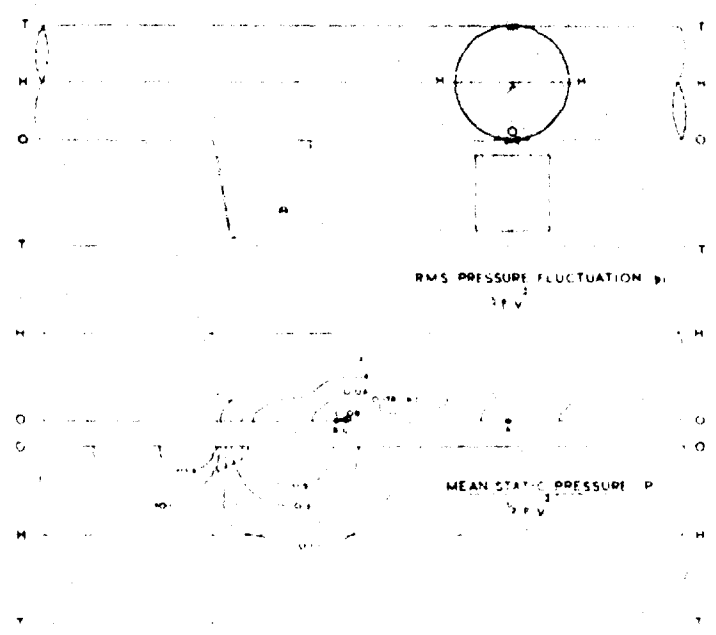
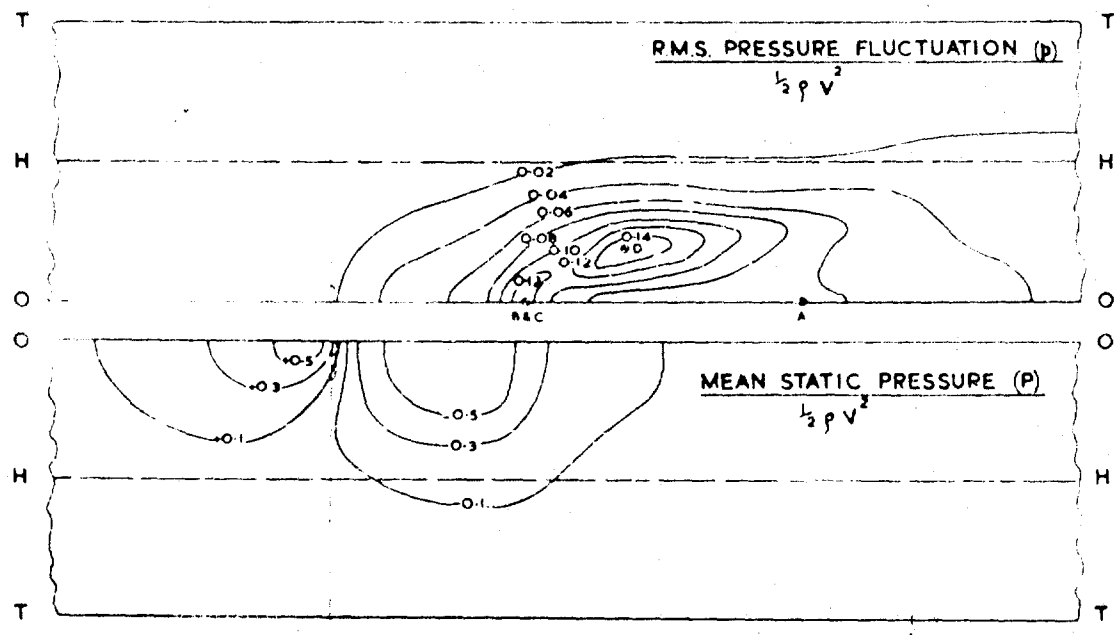


Fig. 20 Installation of transducer for pressure-fluctuation measurements on body with air-brake



(a)  $\theta = 70^\circ$



(b)  $\theta = 90^\circ$

Fig.21 Fluctuating and static pressure distributions on a body surface due to an air-brake

Contours and projected brake area shown on developed body surface

⊕ indicates points at which spectra have been measured

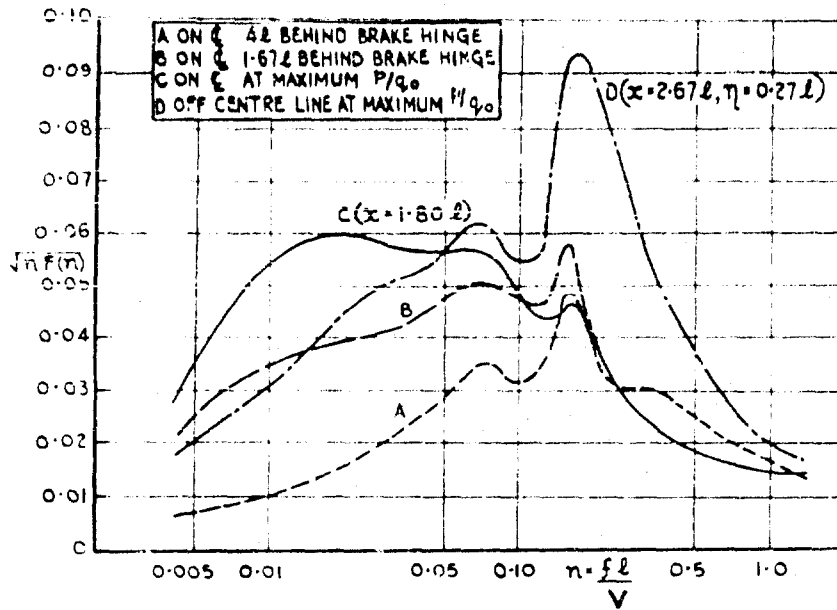
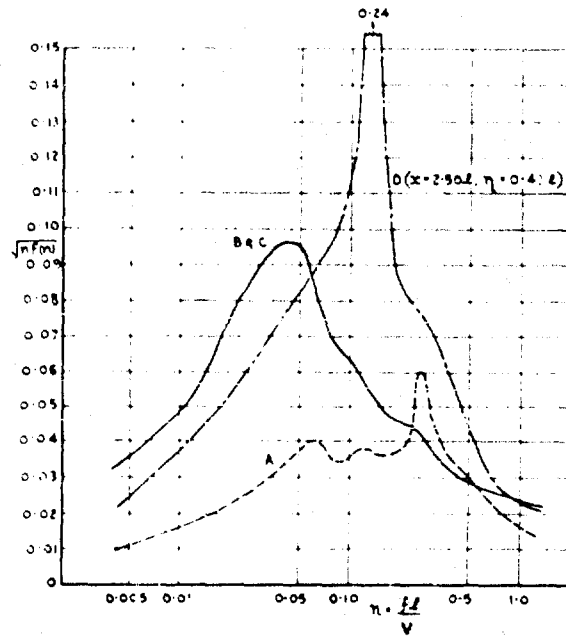
(a)  $\theta = 70^\circ$ (b)  $\theta = 90^\circ$ 

Fig. 22 Pressure fluctuation spectra measured at points indicated in Figure 21

$x$  = distance of pressure transducer behind brake hinge-line

$\eta$  = distance of pressure transducer from  $\phi$  measured round body surface

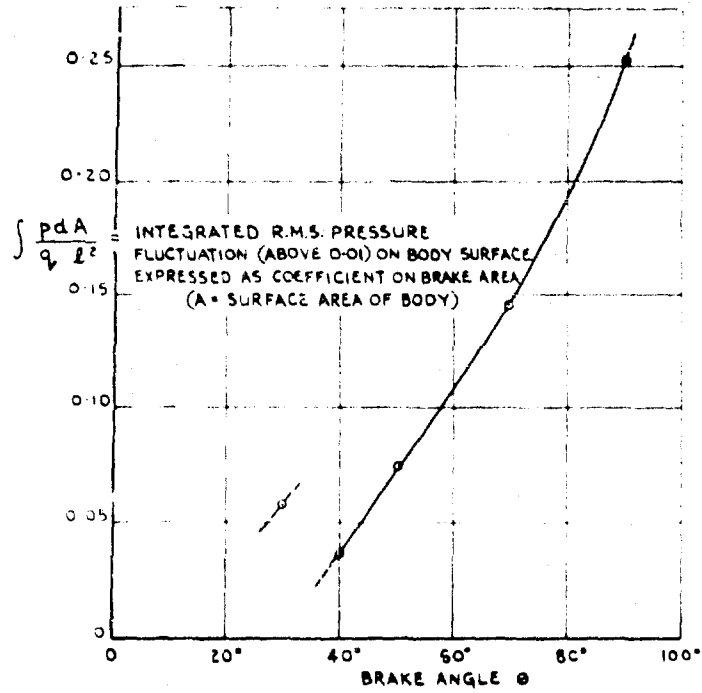


Fig. 23 Effect of air-brake angle on the pressure excitation on a body

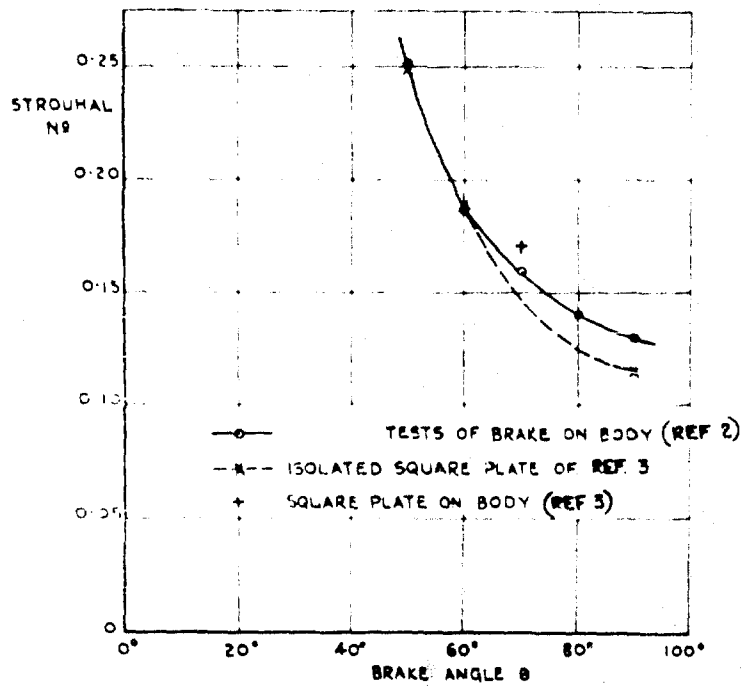


Fig. 24 Variation of Strouhal number with air-brake angle

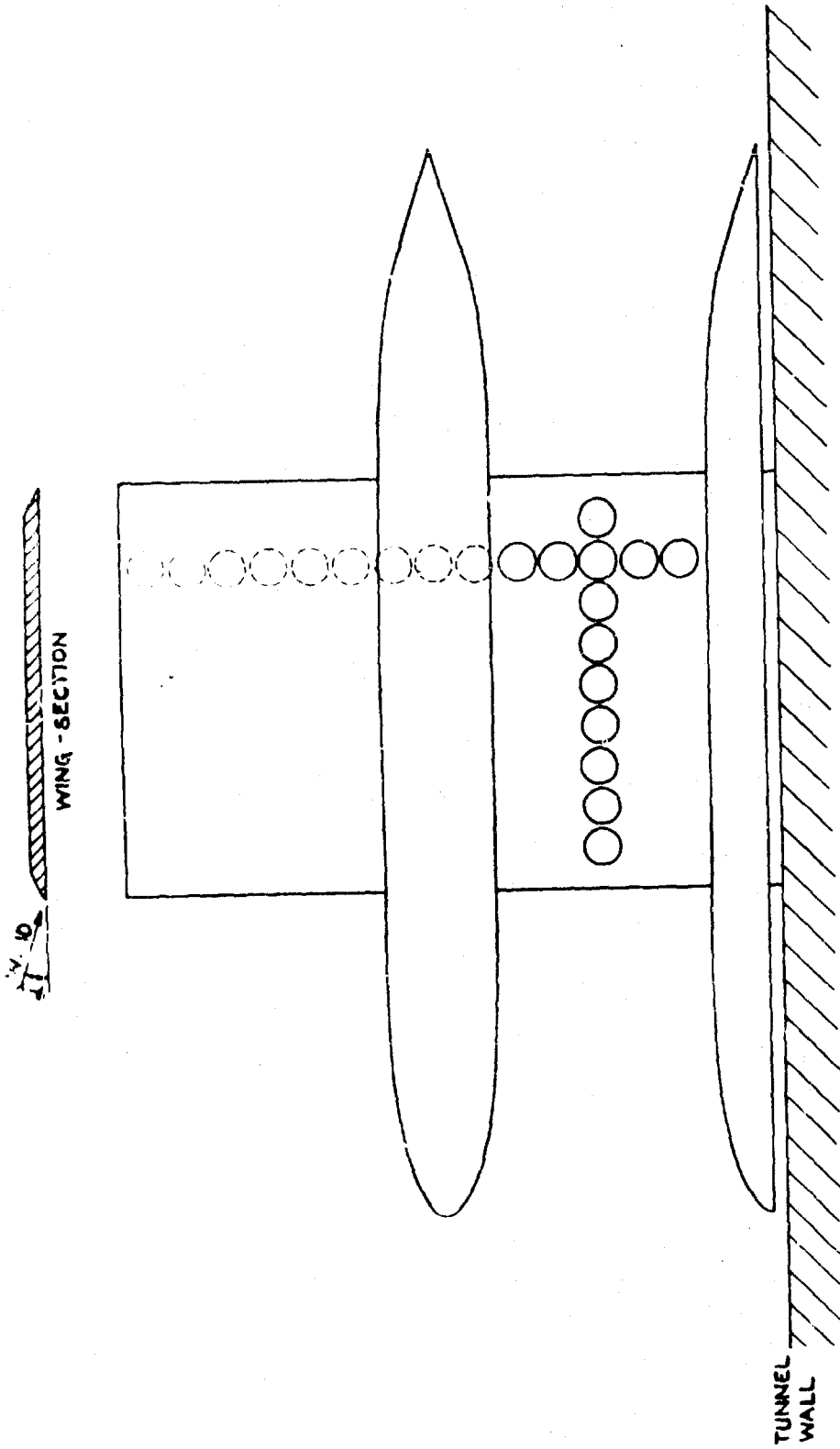


Fig. 25 Wing for correlation coefficient measurements  
Full circles show transducer positions used for tests described in Section 4.3.1

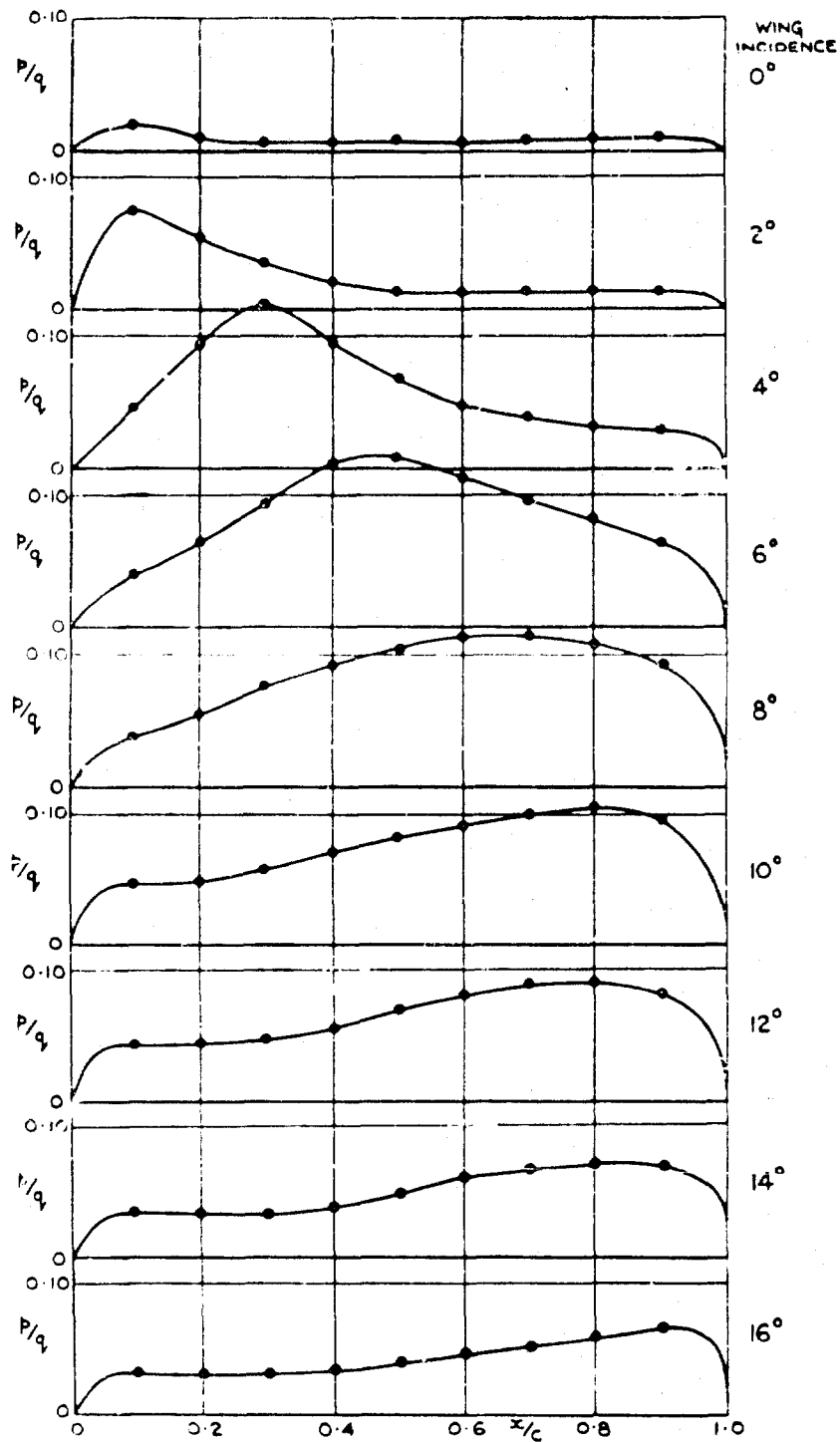


Fig. 26 Chordwise distribution of pressure fluctuations on wing shown in Figure 25.  
nacelle on

$x$  = distance from wing leading edge.  $c$  = wing chord

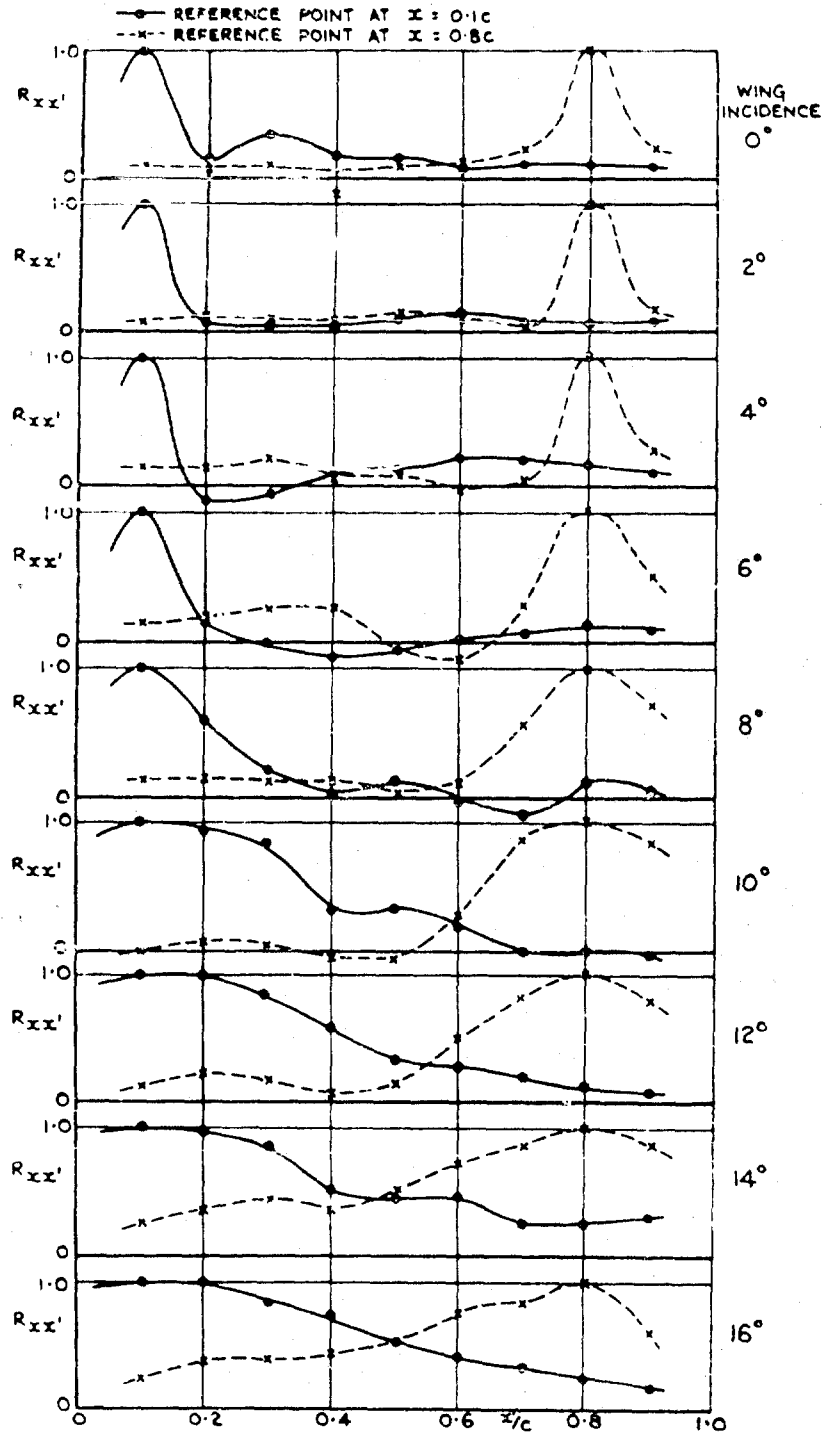


FIG. 27 Chordwise variation of correlation coefficient on wing shown in Figure 25, nacelle on

$x$  &  $x'$  measured from wing leading edge.  $c$  = wing chord

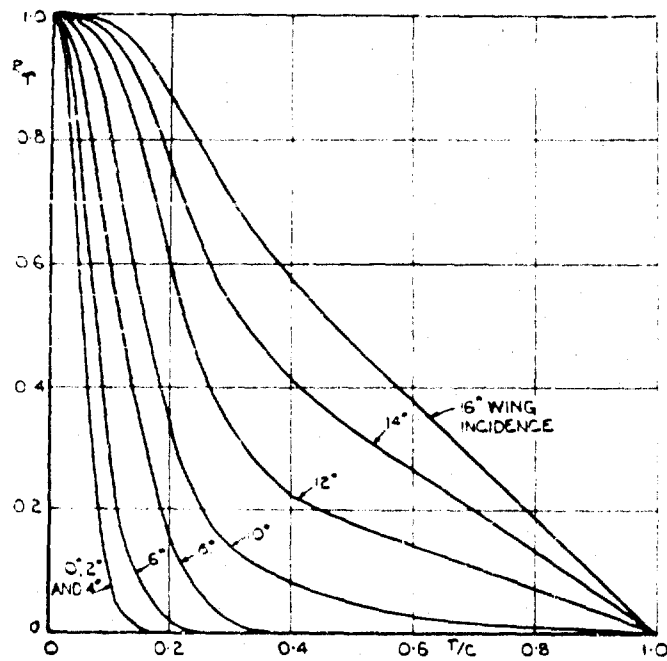


Fig. 28 Smoothed chordwise variation of correlation function on wing shown in Figure 25. Nacelle on  
 $r$  distance apart of measuring points,  $c$  = wing chord

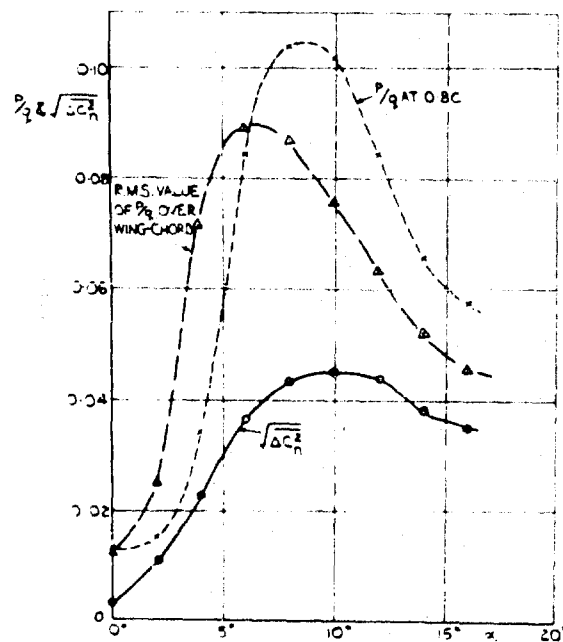


Fig. 29 Variation of section normal-force fluctuation on wing shown in Figure 25. Nacelle on

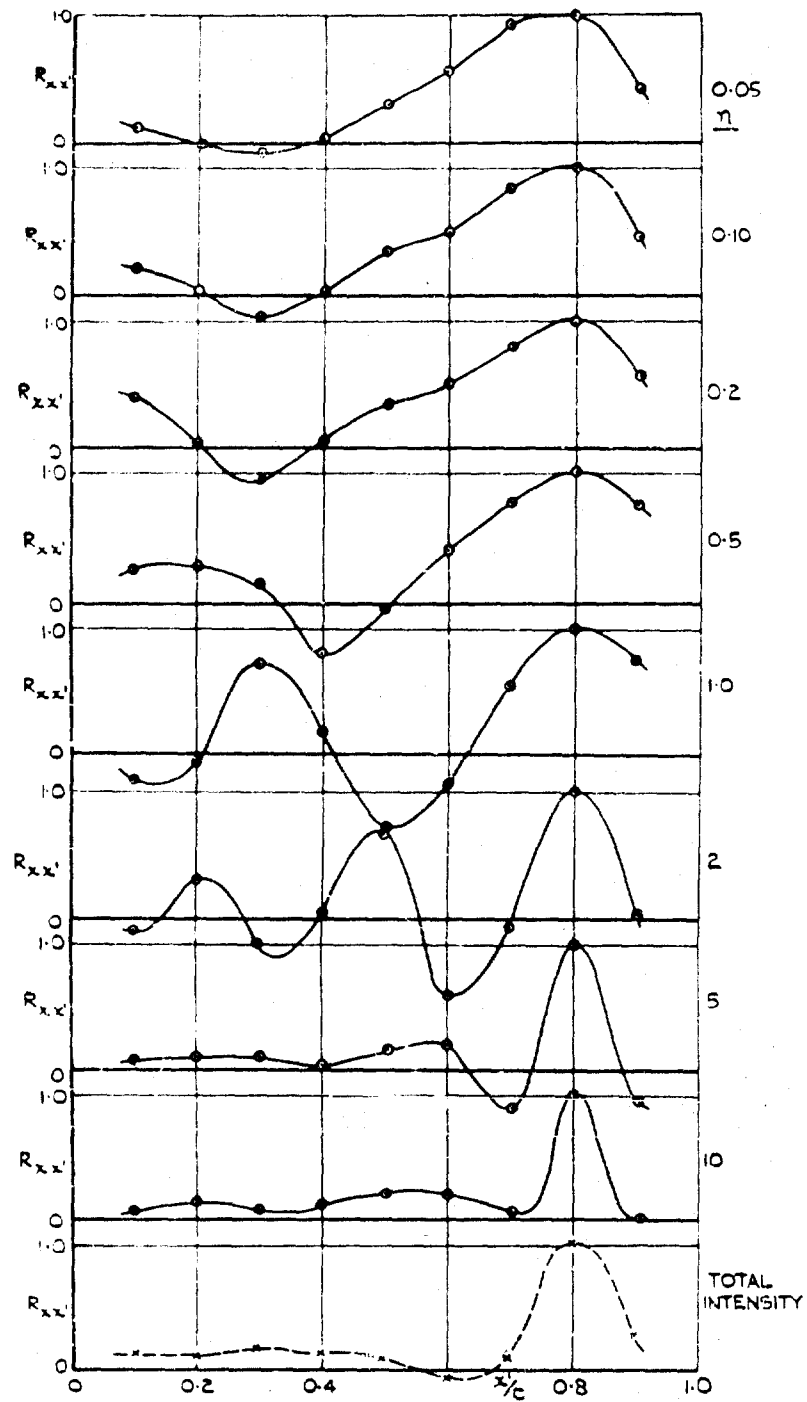
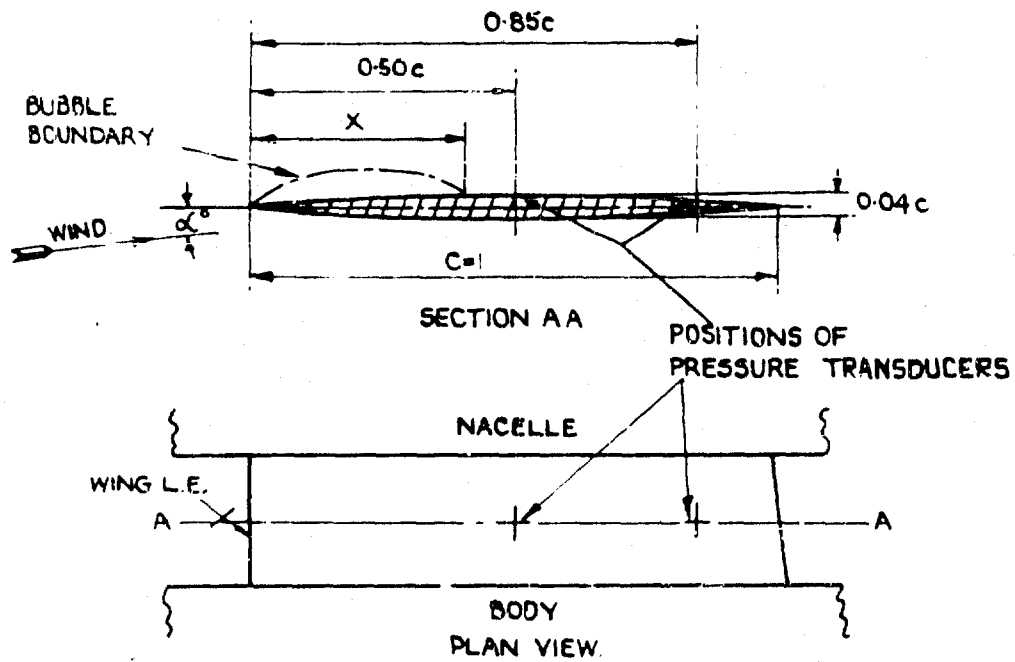


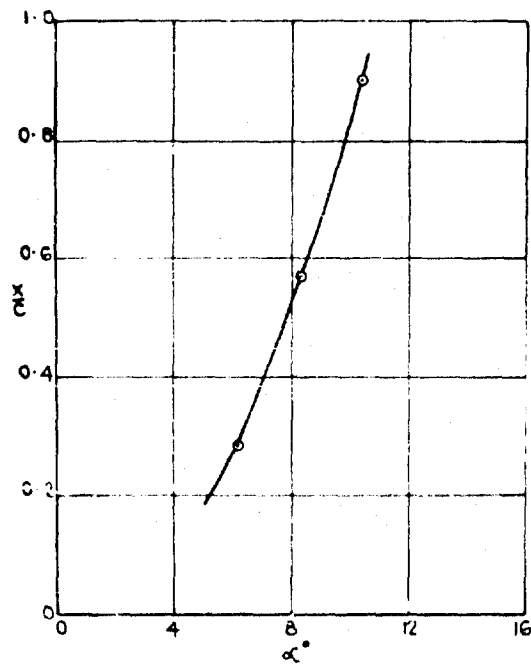
FIG. 30 Chordwise variation of correlation coefficient on wing shown in Figure 25.  
Nacelle on. Wing incidence  $4^\circ$

$x = 0.8c$ ,  $c =$  wing chord

$x$  and  $x'$  measured from the wing leading-edge

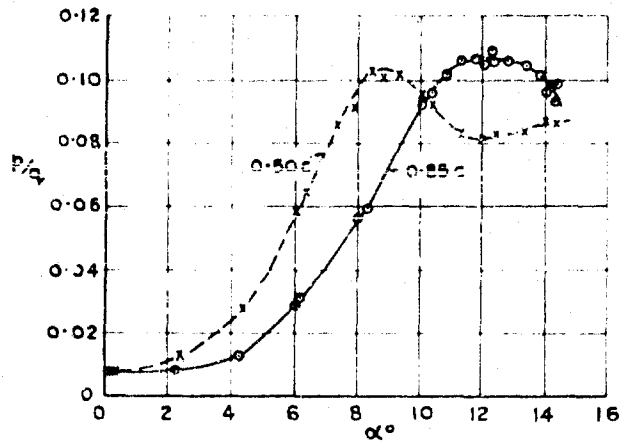


(a) Details of model

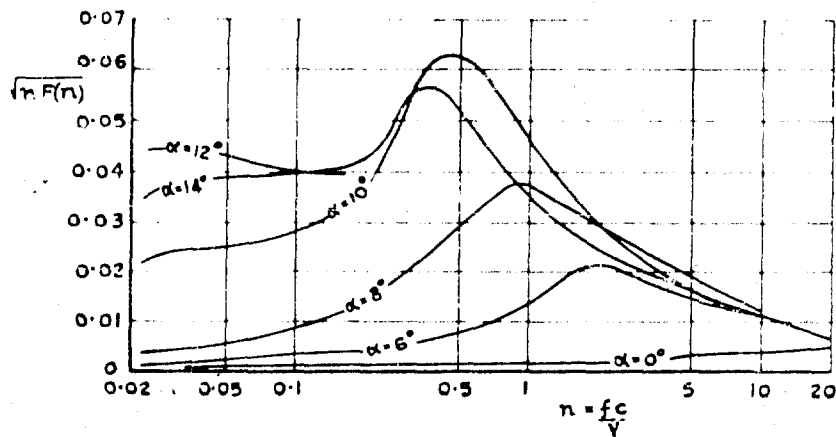


(b) Variation of bubble length with incidence

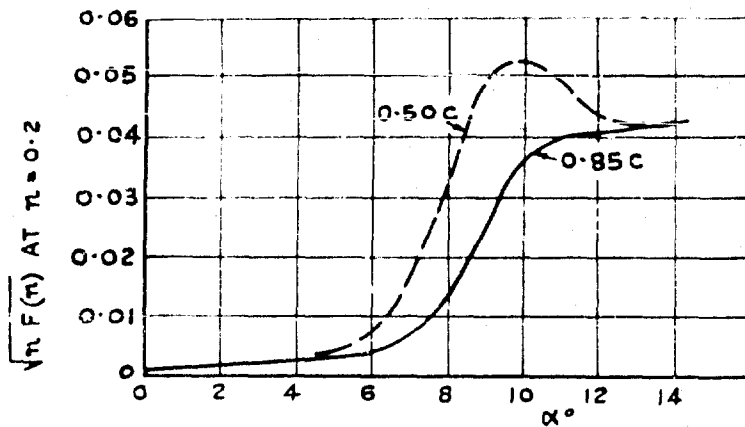
Fig.31 Unswept wing with sharp leading edge



(a) r.m.s. pressure fluctuation

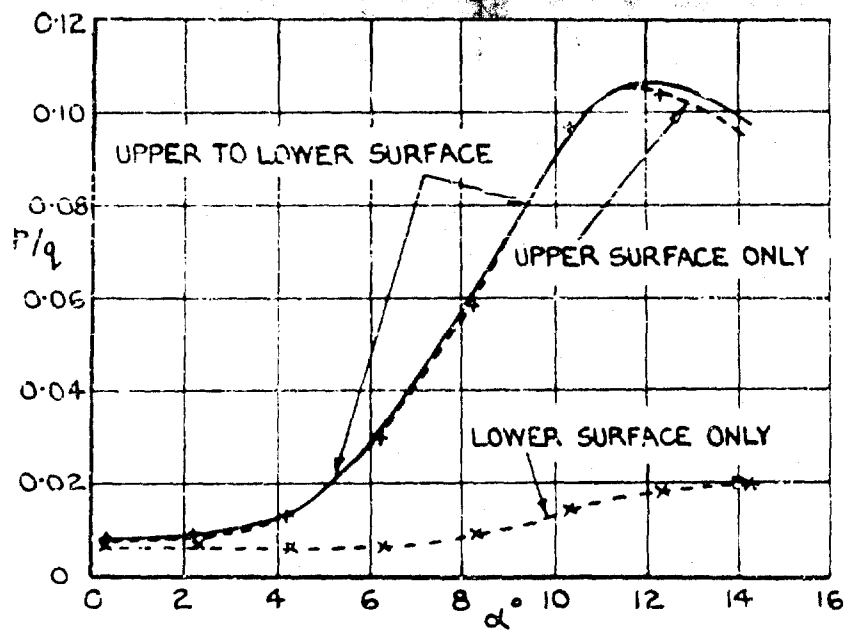


(b) Spectra of pressure fluctuations at 0.85c



(c) 'Low frequency component' of pressure fluctuations

Fig.32 Unswept wing with sharp leading edge. Fluctuations in pressure difference between upper and lower surfaces



(a) r.m.s. pressure fluctuation

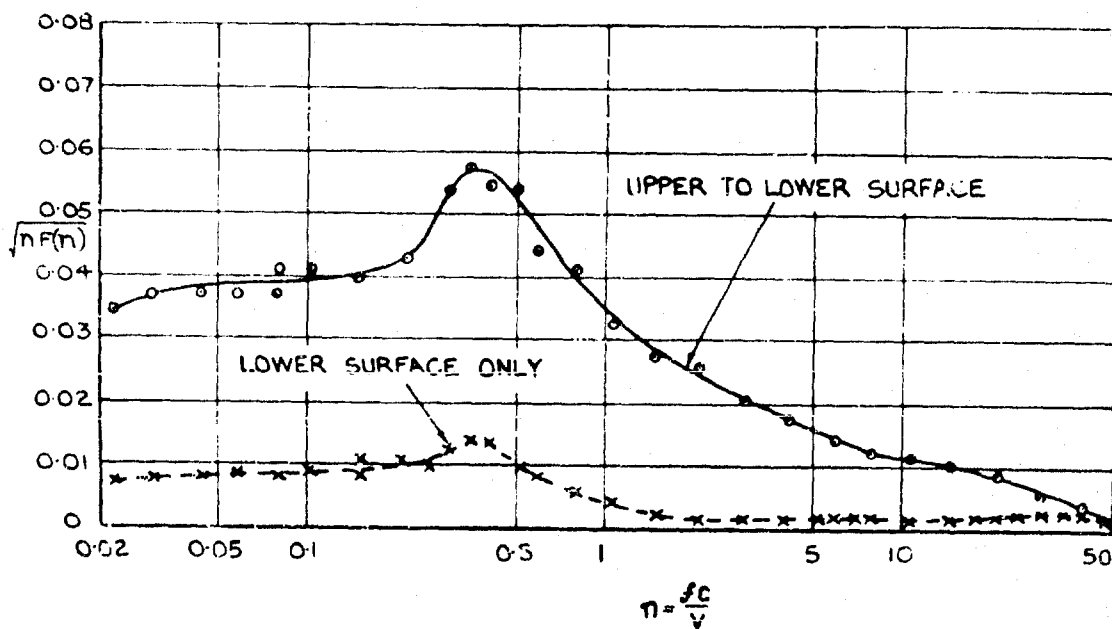
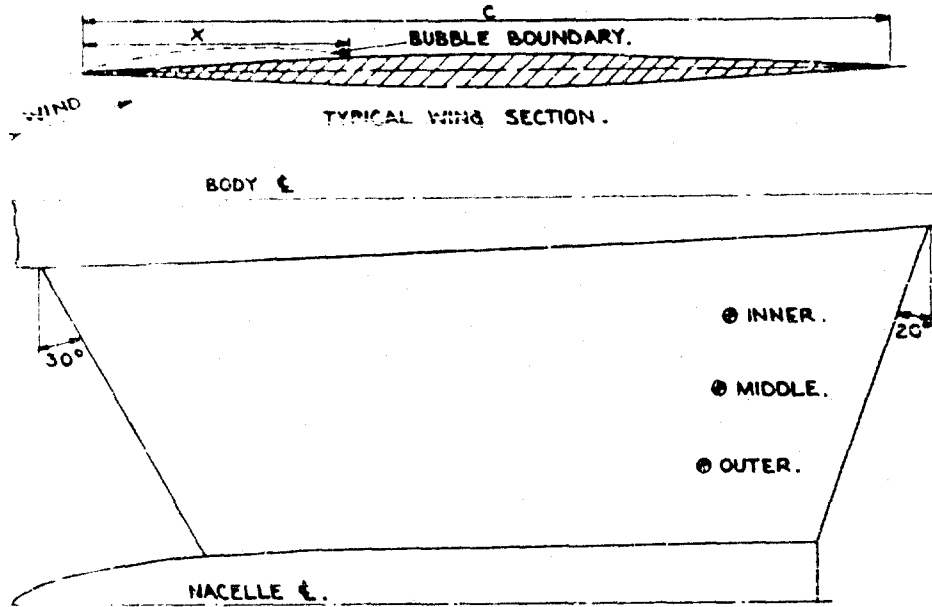
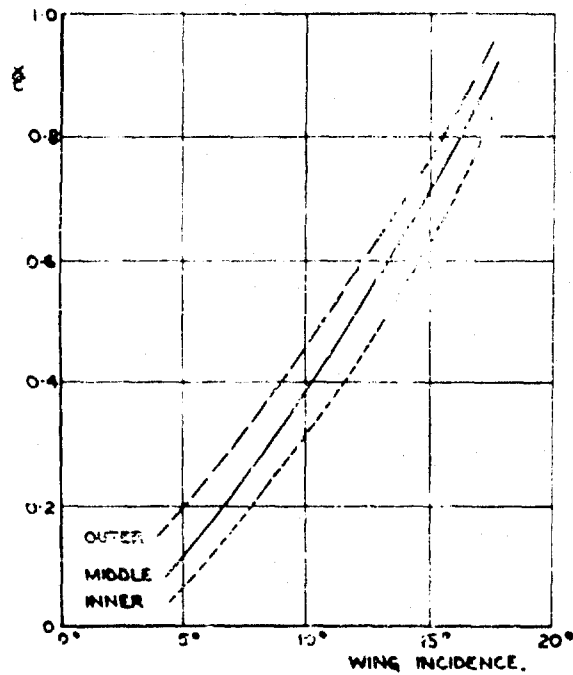
(b) Spectra of pressure fluctuations,  $\alpha = 14^\circ$ 

FIG. 23 Unswep wing with sharp leading edge. Comparison of pressure fluctuations on upper and lower surfaces. Transducer at  $0.85c$



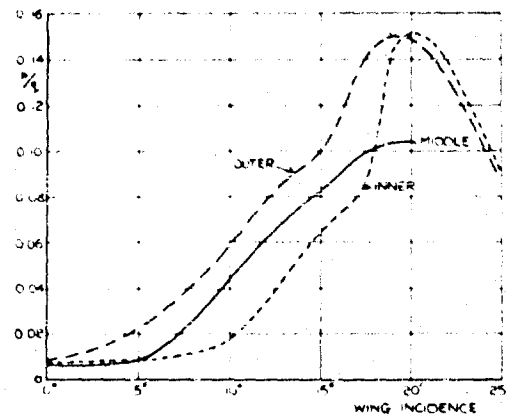
(a) Model details

The three transducer positions shown thus  $\odot$  are at 0.80c

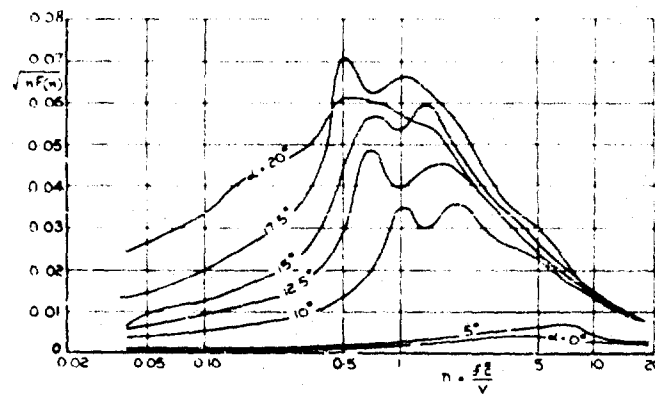


(b) Position of attachment point at spanwise positions of pressure transducers

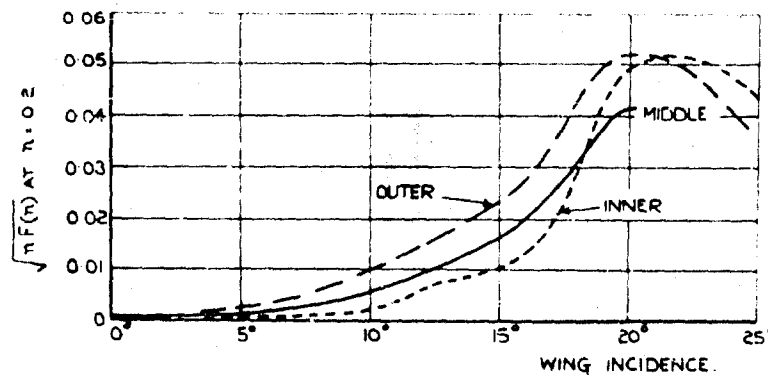
Fig.34 Sharp-edged wing with 30° leading edge sweep



(a) r.m.s. pressure fluctuation at the three transducer positions



(b) Spectra of pressure fluctuations at middle transducer position



(c) 'Low-frequency component' of pressure fluctuations at the three transducer positions

Fig. 35 Pressure fluctuation measurements on a sharp-edged wing with 30° leading edge sweep as shown in Figure 34

 $\bar{c}$  = wing mean chord

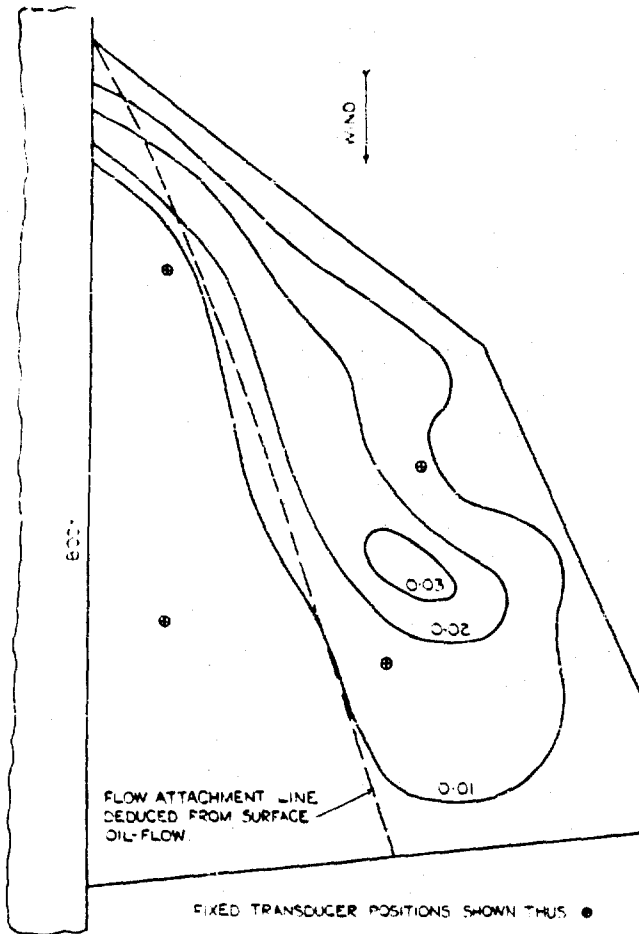


Fig. 36 Upper-surface contours of  $\sqrt{p'F(n)}$  at  $n = 0.2$  on a low-aspect-ratio sharp-edged wing at  $8^\circ$  incidence;  $n = \Gamma C/V$

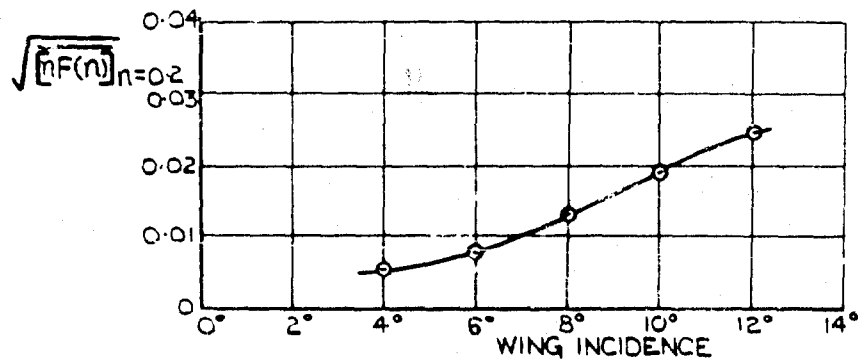
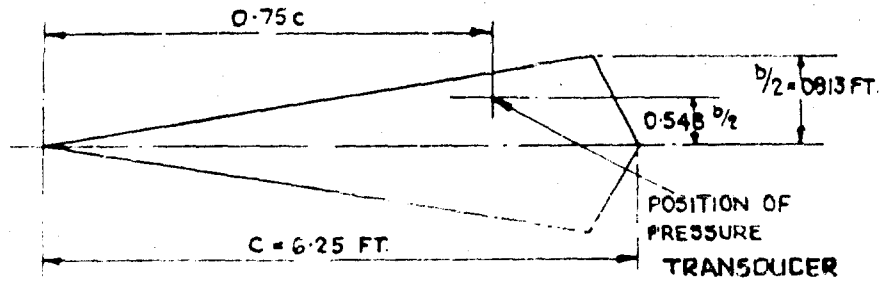
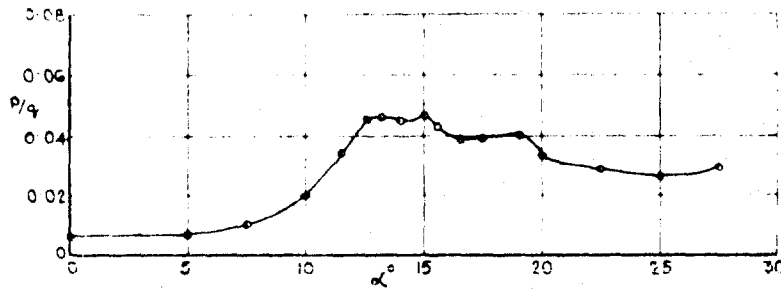


Fig. 37 Variation of r.m.s. upper-surface value of  $\sqrt{p'F(n)}$  at  $n = 0.2$  with incidence for the sharp-edged wing shown in Figure 36, assuming a correlation coefficient of 1.0 throughout

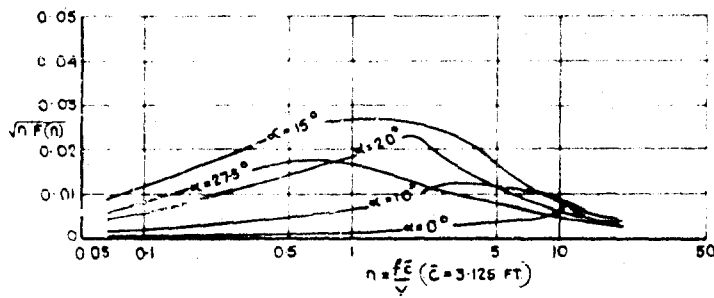
SECTIONS ARE ALL R.A.E. 101 ( $t/c = 0.06$ )



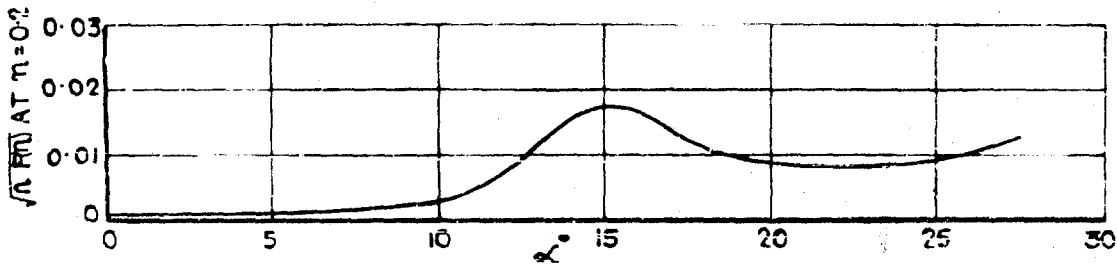
(a) Details of model



(b) r.m.s. pressure fluctuation



(c) Spectra of pressure fluctuations



(d) 'low frequency component' of pressure fluctuations

Fig. 38  $81^\circ$  swept wing - RAE 101 section: fluctuations in pressure difference between upper and lower surface

## DISTRIBUTION

Copies of AGARD publications may be obtained in the various countries at the addresses given below.

On peut se procurer des exemplaires des publications de l'AGARD aux adresses suivantes.

BELGIUM BELGIQUE	Centre National d'Etudes et de Recherches Aéronautiques 11, rue d'Égmont Bruxelles.
CANADA	Director of Scientific Information Services, Defence Research Board Department of National Defence 'A' Building Ottawa, Ontario.
DENMARK DANEMARK	Military Research Board Defence Staff Kastellet Copenhagen Ø.
FRANCE	O.N.E.R.A. (Direction) 25, avenue de la Division-Leclerc Châtillon-sous-Bagneux (Seine)
GERMANY ALLEMAGNE	Wissenschaftliche Gesellschaft für Luftfahrt Zentralstelle der Luftfahrt-dokumentation München 64, Flughafen Attn: Dr. H.J. Rautenberg
GREECE GRECE	Greek Nat. Def. Gen. Staff B. MEO Athens.
ICELAND ISLANDE	Director of Aviation C/o Flugrad Reykjavik Iceland
ITALY ITALIE	Centro Consultivo Studi e Ricerche Ministero Difesa - Aeronautica Rome.

LUXEMBURG  
LUXEMBOURG

Luxemburg Delegation to NATO  
Palais de Chaillot  
Paris 16.

NETHERLANDS  
PAYS BAS

Netherlands Delegation to AGARD  
10 Kanaalstraat  
Delft, Holland.

NORWAY  
NORVEGE

Chief Engineering Division  
Royal Norwegian Air Force  
Deputy Chief of Staff/Material  
Myntgaten 2  
Oslo, Norway  
Attn: Lt. Col. S. Heglund

PORTUGAL

Subsecretariado da Estado da  
Aeronautica  
Av. da Liberdade 252  
Lisbon.  
Attn: Lt. Col. Jose Ferreira do  
Nascimento

TURKEY  
TURQUIE

M. M. Vekaleti  
Erkaniharbiyei Umumiye Riyaseti  
Ilmi Istisare Kurulu Mudurlugu  
Ankara, Turkey  
Attn: Brigadier General Fuat Ulug

UNITED KINGDOM  
ROYAUME UNI

Ministry of Supply  
TIL, Room 009A  
First Avenue House  
High Holborn  
London, W.C.1.

UNITED STATES  
ETATS UNIS

National Advisory Committee for  
Aeronautics  
1512 H Street, N.W.  
Washington 25, D.C.

